Understanding and Extending Subgraph GNNs by Rethinking Their Symmetries

Fabrizio Frasca[*]
Imperial College London & Twitter
ffrasca@twitter.com

Beatrice Bevilacqua[*]
Purdue University
bbevilac@purdue.edu

Michael M. Bronstein
University of Oxford & Twitter
mbronstein@twitter.com

Haggai Maron
NVIDIA Research
hmaron@nvidia.com

Abstract

Subgraph GNNs are a recent class of expressive Graph Neural Networks (GNNs) which model graphs as collections of subgraphs. So far, the design space of possible Subgraph GNN architectures as well as their basic theoretical properties are still largely unexplored. In this paper, we study the most prominent form of subgraph methods, which employs node-based subgraph selection policies such as ego-networks or node marking and deletion. We address two central questions: (1) *What is the upper-bound of the expressive power of these methods?* and (2) *What is the family of equivariant message passing layers on these sets of subgraphs?*. Our first step in answering these questions is a novel symmetry analysis which shows that modelling the symmetries of node-based subgraph collections requires a significantly smaller symmetry group than the one adopted in previous works. This analysis is then used to establish a link between Subgraph GNNs and Invariant Graph Networks (IGNs). We answer the questions above by first bounding the expressive power of subgraph methods by 3-WL, and then proposing a general family of message-passing layers for subgraph methods that generalises all previous node-based Subgraph GNNs. Finally, we design a novel Subgraph GNN dubbed `SUN`, which theoretically unifies previous architectures while providing better empirical performance on multiple benchmarks.

1 Introduction

Message Passing Neural Networks (MPNNs) are arguably the most commonly used version of Graph Neural Networks (GNNs). The limited expressive power of MPNNs [36, 55] has led to a plethora of works aimed at designing expressive GNNs while maintaining the simplicity and scalability of MPNNs [11, 39, 49, 30]. Several recent studies have proposed a new class of such architectures [14, 59, 7, 61, 43, 42], dubbed *Subgraph GNNs*, which apply MPNNs to collections ('bags') of subgraphs extracted from the original input graph and then aggregate the resulting representations. Subgraphs are selected according to a predefined policy; in the most popular ones, each subgraph is tied to a specific node in the original graph, for example by deleting it or extracting its local ego-network. Subgraph GNNs have demonstrated outstanding empirical performance, with state-of-the-art results on popular benchmarks like the ZINC molecular property prediction [61, 7].

While offering great promise, it is fair to say that we still lack a full understanding of Subgraph GNNs. Firstly, on the theoretical side, it is known that subgraph methods are strictly stronger than

[*]Equal contribution. Author ordering determined by coin flip.

36th Conference on Neural Information Processing Systems (NeurIPS 2022).

the Weisfeiler-Leman (WL) test [54, 39], but an upper-bound on their expressive power is generally unknown. Secondly, on a more practical level, Subgraph GNN architectures differ considerably in the way information is aggregated and shared across the subgraphs, and an understanding of the possible aggregation and sharing rules is missing. Both aspects are important: an understanding of the former can highlight the limitations of emerging architectures, a study of the latter paves the way for improved Subgraph GNNs.

Main contributions. The goal of this paper is to provide a deeper understanding of node-based Subgraph GNNs in light of the two aforementioned aspects. The main theoretical tool underpinning our contributions is a novel analysis of the symmetry group that acts on the sets of subgraphs. While several previous approaches [43, 14, 7] have (often implicitly) assumed that a subgraph architecture should be equivariant to independent node and subgraph permutations, we leverage the fact that node-based policies induce an inherent bijection between the subgraphs and the nodes. This observation allows us to align the two groups and model the symmetry with a single (smaller) permutation group that acts on nodes and subgraphs *jointly*. Other works [61, 56, 59] have (again, implicitly) recognised such node-subgraph correspondence but without studying the implications on the symmetry group, and resorting, as a result, to a partial and heuristic choice of equivariant operations.

The use of this stricter symmetry group raises a fruitful connection with k-order Invariant Graph Networks (`k-IGNs`) [33, 32], a well studied family of architectures for processing graphs and hypergraphs designed to be equivariant to the same symmetry group. This connection allows us to transfer and reinterpret previous results on `IGNs` to our Subgraph GNN setup. As our first contribution we show that the expressive power of Subgraph GNNs with node-based policies is bounded by that of the `3-WL` test. This is shown by proving that all previous Subgraph GNNs can be implemented by a `3-IGN` and by leveraging the fact that the expressive power of these models is bounded by `3-WL` [21, 5].

Our second contribution is the proposal of a general layer formulation for Subgraph GNNs, based on the observation that these methods maintain an $n \times n$ representation of n subgraphs with n nodes, following the same symmetry structure of `2-IGNs` (same permutation applied to both rows and columns of this representation). We propose a novel extension of `2-IGNs` capturing both local (message-passing-like) and global operations. This extension easily recovers previous methods facilitating their comparison. Also, we present a number of new operations that previous methods did not implement. We build upon these observations to devise a new Subgraph GNN dubbed `SUN`, (*Subgraph Union Network*). We prove that `SUN` generalises all previous node-based Subgraph GNNs and we empirically compare it to these methods, showing it can outperform them.

2 Previous and related work

Expressive power of GNNs. The expressive power of GNNs is a central research focus since it was realised that message-passing type GNNs are constrained by the expressivity of the WL isomorphism test [36, 55]. Other than the aforementioned subgraph-based methods, numerous approaches for more powerful GNNs have been proposed, including positional and structural encodings [1, 45, 11, 17, 28, 31], higher-order message-passing schemes [36, 38, 10, 9], equivariant models [24, 33, 32, 53, 15, 51, 40]. We refer readers to the recent survey by Morris et al. [39] for additional details. Finally we note that, in a related and concurrent work, Qian et al. [46] propose a theoretical framework to study the expressive power of subgraph-based GNNs by relating them to the `k-WL` hierarchy, and explore how to sample subgraphs in a data-driven fashion.

Invariant graph networks. `IGNs` were recently introduced in a series of works by Maron et al. [33, 32, 34] as an alternative to MPNNs for processing graph and hyper-graph data. For $k \geq 2$, `k-IGNs` represent hyper-graphs with hyper-edges up to size k with k-order tensor $\mathcal{Y} \in \mathbb{R}^{n^k}$, where each entry holds information about a specific hyper-edge. On these they apply linear S_n-equivariant layers interspersed with pointwise nonlinearities. These models have been thoroughly studied in terms of: (i) their expressive power; (ii) the space of their equivariant linear layers. As for (i), `IGNs` were shown to have exactly the same graph separation power as the `k-WL` graph isomorphism test [32, 5, 21] and, for sufficiently large k, to have a universal approximation property w.r.t. S_n-invariant and equivariant functions [34, 26, 47]. Concerning (ii), the work in [33] completely characterised the space of linear layers equivariant to S_n from $\mathbb{R}^{n^k}$ to $\mathbb{R}^{n^{k'}}$: the authors derived a basis of bell$(k + k')$ linear operators consisting of indicator tensors of equality patterns over the multi-index set $\{1, \dots, n\}^{k+k'} = [n]^{k+k'}$. Albooyeh et al. [2] showed these layers can be (re-)written

as sums of pooling-broadcasting operations between elements of $\mathcal{Y}$ indexed by the orbits [2] of the action of S_n on $[n]^k$ and $[n]^{k'}$. Take, e.g., $k = k' = 2$. In this case there are only two orbits: $\{i, i\},\ i \in [n]$ corresponding to on-diagonal terms, and $\{i, j\},\ i \neq j \in [n]$, off-diagonal terms. According to Albooyeh et al. [2] any equivariant linear layer $L : \mathbb{R}^{n^2} \to \mathbb{R}^{n^2}$ can be represented as a composition of pooling and broadcasting operations on the elements indexed by these orbits. One example is the linear map that sums the on-diagonal elements and broadcasts the result to the off-diagonal ones: $L(\mathcal{Y})_{ij} = \sum_k \mathcal{Y}_{kk}$ for $i \neq j$, 0 otherwise. See Appendix B, for additional details. These results particularly important as they underpin most of our theoretical derivations. Lastly, a more comprehensive coverage of `IGN`s can be found in [39].

Subgraph GNNs. Despite motivated by diverse premises, a collection of concurrent methods share the overarching design whereby graphs are modelled through the application of a GNN to their subgraphs. Bevilacqua et al. [7] first explicitly formulated the concept of bags of subgraphs generated by a predefined policy and studied layers to process them in an equivariant manner: the same GNN can encode each subgraph independently (DS-GNN), or information can be shared between these computations in view of the alignment of nodes across the bag [35] (DSS-GNN). Building upon the Reconstruction Conjecture [25, 52], Reconstruction GNNs [14] obtain node-deleted subgraphs, process them with a GNN and then aggregate the resulting representations by means of a set model. Nested GNNs [59] and GNN-As-Kernel models (GNN-AK) [61] shift their computation from rooted subtrees to rooted subgraphs, effectively representing nodes by means of GNNs applied to their enclosing ego-networks. Similarly to DSS-GNNs [7], GNN-AK models may feature information sharing modules aggregating node representations across subgraphs. ID-GNNs [56] also process ego-network subgraphs, but their roots are 'marked' so to specifically alter the exchange of messages involving them. Intuitively, the use of subgraphs implicitly breaks those local symmetries which determine the notorious expressiveness bottleneck of MPNNs. We note that other works can be interpreted as Subgraph GNNs, including those by Papp et al. [43], Papp and Wattenhofer [42].

3 Node-based Subgraph GNNs

Notation. Let $G = (A, X)$ be a member of the family $\mathcal{G}$ of *node-attributed*, undirected, finite, simple graphs[3]. The *adjacency matrix* $A \in \mathbb{R}^{n \times n}$ represents G's edge set E over its set of n nodes V. The *feature matrix* $X \in \mathbb{R}^{n \times d}$ gathers the node features; we denote by $x_j \in \mathbb{R}^{d \times 1}$ the features of node j corresponding to the j-th row of X. B_G is used to denote a multiset (bag) of m subgraphs of G. Adjacency and feature matrices for subgraphs in B_G are arranged in tensors $\mathcal{A} \in \mathbb{R}^{m \times n \times n}$ and $\mathcal{X} \in \mathbb{R}^{m \times n \times d}$. Superscript $^{i,(t)}$ refers to representations on subgraph i at the t-th layer of a stacking, as in $x_j^{i,(t)}$. Finally, we denote $[n] = \{1, \dots, n\}$. All proofs are deferred to Appendices B and D.

Formalising Subgraph GNNs. Subgraph GNNs compute a representation of $G \in \mathcal{G}$ as

$$(A, X) \mapsto \big(\mu \circ \rho \circ \mathcal{S} \circ \pi\big)(A, X). \tag{1}$$

Here, $\pi : G \mapsto \{G^1, ..., G^m\} = \{(A^1, X^1), ..., (A^m, X^m)\} = B_G^{(0)}$ is a *selection policy* generating a bag of subgraphs from G; $\mathcal{S} = L_T \circ \ldots \circ L_1 : B_G^{(0)} \mapsto B_G^{(T)}$ is a *stacking* of T (node- and subgraph-) permutation equivariant layers; $\rho : (G, B_G^{(T)}) \mapsto x_G$ is a permutation invariant *pooling function*, μ is an MLP. The layers in $\mathcal{S}$ comprise a *base-encoder* in the form of a GNN applied to subgraphs; throughout this paper, we assume it to be a `1-WL` maximally expressive MPNN such as the one in Morris et al. [36]. Subgraph GNNs differ in the implementation of π, $\mathcal{S}$ and, in some cases, ρ. For example, in (n-1)-Reconstruction GNNs [14], π selects node-deleted subgraphs and $\mathcal{S}$ applies a Siamese MPNN to each subgraph independently. To exemplify the variability in $\mathcal{S}$, DSS-GNN [7] extends this method with cross-subgraph node and connectivity aggregation. More details are on how currently known Subgraph GNNs are captured by Equation (1) can be found in Appendix A.

Node-based selection policies. In this work, we focus on a specific family of *node-based* subgraph selection policies, wherein every subgraph is associated with a unique node in the graph. Formally, we call a subgraph selection policy *node-based* if it is of the form $\pi(G) = \{f(G, v)\}_{v \in V}$, for some *selection function* $f(G, v)$ that takes a graph G and a node v as inputs and outputs a subgraph G^v.

[2] For group G acting on set X, the orbits of the action of G on X are defined as $\{G \cdot x \,|\, x \in X\}$. These *partition* X into subsets whose elements can (only) reach all other elements in the subset via the group action.

[3] We do not consider edge features, although an extension to such a setting would be possible.

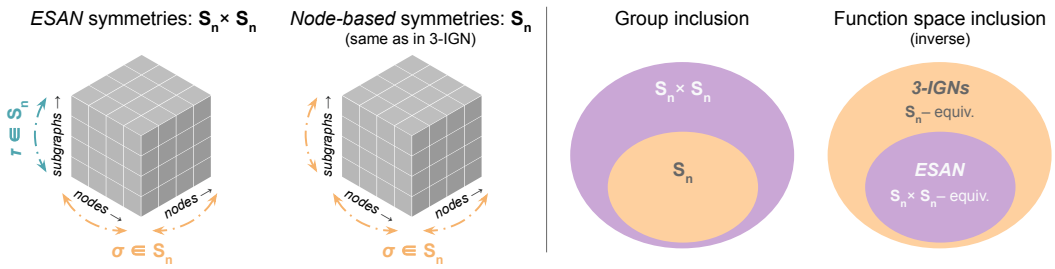

Figure 1: Symmetries of bags of subgraphs (left) and corresponding function space diagrams (right). In ESAN [7] symmetries are modelled as a direct product of node and subgraph permutation groups; however, node-based policies enable the use of one single permutation group, the same as in `3-IGNs`. `3-IGNs` are less constrained, thus more expressive than ESAN and other Subgraph GNNs. See diagram on the right and formal statement in Section 5.

In the following, we refer to v as the *root* of subgraph G^v. We require f to be a bijection and we note that such policies produce $m = n$ different subgraphs. Amongst the most common examples are *node-deletion* (ND), *node-marking* (NM), and *ego-networks* (EGO) policies. For input graph G, $f_{\mathrm{ND}}(G, v)$ removes node v and the associated connectivity; $f_{\mathrm{NM}}(G, v)$ adds a special 'mark' attribute to v's features (with no connectivity alterations), and $f_{\mathrm{EGO}(h)}(G, v)$ returns the subgraph induced by the h-hop-neighbourhood around the root v. EGO policies can be 'marked': $f_{\mathrm{EGO+}(h)}(G, v)$ extracts the h-hop ego-net around v *and* marks this node as done by f_{NM}. For convenience, we denote the class of such node-based selection policies by Π:

Definition 1 (Known node-based selection policies Π)**.** *Let Σ be the set of all node-based subgraph selection policies operating on $\mathcal{G}$. Class $\Pi \subset \Sigma$ collects the node-based policies node-deletion (ND), node-marking (NM), ego-nets (EGO) and marked ego-nets (EGO+) of any depth:* $\Pi = \{\pi_{\mathrm{ND}}, \pi_{\mathrm{NM}}, \pi_{\mathrm{EGO}(h)}, \pi_{\mathrm{EGO+}(h)} \,|\, h > 0\}$.

Node-based Subgraph GNNs are those Subgraph GNNs which, implicitly or explicitly, process bags generated by node-based policies. We group known formulations in the following family:

Definition 2 (Known node-based Subgraph GNNs Υ)**.** *Let Ξ be the set of all node-based Subgraph GNNs. Class $\Upsilon \subset \Xi$ collects known Subgraph GNNs when equipped with `1-WL` base-encoders:* $\Upsilon = \{$(n-1)-Reconstr.GNN, GNN-AK, GNN-AK-ctx, NGNN, ID-GNN, DS-GNN$_\Pi$, DSS-GNN$_\Pi\}$. DS-GNN$_\Pi$, DSS-GNN$_\Pi$ *refer to* DS- *and* DSS-GNN *models equipped with any $\pi \in \Pi$.*

Importantly, all these methods apply MPNNs to subgraphs of the original graph, but differ in the way information is shared between subgraphs/nodes. In all cases, their expressive power is strictly larger than `1-WL`, but an *upper*-bound is currently unknown.

4 Symmetries of node-based subgraph selection policies

In an effort to characterise the representational power of node-based Subgraph GNNs, we first study the symmetry group of the objects they process: 'bags of subgraphs' represented as tensors $(\mathcal{A}, \mathcal{X}) \in \mathbb{R}^{m\times n\times n} \times \mathbb{R}^{m\times n\times d}$, assuming n nodes across m subgraphs. Previous approaches [14, 7, 43] used two permutation groups: one copy of the symmetric group S_n models *node permutations*, while another copy S_m models *subgraph permutations* in the bag. These two were combined by a group product[4] acting *independently* on the nodes and subgraphs in $(\mathcal{A}, \mathcal{X})$. For example, Bevilacqua et al. [7] model the symmetry as:

$$((\tau, \sigma)\cdot\mathcal{A})_{ijk} = \mathcal{A}_{\tau^{-1}(i)\sigma^{-1}(j)\sigma^{-1}(k)}, \quad ((\tau, \sigma)\cdot\mathcal{X})_{ijl} = \mathcal{X}_{\tau^{-1}(i)\sigma^{-1}(j)l}, \qquad (\tau, \sigma) \in S_m \times S_n \quad (2)$$

Our contributions stem from the following crucial observation: When using node-based policies, the subgraphs in $(\mathcal{A}, \mathcal{X})$ can be *ordered consistently with the nodes* by leveraging the bijection $f : v \mapsto G_v$ characterising this policy class. In other words, f suggests a node-subgraph alignment

[4] Bevilacqua et al. [7] use a direct-product, assuming nodes in subgraphs are consistently ordered. Cotta et al. [14] use the larger wreath-product assuming node ordering in the subgraph is unknown.

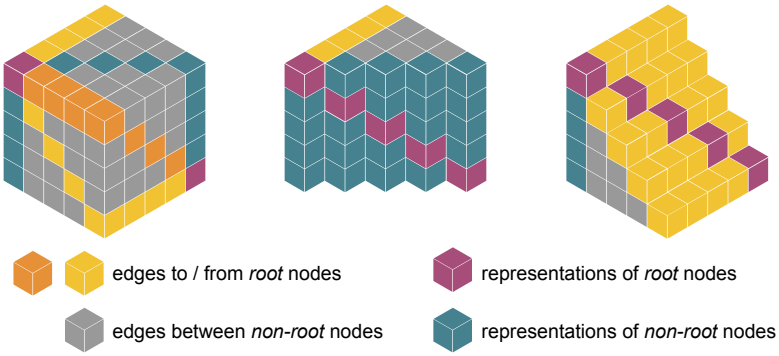

Figure 2: Depiction of cubed tensor $\mathcal{Y}$, its orbit-induced partitioning and the related semantics when $\mathcal{Y}$ is interpreted as a bag of node-based subgraphs, $n = 5$. Elements in the same partition are depicted with the same colour. Left: the whole tensor. Middle and right: sections; elements in purple and green constitute sub-tensor $\mathcal{X}$, the remaining ones sub-tensor $\mathcal{A}$.

inducing a new structure on $(\mathcal{A}, \mathcal{X})$, whereby the subgraph order is not independent of that of nodes anymore. Importantly, this new structure is preserved *only* by those permutations operating identically on both nodes and subgraphs. Following this observation, the symmetry of a node-based bag of subgraphs is modelled more accurately using only *one single permutation group* S_n jointly acting on both nodes and subgraphs:

$$(\sigma \cdot \mathcal{A})_{ijk} = \mathcal{A}_{\sigma^{-1}(i)\sigma^{-1}(j)\sigma^{-1}(k)}, \quad (\sigma \cdot \mathcal{X})_{ijl} = \mathcal{X}_{\sigma^{-1}(i)\sigma^{-1}(j)l}, \qquad \sigma \in S_n \tag{3}$$

It should be noted that S_n is *significantly smaller* than $S_n \times S_n$[5]. Informally, the latter group contains many permutations which are not in the former: those acting differently on nodes and subgraphs and, thus, not preserving the new structure of $(\mathcal{A}, \mathcal{X})$. Since they are restricted by a smaller set of equivariance constraints, we expect GNNs designed to be equivariant to S_n to be be more expressive than those equivariant to the larger groups considered by previous works [34] (see Figure 1).

The insight we obtain from Equation (3) is profound: it reveals that the symmetry structure of $\mathcal{A}$ exactly matches the symmetries of third-order tensors used by `3-IGNs`, and similarly, that the symmetry structure for $\mathcal{X}$ matches the symmetries of second-order tensors used by `2-IGNs`. In the following, we will make use of this insight and the fact that `IGNs` are well-studied objects to prove an upper-bound on the expressive power of Subgraph GNNs and to design principled extensions to these models. We remark that bags of node-based subgraphs can also be represented as tensors $\mathcal{Y} \in \mathbb{R}^{n^3 \times d}$, the same objects on which `3-IGNs` operate. Here, $\mathcal{X}$ is embedded in the main diagonal plane of $\mathcal{Y}$, $\mathcal{A}$ in its remaining entries. Within this context, it is informative to study the semantics of the 5 orbits induced by the action of S_n on $\mathcal{Y}$'s multi-index set $[n]^3$: each of these uniquely identify root nodes, non-root nodes, edges to and from root nodes as well as edges between non-root nodes (see Figure 2 and additional details in Appendix B.1.1). We build upon this observation, along with the layer construction by Albooyeh et al. [2], to prove many of the results presented in the following.

5 A representational bound for Subgraph GNNs

In this section we prove that the expressive power of known node-based Subgraph GNNs is bounded by `3-WL` by showing that they can be implemented by `3-IGNs`, which have the same expressive power as `3-WL`. Underpinning the possibility of `IGNs` to upper-bound a certain Subgraph GNN $\mathcal{N}$ in its expressive power is the ability of `IGNs` to (i) implement $\mathcal{N}$'s subgraph selection policy (π) and (ii) implement $\mathcal{N}$'s (generalised) message-passing and pooling equations ($\mu \circ \rho \circ \mathcal{S}$). This would ensure that whenever $\mathcal{N}$ assigns distinct representations to two non-isomorphic graphs, an `IGN` implementing $\mathcal{N}$ would do the same. We start by introducing a recurring, useful concept.

Definition 3 ("implements"). *Let $f : D_f \to C_f$, $g : D_g \to C_g$ be two functions and such that $D_g \subseteq D_f, C_g \subseteq C_f$. We say f* implements *g (and write $f \cong g$) when $\forall x \in D_g, f(x) = g(x)$.*

[5] More formally, S_n's orbits on the indices in (3) refine the orbits of the product group in (2).

Our first result shows that 3-IGNs can implement the selection policies in class Π (Definition 1), which, to the best of our knowledge, represent *all known* node-based policies utilised by previously proposed Subgraph GNNs.

Lemma 4 (3-IGNs implement known node-based selection policies)**.** *For any $\pi \in \Pi$ there exists a stacking of 3-IGN layers $\mathcal{M}_\pi$ s.t. $\mathcal{M}_\pi \cong \pi$.*

Intuitively, 3-IGNs start from a $\mathbb{R}^{n^2}$ representation of G and, first, move to a $\mathbb{R}^{n^3}$ tensor 'copying' this latter along its first (subgraph) dimension. This is realised via an appropriate broadcast operation. Then, they proceed by adding a 'mark' to the features of some nodes and/or by nullifying elements corresponding to some edges. We refer readers to Figure 2 and Appendix B.1.2 for additional details on how nodes in each subgraph are represented in 3-IGNs. Next, we show 3-IGNs can implement layers of any model $\in \Upsilon$.

Lemma 5 (3-IGNs implement Subgraph GNN layers)**.** *Let G_1, G_2 be two graphs in $\mathcal{G}$ and $\mathcal{N}$ a model in family Υ equipped with Morris et al. [36] message-passing base-encoders. Let $B_1^{(t)}, B_2^{(t)}$ be bags of subgraphs in the input of some intermediate layer L in $\mathcal{N}$. Then there exists a stacking of 3-IGN layers $\mathcal{M}_L$ for which $\mathcal{M}_L(B_i^{(t)}) = B_i^{(t+1)} = L(B_i^{(t)})$ for $i = 1, 2$.*

Lemmas 4 and 5 allow us to upper-bound the expressive power of all known instances of node-based Subgraph GNNs by that of 3-IGNs:

Theorem 6 (3-IGNs upper-bound node-based Subgraph GNNs)**.** *For any pair of non-isomorphic graphs G_1, G_2 in family $\mathcal{G}$ and Subgraph GNN model $\mathcal{N} \in \Upsilon$ equipped with Morris et al. [36] message-passing base-encoders, if there exists weights Θ such that G_1, G_2 are distinguished by instance $\mathcal{N}_\Theta$, then there exist weights Ω for a 3-IGN instance $\mathcal{M}_\Omega$ such that G_1, G_2 are distinguished by $\mathcal{M}_\Omega$ as well.*

Theorem 6 has profound consequences in the characterisation of the expressive power of node-based Subgraph GNNs, as we show in the following

Corollary 7 (3-WL upper-bounds node-based Subgraph GNNs)**.** *Let $G_1, G_2 \in \mathcal{G}$ be two non-isomorphic graphs and $\mathcal{N}_\Theta \in \Upsilon$ one instance of model $\mathcal{N}$ with weights Θ. If $\mathcal{N}_\Theta$ distinguishes G_1, G_2, then the 3-WL algorithm does so as well.*

Proof idea: If there is a pair of graphs undistinguishable by 3-WL, but for which there exists a Subgraph GNN separating them, there must exists a 3-IGN separating these (Theorem 6). This is in contradiction with the result by Geerts [21], Azizian and Lelarge [5][6].

6 A design space for Subgraph GNNs

As discussed, different formulations of Subgraph GNNs differ primarily in the specific rules for updating node representations across subgraphs. However, until now it is not clear whether existing rules exhaust all the possible equivariant options. We devote this section to a systematic characterisation of the 'layer space' of Subgraph GNNs.

In the spirit of the previous Section 5, where we "embedded" Subgraph GNNs in 3-IGNs, one option would be to consider all bell$(6) = 203$ linear equivariant operations prescribed by this formalism. However, this choice would be problematic for three main reasons: (i) This layer space is *too vast* to be conveniently explored; (ii) It includes operations involving $\mathcal{O}(n^3)$ space complexity, impractical in most applications; (iii) The linear IGN basis does not directly support local message passing, a key operation in subgraph methods. Following previous Subgraph GNN variants, which use $\mathcal{O}(n^2)$ storage for the representation of n nodes in n subgraphs, we set the desideratum of $\mathcal{O}(n^2)$ memory complexity as our main constraint, and use this restriction to reduce the design space. Precisely, we are interested in modelling S_n-equivariant transformations on the subgraph-node tensor $\mathcal{X}$.

6.1 Extended 2-IGNs

As we have already observed in Equation 3 in Section 4, such a second order tensor $\mathcal{X}$ abides by the same symmetry structure of 2-IGNs. We therefore gain intuition from the characterisation of linear equivariant mappings as introduced by Maron et al. [33], and propose an extension of this formalism.

[6] k-WL is equivalent to (k-1)-FWL, i.e. the "Folklore" WL test, see [36].

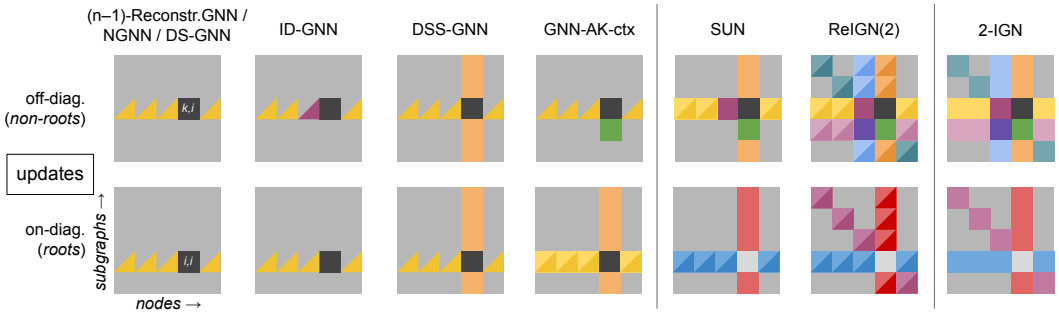

Figure 3: Comparison of aggregation and update rules in Subgraph GNNs, illustrated on an $n \times n$ matrix (n subgraphs with n nodes). Top row: off-diagonal updates; bottom row: diagonal (root node) updates. Each colour represents a different parameter. Full squares: global sum pooling; triangles: local pooling; two triangles: both local and global pooling. See Appendix C for more details.

`2-IGN` layer space. A `2-IGN` layer L_Θ updates $\mathcal{X} \in \mathbb{R}^{n\times n\times d}$ as $\mathcal{X}^{(t+1)} = L_\Theta\big(\mathcal{X}^{(t)}\big)$ by applying a specific transformation to on- (x_i^i) and off-diagonal terms ($x_j^i, i \neq j$):

$$x_i^{i,(t+1)} = \upsilon_{\theta_1}\Big(x_i^{i,(t)}, \square_j\, x_j^{j,(t)}, \square_{j\neq i}\, x_j^{i,(t)}, \square_{h\neq i}\, x_i^{h,(t)}, \square_{h\neq j}\, x_j^{h,(t)}\Big) \tag{4}$$

$$x_i^{k,(t+1)} = \upsilon_{\theta_2}\Big(x_i^{k,(t)}, x_k^{i,(t)}, \square_{h\neq j}\, x_j^{h,(t)}, \square_{h\neq i}\, x_i^{h,(t)}, \square_{j\neq k}\, x_j^{k,(t)}, \square_{j\neq i}\, x_j^{i,(t)}, \square_{h\neq k}\, x_k^{h,(t)}, x_k^{k,(t)}, x_i^{i,(t)}, \square_j\, x_j^{j,(t)}\Big)$$

Here, $\square$ indicates a permutation invariant aggregation function, $\upsilon_{\theta_1}, \upsilon_{\theta_2}$ apply a specific $d \times d'$ linear transformation to each input term and sum the outputs including bias terms.

`ReIGN(2)` layer space. As `2-IGN` layers are linear, the authors advocate setting $\square \equiv \sum$, performing pooling as *global* summation. Here, we extend this formulation to additionally include different *local* aggregation schemes. In this new extended formalism, entry x_i^k represents node i in subgraph k; accordingly, each aggregation in Equation 4 can be also performed locally, i.e. extending only over i's neighbours, as prescribed by the connectivity of subgraph k or of the original input graph. As an example, when updating entry $x_i^{k,(t)}$, term $\square_{j\neq k}\, x_j^{k,(t)}$ is expanded as $\big(\square_{j\neq k}\, x_j^{k,(t)}, \square_{j\sim_k i}\, x_j^{k,(t)}, \square_{j\sim i}\, x_j^{k,(t)}\big)$, with $\sim_k$ denoting adjacency in subgraph k, and $\sim$ that in the original graph connectivity. Each term in the expansion is associated with a specific learnable linear transformation. We report a full list of pooling operations in Appendix D, Table 3. These local pooling operations allow to readily recover sparse message passing, which constitutes the main computational primitive of all popular (Subgraph) GNNs. Other characteristic Subgraph GNN operations are also recovered by this formalism: for example, $\square_{h\neq i}\, x_i^{h,(t)}$ operates global pooling of node i's representations across subgraphs, as previously introduced in Bevilacqua et al. [7], Zhao et al. [61]. We also note that additional, novel, operations are supported, e.g. the transpose $x_k^{i,(t)}$. We generally refer to this framework as `ReIGN(2)` ("Rethought `2-IGN`").

`ReIGN(2)` architectures. `ReIGN(2)` induces (linear) layers in the same form of Equation 4, but where $\square$ terms are expanded to both local and global operations, as explained. These layers can operate on any bag generated by a node-based selection policy $\bar{\pi}$, and can be combined together in `ReIGN(2)` stacks of the form $\mathcal{S}_\mathcal{R} = L^{(T)} \circ \sigma \circ L^{(T-1)} \circ \sigma \circ \ldots \circ \sigma \circ L^{(1)}$, where σ's are pointwise nonlinearities and L's are `ReIGN(2)` layers. This allows us to define `ReIGN(2)` models as Subgraph GNNs in the form of Equation 1, where $\mathcal{S}$ is a `ReIGN(2)` layer stacking and π is node-based: $\mathcal{R}_{\bar{\pi}} = \mu \circ \rho \circ \mathcal{S}_\mathcal{R} \circ \bar{\pi}$.

More generally, `ReIGN(2)` induces a 'layer space' for node-based Subgraph GNNs: the expanded terms in its update equations represent a pool of atomic operations that can be selected and combined to define new equivariant layers. Compared to that of `3-IGN`s, this space is of tractable size, yet it recovers previously proposed Subgraph GNNs and allows to define novel interesting variants.

Recovering previous Subgraph GNNs. The following result states that the `ReIGN(2)` generalises all known subgraph methods in Υ, as their layers are captured by a `ReIGN(2)` stacking.

Theorem 8 (ReIGN(2) implements node-based Subgraph GNNs)**.** *Let $\mathcal{N}$ be a model in family Υ equipped with Morris et al. [36] message-passing base-encoders. For any instance $\mathcal{N}_\Theta$, there exists ReIGN(2) instance $\mathcal{R}_\Omega$ such that $\mathcal{R}_\Omega \cong \mathcal{N}_\Theta$.*

This shows that known methods are generalised without resorting to the $\mathcal{O}(n^3)$ computational complexity of 3-IGNs. Figure 3 illustrates the aggregation and sharing rules used by previous Subgraph GNNs to update root and non-root nodes, and compare them with those of ReIGN(2) and 2-IGNs. We visualise these on the subgraph-node sub-tensor gathering node representations across subgraphs; here, root nodes occupy the main diagonal, non-root nodes all the remaining off-diagonal entries. As for to the 2-IGN Equations 4, the elements in these two partitions may be updated differently, so we depict them separately in, respectively, the bottom and top rows. In each depiction we colour elements depending on the set of weights parameterising their contribution in the update process, with two main specifications: (i) Elements sharing the same colour are pooled together; (ii) Triangles indicate such pooling is performed locally based on the subgraph connectivity at hand (two triangles indicate both local and global pooling ops are performed). E.g., note how DS-GNN equivalently updates the representations of root and non-root nodes via the same (local) message-passing layer (triangles, yellow, leftmost picture). By illustrating how ReIGN(2) generalises previous node-based methods, this figure is to be interpreted as visual support for the Proof of Theorem 8 (see Appendix D). Additional details and discussions on Figure 3 are found in Appendix C.

Notably, as methods in Υ have been shown to be strictly stronger than 2-WL [7, 14, 61, 59, 56], Theorem 8 implies the same lower bound for ReIGN(2). Nevertheless, when employing policies in Π and 3-IGN-computable invariant pooling functions ρ (as those used by models in Υ), ReIGN(2)s are upper-bounded by 3-IGNs:

Proposition 9 (3-IGNs implement ReIGN(2))**.** *For any pair of non-isomorphic graphs G_1, G_2 in family $\mathcal{G}$, if there exist policy $\bar{\pi} \in \Pi$, parameters Θ and 3-IGN-computable invariant pooling function ρ such that the ReIGN(2) instance $\mathcal{R}_{\rho,\Theta,\bar{\pi}}$ distinguishes G_1, G_2, then there exist weights Ω for a 3-IGN instance $\mathcal{M}_\Omega$ such that G_1, G_2 are distinguished by $\mathcal{M}_\Omega$ as well.*

This proposition entails an upper-bound on the expressive power of ReIGN(2).

Corollary 10 (3-WL upper-bounds ReIGN(2))**.** *The expressive power of a ReIGN(2) model with policy $\pi \in \Pi$ and 3-IGN-computable invariant pooling function ρ is upper-bounded by 3-WL.*

We note that there may be layers equivariant to S_n over $\mathbb{R}^{n^2}$ not captured by ReIGN(2). Yet, previously proposed Subgraph GNN layers do not exhaust the ReIGN(2) design space, which remains largely unexplored. One, amongst possible novel constructions, is introduced next.

6.2 A unifying architecture: Subgraph Union Networks

We now show how the ReIGN(2) layer space can guide the design of novel, expressive, Subgraph GNNs. Our present endeavour is to conceive a computationally tractable architecture subsuming known node-based models: in virtue of this latter desideratum, we will dub this architecture "Subgraph Union Network" (SUN). To design the base equivariant layer for SUN, we select and combine specific aggregation terms suggested by the ReIGN(2) framework:

$$x_i^{i,(t+1)} = \sigma\Big(\upsilon_{\theta_1}\big(x_i^{i,(t)}, \sum_{j\sim_i i} x_j^{i,(t)}, \sum_j x_j^{i,(t)}, \sum_h x_i^{h,(t)}, \sum_{j\sim i}\sum_h x_j^{h,(t)}\big)\Big) \tag{5}$$

$$x_i^{k,(t+1)} = \sigma\Big(\upsilon_{\theta_2}\big(x_i^{k,(t)}, \sum_{j\sim_k i} x_j^{k,(t)}, x_i^{i,(t)}, x_k^{k,(t)}, \sum_j x_j^{k,(t)}, \sum_h x_i^{h,(t)}, \sum_{j\sim i}\sum_h x_j^{h,(t)}\big)\Big) \tag{6}$$

where υ's sum their inputs after applying a specific linear transformations to each term. One of the novel features of SUN is that roots are transformed by a *different set of parameters* (θ_1) than the other nodes [7] (θ_2, see Figure 2). In practice, the first and last two terms in each one of Equations (5) and (6) can be processed by maximally expressive MPNNs [36, 55], the remaining terms by MLPs. We test these variants in our experiments, with their formulations in Appendix G. SUN remains an instantiation of the ReIGN(2) framework:

Proposition 11 (A ReIGN(2) stacking implements SUN layers)**.** *For any SUN layer L defined according to Equations 5 and 6, there exists a ReIGN(2) layer stacking $\mathcal{S}_L$, such that $\mathcal{S}_L \cong L$.*

[7] As a result, the architecture can mark root nodes, for example.

Table 1: Test mean MAE on the Counting Substructures and ZINC-12k datasets. All Subgraph GNNs employ a GIN base-encoder. †This version of GNN-AK+ does not follow the standard evaluation procedure.

Method	Counting Substructures (MAE ↓)			
	Triangle	Tailed Tri.	Star	4-Cycle
GCN [27]	0.4186	0.3248	0.1798	0.2822
GIN [55]	0.3569	0.2373	0.0224	0.2185
PNA [13]	0.3532	0.2648	0.1278	0.2430
PPGN [32]	0.0089	0.0096	0.0148	**0.0090**
GNN-AK [61]	0.0934	0.0751	0.0168	0.0726
GNN-AK-CTX [61]	0.0885	0.0696	0.0162	0.0668
GNN-AK+ [61]	0.0123	0.0112	0.0150	0.0126
SUN (EGO)	0.0092	0.0105	0.0064	0.0140
SUN (EGO+)	**0.0079**	**0.0080**	**0.0064**	0.0105

Method	ZINC (MAE ↓)
GCN [27]	0.321 ± 0.009
GIN [55]	0.163 ± 0.004
PNA [13]	0.133 ± 0.011
GSN [11]	0.101 ± 0.010
CIN [9]	**0.079** ± 0.006
NGNN [59]	0.111 ± 0.003
DS-GNN (EGO) [7]	0.115 ± 0.004
DS-GNN (EGO+) [7]	0.105 ± 0.003
DSS-GNN (EGO) [7]	0.099 ± 0.003
DSS-GNN (EGO+) [7]	0.097 ± 0.006
GNN-AK [61]	0.105 ± 0.010
GNN-AK-CTX [61]	0.093 ± 0.002
GNN-AK+ [61]†	$0.086 \pm$???
GNN-AK+ [61]	0.091 ± 0.011
SUN (EGO)	0.083 ± 0.003
SUN (EGO+)	0.084 ± 0.002

Finally, we show that a stacking of SUN layers can implement any layer of known node-based Subgraph Networks, making this model a principled generalisation thereof.

Proposition 12 (A SUN stacking implements known Subgraph GNN layers)**.** *Let $\mathcal{N}$ be a model in family Υ employing Morris et al. [36] as a message-passing base-encoder. Then, for any layer L in $\mathcal{N}$, there exists a stacking of SUN layers $\mathcal{S}_L$ such that $\mathcal{S}_L \cong L$.*

Beyond SUN. As it can be seen in Figure 3, SUN does not use all possible operations in the ReIGN(2) framework. Notably, two interesting operations that are not a part of SUN are: (i) The 'transpose': $x_i^k = \upsilon_\theta(x_k^i)$, which shares information between the i-th node in the k-th subgraph and the k-th node in the i-th subgraph; (ii) Local vertical pooling $x_i^k = \upsilon_\theta(\sum_{h \sim i} x_i^h)$. The exploration of these and other operations is left to future work.

7 Experiments

We experimentally validate the effectiveness of one ReIGN(2) instantiation, comparing SUN to previously proposed Subgraph GNNs[8]. We seek to verify whether its theoretical representational power practically enables superior accuracy in expressiveness tasks and real-world benchmarks. Concurrently, we pay attention to the *generalisation ability* of models in comparison. SUN layers are less constrained in their weight sharing pattern, resulting in a more complex model. As this is traditionally associated with inferior generalisation abilities in low data regimes, we deem it important to additionally assess this aspect. Our code is also available.[9]

Synthetic. Counting substructures and regressing graph topological features are notoriously hard tasks for GNNs [12, 17, 13]. We test the representational ability of SUN on common benchmarks of this kind [12, 13]. Table 1 reports results on the substructure counting suite, on which SUN attains state-of-the-art results in 3 out of 4 tasks. Additional results on the regression of global, structural properties are reported in Appendix G.

Real-world. On the molecular ZINC-12k benchmark (constrained solubility regression) [50, 22, 16], SUN exhibits best performance amongst all domain-agnostic GNNs under the 500k parameter budget, including other Subgraph GNNs (see Table 1). A similar trend is observed on the large-scale Molhiv dataset from the OGB [23] (inhibition of HIV replication). Results are in Table 2. Remarkably, on both datasets, SUN either outperforms or approaches HIMP [19], GSN [11] and CIN [9], GNNs which explicitly model rings. We experiment on smaller-scale TUDatasets [37] in Appendix G, where we also compare selection policies.

[8]For GNN-AK variants [61], we run the code provided by the authors, for which the 'context' and 'subgraph' embeddings sum only over ego-network nodes.

[9]https://github.com/beabevi/SUN

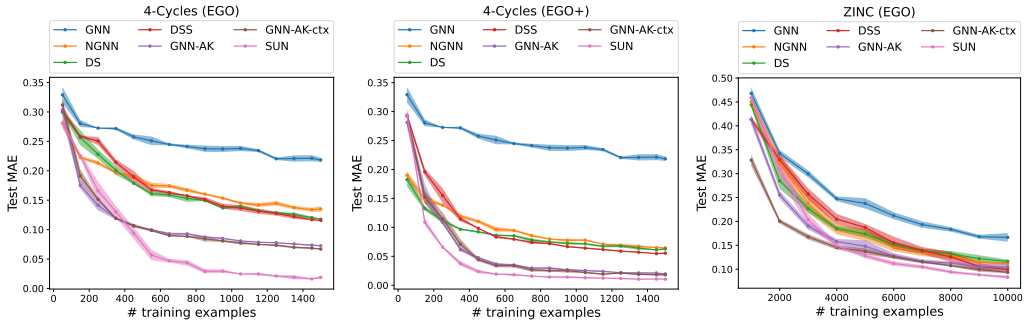

(a) (b) (c)

Figure 4: Generalisation capabilities of Subgraph GNNs in the counting prediction task (Figures 4a and 4b) and in the ZINC-12k dataset (Figure 4c).

Generalisation from limited data. In this set of experiments we compare the test performance of Subgraph GNNs when trained on increasing fractions of the available training data. Each architecture is selected by tuning the hyperparameters with the entire training and validation sets. We run this experiment on the 4-cycle counting task and the real-world ZINC-12k. We illustrate results in Figures 4a to 4c. Except for a short initial phase in the EGO policy, `SUN` generalises better than other Subgraph GNNs on cycle-counting. On ZINC-12k, `SUN` outruns DSS-, DS-GNN and GNN-AK variants from, respectively, $20, 30$ and 40% of the samples. These results demonstrate that `SUN`'s expressiveness is not at the expense of sample efficiency, suggesting that its modelled symmetries guarantee strong representational power while retaining important inductive biases for learning on graphs.

Table 2: Test results for OGB dataset. GIN base-encoder for each Subgraph GNN.

Method	OGBG-MOLHIV **ROC-AUC (%)**
GCN [27]	76.06±0.97
GIN [55]	75.58±1.40
PNA [13]	79.05±1.32
DGN [6]	79.70±0.97
HIMP [19]	78.80±0.82
GSN [11]	80.39±0.90
CIN [9]	**80.94**±0.57
RECONSTR.GNN [14]	76.32±1.40
DS-GNN (EGO+) [7]	77.40±2.19
DSS-GNN (EGO+) [7]	76.78±1.66
GNN-AK+ [61]	79.61±1.19
SUN (EGO+)	80.03±0.55

8 Conclusions

Our work unifies, extends, and analyses the emerging class of Subgraph GNNs. Notably, we demonstrated that the expressive power of these methods is bounded by `3-WL`. Towards a systematic study of models whose expressivity lies between `1-` and `3-WL`, we proposed a new family of layers for the class of Subgraph GNNs and, unlike most previous works on the expressive power of GNNs, we also investigated the generalisation abilities of these models, for which `SUN` shows considerable improvement. Appendix E lists several directions for future work, including an extension of our work to higher-order node-based policies.

Societal impact. We do not envision any negative, immediate societal impact originating from our theoretical results, which represent most of our contribution. Experimentally, our model has shown promising results on molecular property prediction tasks and strong generalisation ability in low-data regimes. This leads us to believe our work may contribute to positively impactful pharmaceutical research, such as drug discovery [20, 3].

Acknowledgments and Disclosure of Funding

The authors are grateful to Joshua Southern, Davide Eynard, Maria Gorinova, Guadalupe Gonzalez, Katarzyna Janocha for valuable feedback on early versions of the manuscript. They would like to thank Bruno Ribeiro and Or Litany for helpful discussions, Giorgos Bouritsas for constructive conversations about the generalisation experiments and, in particular, Marco Ciccone for the precious exchange on sharpness-aware optimisation and Neapolitan pizza. MB is supported in part by ERC Consolidator grant no 724228 (LEMAN). No competing interests are declared.

References

[1] Ralph Abboud, İsmail İlkan Ceylan, Martin Grohe, and Thomas Lukasiewicz. The surprising power of graph neural networks with random node initialization. In *Proceedings of the Thirtieth International Joint Conference on Artificial Intelligence (IJCAI)*, 2020.

[2] Marjan Albooyeh, Daniele Bertolini, and Siamak Ravanbakhsh. Incidence networks for geometric deep learning. *arXiv preprint arXiv:1905.11460*, 2019.

[3] Han Altae-Tran, Bharath Ramsundar, Aneesh S Pappu, and Vijay Pande. Low data drug discovery with one-shot learning. *ACS Central Science*, 3(4):283–293, 2017.

[4] James Atwood and Don Towsley. Diffusion-convolutional neural networks. In *Advances in Neural Information Processing Systems*, volume 29, 2016.

[5] Waïss Azizian and Marc Lelarge. Expressive power of invariant and equivariant graph neural networks. In *International Conference on Learning Representations*, 2021.

[6] Dominique Beaini, Saro Passaro, Vincent Létourneau, William L. Hamilton, Gabriele Corso, and Pietro Liò. Directional graph networks. In *International Conference on Machine Learning*, 2021.

[7] Beatrice Bevilacqua, Fabrizio Frasca, Derek Lim, Balasubramaniam Srinivasan, Chen Cai, Gopinath Balamurugan, Michael M Bronstein, and Haggai Maron. Equivariant subgraph aggregation networks. In *International Conference on Learning Representations*, 2022.

[8] Lukas Biewald. Experiment tracking with weights and biases, 2020. Software available from wandb.com.

[9] Cristian Bodnar, Fabrizio Frasca, Nina Otter, Yuguang Wang, Pietro Liò, Guido F Montúfar, and Michael Bronstein. Weisfeiler and lehman go cellular: Cw networks. In *Advances in Neural Information Processing Systems*, volume 34, 2021.

[10] Cristian Bodnar, Fabrizio Frasca, Yuguang Wang, Nina Otter, Guido F Montúfar, Pietro Liò, and Michael Bronstein. Weisfeiler and lehman go topological: Message passing simplicial networks. In *International Conference on Machine Learning*, 2021.

[11] Giorgos Bouritsas, Fabrizio Frasca, Stefanos P Zafeiriou, and Michael Bronstein. Improving graph neural network expressivity via subgraph isomorphism counting. *IEEE Transactions on Pattern Analysis and Machine Intelligence*, 2022.

[12] Zhengdao Chen, Lei Chen, Soledad Villar, and Joan Bruna. Can graph neural networks count substructures? In *Advances in Neural Information Processing Systems*, volume 33, 2020.

[13] Gabriele Corso, Luca Cavalleri, Dominique Beaini, Pietro Liò, and Petar Veličković. Principal neighbourhood aggregation for graph nets. In *Advances in Neural Information Processing Systems*, volume 33, 2020.

[14] Leonardo Cotta, Christopher Morris, and Bruno Ribeiro. Reconstruction for powerful graph representations. In *Advances in Neural Information Processing Systems*, volume 34, 2021.

[15] Pim de Haan, Taco S Cohen, and Max Welling. Natural graph networks. In *Advances in Neural Information Processing Systems*, volume 33, 2020.

[16] Vijay Prakash Dwivedi, Chaitanya K Joshi, Thomas Laurent, Yoshua Bengio, and Xavier Bresson. Benchmarking graph neural networks. *arXiv preprint arXiv:2003.00982*, 2020.

[17] Vijay Prakash Dwivedi, Anh Tuan Luu, Thomas Laurent, Yoshua Bengio, and Xavier Bresson. Graph neural networks with learnable structural and positional representations. In *International Conference on Learning Representations*, 2022.

[18] Matthias Fey and Jan Eric Lenssen. Fast graph representation learning with pytorch geometric. *arXiv preprint arXiv:1903.02428*, 2019.

[19] Matthias Fey, Jan-Gin Yuen, and Frank Weichert. Hierarchical inter-message passing for learning on molecular graphs. In *ICML Graph Representation Learning and Beyond (GRL+) Workhop*, 2020.

[20] Thomas Gaudelet, Ben Day, Arian R Jamasb, Jyothish Soman, Cristian Regep, Gertrude Liu, Jeremy B R Hayter, Richard Vickers, Charles Roberts, Jian Tang, David Roblin, Tom L Blundell, Michael M Bronstein, and Jake P Taylor-King. Utilizing graph machine learning within drug discovery and development. *Briefings in Bioinformatics*, 05 2021. ISSN 1477-4054.

[21] Floris Geerts. The expressive power of kth-order invariant graph networks. *arXiv preprint arXiv:2007.12035*, 2020.

[22] Rafael Gómez-Bombarelli, Jennifer N. Wei, David Duvenaud, José Miguel Hernández-Lobato, Benjamín Sánchez-Lengeling, Dennis Sheberla, Jorge Aguilera-Iparraguirre, Timothy D. Hirzel, Ryan P. Adams, and Alán Aspuru-Guzik. Automatic chemical design using a data-driven continuous representation of molecules. *ACS Central Science*, 4(2):268–276, Jan 2018. ISSN 2374-7951. doi: 10.1021/acscentsci.7b00572.

[23] Weihua Hu, Matthias Fey, Marinka Zitnik, Yuxiao Dong, Hongyu Ren, Bowen Liu, Michele Catasta, and Jure Leskovec. Open graph benchmark: Datasets for machine learning on graphs. In *Advances in Neural Information Processing Systems*, volume 33, 2020.

[24] Truong Son Hy, Shubhendu Trivedi, Horace Pan, Brandon M Anderson, and Risi Kondor. Covariant compositional networks for learning graphs. *Anchorage '19: 15th International Workshop on Mining and Learning with Graphs*, 2019.

[25] Paul J. Kelly. A congruence theorem for trees. *Pacific Journal of Mathematics*, 7(1):961–968, 1957.

[26] Nicolas Keriven and Gabriel Peyré. Universal invariant and equivariant graph neural networks. In *Advances in Neural Information Processing Systems*, volume 32, 2019.

[27] Thomas N Kipf and Max Welling. Semi-supervised classification with graph convolutional networks. In *International Conference on Learning Representations*, 2017.

[28] Devin Kreuzer, Dominique Beaini, Will Hamilton, Vincent Létourneau, and Prudencio Tossou. Rethinking graph transformers with spectral attention. In *Advances in Neural Information Processing Systems*, volume 34, 2021.

[29] Jungmin Kwon, Jeongseop Kim, Hyunseo Park, and In Kwon Choi. Asam: Adaptive sharpness-aware minimization for scale-invariant learning of deep neural networks. In *International Conference on Machine Learning*, 2021.

[30] Pan Li and Jure Leskovec. The expressive power of graph neural networks. In Lingfei Wu, Peng Cui, Jian Pei, and Liang Zhao, editors, *Graph Neural Networks: Foundations, Frontiers, and Applications*, pages 63–98. Springer Singapore, Singapore, 2022.

[31] Derek Lim, Joshua David Robinson, Lingxiao Zhao, Tess Smidt, Suvrit Sra, Haggai Maron, and Stefanie Jegelka. Sign and basis invariant networks for spectral graph representation learning. In *ICLR 2022 Workshop on Geometrical and Topological Representation Learning*, 2022.

[32] Haggai Maron, Heli Ben-Hamu, Hadar Serviansky, and Yaron Lipman. Provably powerful graph networks. In *Advances in Neural Information Processing Systems*, volume 32, 2019.

[33] Haggai Maron, Heli Ben-Hamu, Nadav Shamir, and Yaron Lipman. Invariant and equivariant graph networks. In *International Conference on Learning Representations*, 2019.

[34] Haggai Maron, Ethan Fetaya, Nimrod Segol, and Yaron Lipman. On the universality of invariant networks. In *International Conference on Machine Learning*, 2019.

[35] Haggai Maron, Or Litany, Gal Chechik, and Ethan Fetaya. On learning sets of symmetric elements. In *International Conference on Machine Learning*, 2020.

[36] Christopher Morris, Martin Ritzert, Matthias Fey, William L Hamilton, Jan Eric Lenssen, Gaurav Rattan, and Martin Grohe. Weisfeiler and leman go neural: Higher-order graph neural networks. In *Proceedings of the AAAI conference on artificial intelligence*, volume 33, 2019.

[37] Christopher Morris, Nils M Kriege, Franka Bause, Kristian Kersting, Petra Mutzel, and Marion Neumann. TUDataset: A collection of benchmark datasets for learning with graphs. In *ICML Graph Representation Learning and Beyond (GRL+) Workhop*, 2020.

[38] Christopher Morris, Gaurav Rattan, and Petra Mutzel. Weisfeiler and leman go sparse: Towards scalable higher-order graph embeddings. In *Advances in Neural Information Processing Systems*, volume 33, 2020.

[39] Christopher Morris, Yaron Lipman, Haggai Maron, Bastian Rieck, Nils M Kriege, Martin Grohe, Matthias Fey, and Karsten Borgwardt. Weisfeiler and leman go machine learning: The story so far. *arXiv preprint arXiv:2112.09992*, 2021.

[40] Christopher Morris, Gaurav Rattan, Sandra Kiefer, and Siamak Ravanbakhsh. Speqnets: Sparsity-aware permutation-equivariant graph networks. In *ICLR 2022 Workshop on Geometrical and Topological Representation Learning*, 2022.

[41] Mathias Niepert, Pasquale Minervini, and Luca Franceschi. Implicit mle: Backpropagating through discrete exponential family distributions. In *Advances in Neural Information Processing Systems*, volume 34, 2021.

[42] Pál András Papp and Roger Wattenhofer. A theoretical comparison of graph neural network extensions. *arXiv preprint arXiv:2201.12884*, 2022.

[43] Pál András Papp, Karolis Martinkus, Lukas Faber, and Roger Wattenhofer. Dropgnn: Random dropouts increase the expressiveness of graph neural networks. In *Advances in Neural Information Processing Systems*, 2021.

[44] Adam Paszke, Sam Gross, Francisco Massa, Adam Lerer, James Bradbury, Gregory Chanan, Trevor Killeen, Zeming Lin, Natalia Gimelshein, Luca Antiga, Alban Desmaison, Andreas Kopf, Edward Yang, Zachary DeVito, Martin Raison, Alykhan Tejani, Sasank Chilamkurthy, Benoit Steiner, Lu Fang, Junjie Bai, and Soumith Chintala. Pytorch: An imperative style, high-performance deep learning library. In *Advances in Neural Information Processing Systems*, volume 32, 2019.

[45] Omri Puny, Heli Ben-Hamu, and Yaron Lipman. Global attention improves graph networks generalization. *arXiv preprint arXiv:2006.07846*, 2020.

[46] Chendi Qian, Gaurav Rattan, Floris Geerts, Christopher Morris, and Mathias Niepert. Ordered subgraph aggregation networks. *arXiv preprint*, 2022.

[47] Siamak Ravanbakhsh. Universal equivariant multilayer perceptrons. In *International Conference on Machine Learning*, 2020.

[48] Yu Rong, Wenbing Huang, Tingyang Xu, and Junzhou Huang. Dropedge: Towards deep graph convolutional networks on node classification. In *International Conference on Learning Representations*, 2019.

[49] Ryoma Sato. A survey on the expressive power of graph neural networks. *arXiv preprint arXiv:2003.04078*, 2020.

[50] Teague Sterling and John J. Irwin. ZINC 15 – ligand discovery for everyone. *Journal of Chemical Information and Modeling*, 55(11):2324–2337, 11 2015. doi: 10.1021/acs.jcim.5b00559.

[51] Erik Thiede, Wenda Zhou, and Risi Kondor. Autobahn: Automorphism-based graph neural nets. In *Advances in Neural Information Processing Systems*, volume 34, 2021.

[52] Stanislaw M. Ulam. *A collection of mathematical problems*, volume 8. Interscience Publishers, 1960.

[53] Clément Vignac, Andreas Loukas, and Pascal Frossard. Building powerful and equivariant graph neural networks with structural message-passing. In *Advances in Neural Information Processing Systems*, volume 33, 2020.

[54] Boris Weisfeiler and Andrei Leman. The reduction of a graph to canonical form and the algebra which appears therein. *NTI, Series*, 2(9):12–16, 1968.

[55] Keyulu Xu, Weihua Hu, Jure Leskovec, and Stefanie Jegelka. How powerful are graph neural networks? In *International Conference on Learning Representations*, 2019.

[56] Jiaxuan You, Jonathan Gomes-Selman, Rex Ying, and Jure Leskovec. Identity-aware graph neural networks. *AAAI Conference on Artificial Intelligence (AAAI)*, 2021.

[57] Chulhee Yun, Suvrit Sra, and Ali Jadbabaie. Small relu networks are powerful memorizers: a tight analysis of memorization capacity. In *Advances in Neural Information Processing Systems*, volume 32, 2019.

[58] Manzil Zaheer, Satwik Kottur, Siamak Ravanbakhsh, Barnabas Poczos, Russ R Salakhutdinov, and Alexander J Smola. Deep sets. In *Advances in Neural Information Processing Systems*, volume 30, 2017.

[59] Muhan Zhang and Pan Li. Nested graph neural networks. In *Advances in Neural Information Processing Systems*, volume 34, 2021.

[60] Muhan Zhang, Zhicheng Cui, Marion Neumann, and Yixin Chen. An end-to-end deep learning architecture for graph classification. *Proceedings of the AAAI Conference on Artificial Intelligence*, 2018.

[61] Lingxiao Zhao, Wei Jin, Leman Akoglu, and Neil Shah. From stars to subgraphs: Uplifting any GNN with local structure awareness. In *International Conference on Learning Representations*, 2022.

Checklist

1. For all authors...
   (a) Do the main claims made in the abstract and introduction accurately reflect the paper's contributions and scope? [Yes]
   (b) Did you describe the limitations of your work? [Yes] We discussed limitations of several previous works, as well as our own model, throughout the paper as our main contribution.
   (c) Did you discuss any potential negative societal impacts of your work? [Yes] See Section 8.
   (d) Have you read the ethics review guidelines and ensured that your paper conforms to them? [Yes]
2. If you are including theoretical results...
   (a) Did you state the full set of assumptions of all theoretical results? [Yes]
   (b) Did you include complete proofs of all theoretical results? [Yes] See Appendices B and D.
3. If you ran experiments...
   (a) Did you include the code, data, and instructions needed to reproduce the main experimental results (either in the supplemental material or as a URL)? [Yes] See Section 7 and Appendix G.
   (b) Did you specify all the training details (e.g., data splits, hyperparameters, how they were chosen)? [Yes] See Appendix G.
   (c) Did you report error bars (e.g., with respect to the random seed after running experiments multiple times)? [Yes] We report the standard deviation computed over multiple seeds for experiments on ZINC12k (Table 1), ogbg-molhiv (Table 2) and on all generalisation experiments (Figures 4a to 4c). We report the standard deviation for the "Counting Substructures" experiments (Table 1) in Appendix G.
   (d) Did you include the total amount of compute and the type of resources used (e.g., type of GPUs, internal cluster, or cloud provider)? [Yes] See Appendix G.
4. If you are using existing assets (e.g., code, data, models) or curating/releasing new assets...
   (a) If your work uses existing assets, did you cite the creators? [Yes]
   (b) Did you mention the license of the assets? [Yes] See Appendix G.
   (c) Did you include any new assets either in the supplemental material or as a URL? [N/A]
   (d) Did you discuss whether and how consent was obtained from people whose data you're using/curating? [N/A]
   (e) Did you discuss whether the data you are using/curating contains personally identifiable information or offensive content? [N/A]
5. If you used crowdsourcing or conducted research with human subjects...
   (a) Did you include the full text of instructions given to participants and screenshots, if applicable? [N/A]
   (b) Did you describe any potential participant risks, with links to Institutional Review Board (IRB) approvals, if applicable? [N/A]
   (c) Did you include the estimated hourly wage paid to participants and the total amount spent on participant compensation? [N/A]

Supplementary Materials for
Understanding and Extending Subgraph GNNs by Rethinking Their Symmetries

A Subgraph GNNs

A.1 Review of Subgraph GNN architectures

Here we review a series of previously proposed Subgraph GNNs, showing how the proposed architectures are captured by the formulation of Equation 1. We report this here for convenience:

$$(A, X) \mapsto \big(\mu \circ \rho \circ \mathcal{S} \circ \pi\big)(A, X).$$

$(n-k)$-Reconstruction GNN by Cotta et al. [14] is the simplest Subgraph GNN: it applies a Siamese MPNN base-encoder γ to k-node-deleted subgraphs of the original graph and then processes the resulting representations with a set network. When $k = 1$, these models are *node-based* Subgraph GNNs. More formally, $\pi = \pi_{\mathrm{ND}}$, a DeepSets network [58] implements $\mu \circ \rho$, and $\mathcal{S}$ is realised with layers of the form:

$$X^{i,(t+1)} = \gamma_t(A^i, X^{i,(t)}) \tag{7}$$

Equivariant Subgraph Aggregation Network (ESAN) by Bevilacqua et al. [7] extends Reconstruction GNNs in two main ways: First, introducing subgraph selection policies that allow for more general sets of subgraphs such as edge-deleted policies. Second, performing an in-depth equivariance analysis which advocates the use of the DSS layer structure introduced by Maron et al. [35]. This choice gives rise to a more expressive architecture that shares information between subgraphs. Formally, in ESAN, $\mathcal{S}$ is defined as a sequence of equivariant layers which process subgraphs as well as the aggregated graph $G_{\mathrm{agg}} = \big(A^{\mathrm{agg}}, X^{\mathrm{agg}}\big) = \sum_{G^i \in B_G} G^i$. Each layer in $\mathcal{S}$ is of the following form:

$$X^{i,(t+1)} = \gamma_t^0(A^i, X^{i,(t)}) + \gamma_t^1(A^{\mathrm{agg}}, X^{\mathrm{agg},(t)}) \tag{8}$$

with γ_t^0, γ_t^1 being two *distinct* MPNN base-encoders. The above architecture is referred to as DSS-GNN. Bevilacqua et al. [7] also explore disabling component γ^1 and term this simplified model DS-GNN (which reduces to a Reconstruction GNN of Cotta et al. [14] under node-deletion policies[10]). In the same work, the considered policies are edge-covering [7, Definition 7], that is, each edge in the original connectivity appears in the connectivity of at least one subgraph. In view of this observation, the authors consider and implement a simplified version of DSS-GNN, whereby γ^1's operate on the original connectivity A, rather than A^{agg}, that is:

$$X^{i,(t+1)} = \gamma_t^0(A^i, X^{i,(t)}) + \gamma_t^1(A, X^{\mathrm{agg},(t)}). \tag{9}$$

Both DS- and DSS-GNN are *node-based* Subgraph GNNs when equipped with policies in Π. Also, these policies are clearly edge-covering and, in this work, we will consider DSS-GNN as defined by Equation 9.

GNN as Kernel (GNN-AK). Zhao et al. [61] employs an ego-network policy ($\pi = \pi_{\mathrm{EGO}}$), while each layer in $\mathcal{S}$ is structured as $A \circ S$, where S is a stacking of layers in the form of Equation 7 and A is an aggregation/pooling block in the form:

$$x_j^{i,(t+1)} = \phi\big(h_j^{j,(t)}, \sum_{\ell} h_\ell^{j,(t)}\big) \tag{10}$$

with ϕ either concatenation or summation, $h_j^{i,(t)} = \big(\gamma_t(A^i, X^{i,(t)})\big)_j^\top$, for MPNN γ_t. The authors introduce an additional variant (GNN-AK-ctx in the following) which also pools information from nodes in other subgraphs:

$$x_j^{i,(t+1)} = \phi\big(h_j^{j,(t)}, \sum_{\ell} h_\ell^{j,(t)}, \sum_{\ell} h_j^{\ell,(t)}\big). \tag{11}$$

In this paper we consider a more general case of global summation in Equations (10)-(11) [11].

[10] For this reason, we will only consider DS-GNN in the following proofs.

[11] The original paper considers summation over each ego network which is specific to a particular policy. Such summations can be dealt with by adding masking node features.

Nested GNN (NGNN). Zhang and Li [59] also uses $\pi = \pi_{\text{EGO}}$ and applies an independent MPNN to each ego-network, effectively structuring $\mathcal{S}$ as a stack of layers in the form of Equation 7. This architecture differs in the way block ρ is realised, namely by pooling the obtained local representations and running an additional MPNN γ_ρ on the original graph:

$$x_j^{(\rho)} = \sum_\ell x_\ell^{j,(T)}, \qquad x_G = \sum_j \left(\gamma_\rho(A, X^{(\rho)})\right)_j \tag{12}$$

ID-GNN. You et al. [56] proposes distinguishing messages propagated by ego-network roots. This architecture uses $\pi = \pi_{\text{EGO}+(T)}$ policy and $\mathcal{S}$ as a T-layer stacking performing independent *heterogeneous* message-passing on each subgraph:

$$x_j^{i,(t+1)} = \upsilon_t\big(x_j^{i,(t)}, \sum_{\ell \sim_i j, \ell \neq i} \mu_{0,t}(x_\ell^{i,(t)}) + \mathbb{1}_{[i \sim_i j]} \cdot \mu_{1,t}(x_i^{i,(t)})\big) \tag{13}$$

where $\mathbb{1}_{[i \sim_i j]}$ if $i \sim_i j$, 0 otherwise, and $\sim_i$ denotes the connectivity induced by A^i. GNN-AK, GNN-AK-ctx, NGNN and ID-GNN are all, intrinsically, *node-based* Subgraph GNNs.

Interestingly, we notice that the contemporary work by Papp and Wattenhofer [42] suggested using a node marking policy as a more powerful alternative to node deletion. Finally, we note that the model by Vignac et al. [53] may potentially be considered as a Subgraph GNN as well.

A.2 The computational complexity of Subgraph GNNs

Other than proposing Subgraph GNN architectures, the works by Bevilacqua et al. [7], Zhang and Li [59], Zhao et al. [61] also study their computational complexity. In particular, Bevilacqua et al. [7] describe both the space and time complexity of a subgraph method equipped with generic subgraph selection policy and an MPNN as a base encoder. Given the inherent locality of traditional message-passing, the authors derive asymptotic bounds accounting for the sparsity of input graphs. Let n, d refer to, respectively, the number of nodes and *maximum node degree* of an input graph generating a subgraph bag of size b. The forward-pass asymptotic time complexity amounts to $\mathcal{O}(b \cdot n \cdot d)$, while the memory complexity to $\mathcal{O}(b \cdot (n + n \cdot d))$. For a node-based selection policy, $b = n$ so these become, respectively, $\mathcal{O}(n^2 \cdot d)$ and $\mathcal{O}(n \cdot (n + nd))$. The authors stress the explicit dependence on d, which is, on the contrary, lacking in `3-IGNs`. As we show in Appendix B, `3-IGNs` subsume node-based subgraph methods, but at the cost of a cubic time and space complexity ($\mathcal{O}(n^3)$) [7]. Amongst others, this is one reason why Subgraph GNNs may be preferable when applied to sparse, real world graphs (where we typically have $d \ll n$).

As we have noted in the above, more sophisticated Subgraph GNNs layers may feature "global" pooling terms other than local message-passing: see, e.g., term X^{agg} for DSS-GNN [7] in Equations (8) and (9) or the "subgraph" and "context" encodings in the GNN-AK-ctx model [61] (second and third term in the summation of Equation (11)). In principle, each of these operations require a squared asymptotic computational complexity ($\mathcal{O}(n^2)$). However, we note that these terms are shared in the update equations of nodes / subgraphs: in practice, it is only sufficient to perform the computation once. In this case, the asymptotic time complexity would amount to $\mathcal{O}(n^2 \cdot d + n^2)$, i.e., still $\mathcal{O}(n^2 \cdot d)$. Therefore, these Subgraph GNNs retain the same asymptotic complexity described above.

Our proposed `SUN` layers involve the same "local" message-passing and "global" pooling operations: the above analysis is directly applicable, yielding the same asymptotic bounds.

We conclude this section by noting that, for some specific selection policies, these bounds can be tightened. In particular, let us consider ego-networks and refer to c as the maximum ego-network size. As observed by Zhang and Li [59], the time complexity of a Subgraph GNN equipped with such policy becomes $\mathcal{O}(n \cdot c \cdot d)$. Importantly, When ego-networks are of limited depth, the size of the subgraphs may be significantly smaller than that of the input graph; in other words $c \ll n$, reducing the overall forward-pass complexity.

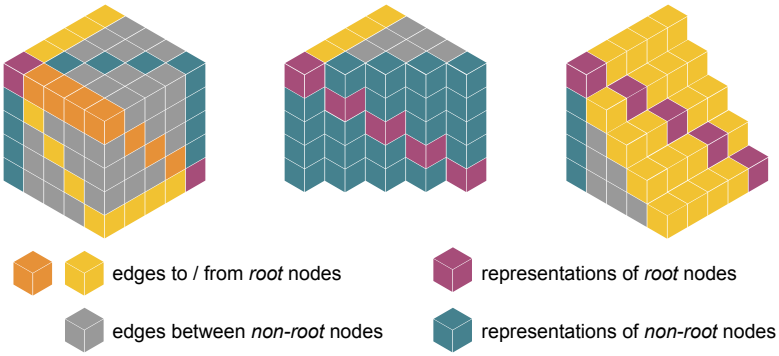

Figure 5: Depiction of cubed tensor $\mathcal{Y}$, its orbit-induced partitioning and the related semantics when $\mathcal{Y}$ is interpreted as a bag of node-based subgraphs, $n = 5$. Elements in the same partition are depicted with the same colour. Left: the whole tensor. Middle and right: sections displaying orbit representations $X_{iii}, X_{ijj}, X_{iij}$ in their entirety.

B Proofs for Section 5 – Subgraph GNNs and 3-IGNs

B.1 3-IGNs as computational models

Before proving the results in Section 5, we first describe here a list of simple operations that are computable by `3-IGNs`. These opearations are to be intended as 'computational primitives' that can then be invoked and reused together in a way to program these models to implement more complex functions. We believe this effort not only serves our need to define those atomic operations required to simulate Subgraph GNNs, but also, it points out to an interpretation of `IGNs` as (abstract) comprehensive computational models beyond deep learning on hypergraphs. We start by describing the objects on which `3-IGNs` operate, and how they can be interpreted as bags of subgraphs.

B.1.1 The 3-IGN computational data structure

The main object on which a `3-IGN` operates is a 'cubed' tensor in $\mathbb{R}^{n^3 \times d}$, typically referred to as $\mathcal{Y}$ in the following. An S_n permutation group act on the first three dimensions of this tensor as:

$$\left(\sigma \cdot \mathcal{Y}\right)_{ijkl} = \mathcal{Y}_{\sigma^{-1}(i)\sigma^{-1}(j)\sigma^{-1}(k)l} \quad \forall \sigma \in S_n$$

whereas the last dimension (l above) hosts d 'channels' not subject to the permutation group.

The action of the permutation group on $[n]^k$ decomposes it into orbits, that is equivalence classes associated with the relation $\sim_S$ defined as:

$$\forall x, y \in [n]^k, x \sim_S y \iff \exists \sigma \in S_n : \sigma(x) = y$$

Orbits induce a partitioning of $[n]^k$. In particular, for $k = 3$ we have:

$$\begin{aligned}
[n]^3 &= \mathbf{o}_{iii} \sqcup \mathbf{o}_{iij} \sqcup \mathbf{o}_{iji} \sqcup \mathbf{o}_{ijj} \sqcup \mathbf{o}_{ijk} \\
\mathbf{o}_{iii} &= \big\{(i,i,i) \,|\, i \in [n]\big\}, \\
\mathbf{o}_{iij} &= \big\{(i,i,j) \,|\, i,j \in [n], i \neq j\big\}, \\
\mathbf{o}_{iji} &= \big\{(i,j,i) \,|\, i,j \in [n], i \neq j\big\}, \\
\mathbf{o}_{ijj} &= \big\{(i,j,j) \,|\, i,j \in [n], i \neq j\big\}, \\
\mathbf{o}_{ijk} &= \big\{(i,j,k) \,|\, i,j \in [n], i \neq j \neq k\big\}
\end{aligned} \tag{14}$$

As studied in Albooyeh et al. [2][12], each of these orbits indexes a specific face-vector, that is a (vectorised) sub-tensor of $\mathcal{Y}$ with a certain number of free index variables, which determines its 'size'.

[12]The authors study the more general case of incidence tensors of any order, for which our three-way cubed tensor is a special case.

Importantly, this entails that the partitioning in Equation 14 induces the same partitioning on $\mathcal{Y}$, so that we can interpret the cubed tensor $\mathcal{Y}$ as a disjoint union of following face-vectors[13]:

$$\begin{aligned} \mathcal{Y} \cong X_{iii} \sqcup X_{iij} \sqcup X_{iji} \sqcup X_{ijj} \sqcup X_{ijk} \qquad (15) \\ X_{iii} = \big(\mathcal{Y}\big)_{\mathbf{o}_{iii}} \qquad \text{(size 1)}, \\ X_{iij} = \big(\mathcal{Y}\big)_{\mathbf{o}_{iij}} \qquad \text{(size 2)}, \\ X_{iji} = \big(\mathcal{Y}\big)_{\mathbf{o}_{iji}} \qquad \text{(size 2)}, \\ X_{ijj} = \big(\mathcal{Y}\big)_{\mathbf{o}_{ijj}} \qquad \text{(size 2)}, \\ X_{ijk} = \big(\mathcal{Y}\big)_{\mathbf{o}_{ijk}} \qquad \text{(size 3)} \end{aligned}$$

or, more compactly, as $\mathcal{Y} \cong \bigsqcup_{\omega} X_{\omega}, \omega \in \Omega = \{iii, iij, iji, ijj, ijk\}$. According to this notation, we consider subscripts in Ω for X as indexing variables for $\mathcal{Y}$. Importantly, since they directly reflect the set of indexes in $\mathbf{o_{iii}}$, $\mathbf{o_{iij}}$, $\mathbf{o_{iji}}$, $\mathbf{o_{ijj}}$, $\mathbf{o_{ijk}}$, when subscripting X, i, j, k are always distinct amongst each other. At the same time, as it can be observed from the definition above, we keep duplicate indexing variables in the subscripts of X's to highlight the characteristic equality pattern of the corresponding orbit. As an example, element $\big(\mathcal{Y}\big)_{1,1,1} \in \mathbb{R}^d$ uniquely belongs to face-vector X_{iii}, elements $\big(\mathcal{Y}\big)_{1,1,2}, \big(\mathcal{Y}\big)_{1,2,1}, \big(\mathcal{Y}\big)_{1,2,2}$ to, respectively, face-vectors $X_{iij}, X_{iji}, X_{ijj}$, $\big(\mathcal{Y}\big)_{1,2,3}$ to X_{ijk}. Since each of these face-vectors is uniquely associated with a particular orbit, we will more intuitively refer to them as 'orbit representations' in the following.

From the considerations above, it is interesting to notice that orbit representations have a precise, characteristic collocation within the cubed tensor $\mathcal{Y}$, directly induced by the equality patterns of the orbits they are indexed by. In particular, X_{iii} corresponds to elements on the main diagonal of the cube, X_{iij}, X_{iji}, X_{ijj} to its three diagonal planes (with main-diagonal excluded), while X_{ijk} corresponds to the the overall adjacency cube (with the main diagonal and the three diagonal planes excluded). The described partitioning is visually depicted in Albooyeh et al. [2, Figure in page 6] and Figure 5 (corresponding to Figure 2 in the main paper).

B.1.2 Bag-of-subgraphs interpretation

An important observation underpinning the majority of our results is that the described cubed tensor $\mathcal{Y}$ can represent bags of node-based subgraphs — this is in contrast with standard interpretations whereby this tensor represents a 3-hypergraph [33, 32]. In particular, as depicted in Figure 1, we arrange subgraphs on the first axis, whereas the second and third axes index nodes.

Accordingly, the adjacency matrix and node representations for subgraph $\bar{i}$ are in sub-tensor $\mathcal{Z}_{\bar{i}} = (\mathcal{Y})_{\bar{i},j,k,l} \in \mathbb{R}^{n^2 \times d}$, with $j, k = 1, \ldots, n, l = 1, \ldots, d$. Here, coherently with [33], we assume node representations are stored in the on-diagonal entries ($j = k$) of $\mathcal{Z}_{\bar{i}}$, while off-diagonal terms ($j \neq k$) host edges, i.e. connectivity information.

We note that this interpretation of $\mathcal{Y}$ assigns meaningful semantics to orbit representations (see Figure 5 for a visual illustration):

- X_{iii} stores representations for root nodes;
- X_{ijj} stores representations for non-root nodes;
- X_{iij} stores connections incoming into root nodes;
- X_{iji} stores connections outgoing from root nodes;
- X_{ijk} stores connections between non-root nodes.

To come back to the examples above, and consistently with the aforementioned semantics, $\big(\mathcal{Y}\big)_{1,1,1}$ represents subgraph 1's root node (that is node 1); $\big(\mathcal{Y}\big)_{1,1,2}, \big(\mathcal{Y}\big)_{1,2,1}$ the connectivity between such root node and node 2 in the same subgraph; $\big(\mathcal{Y}\big)_{1,2,2}$ represents node 2 in subgraph 1; $\big(\mathcal{Y}\big)_{1,2,3}$ the connectivity from node 3 to node 2 in subgraph 1.

[13] The use of symbol '$\cong$', referring to an isomorphism, follows Albooyeh et al. [2].

It is important to note how this interpretation induces a correspondence between the 3-IGN tensor $\mathcal{Y}$ and tensors $\mathcal{A}, \mathcal{X}$ introduced in the main paper, Section 4. $\mathcal{X}$ gathers node features across subgraphs and is therefore in correspondence with $X_{iii} \sqcup X_{ijj}$; $\mathcal{A}$ hosts subgraph connectivity information and is thus in correspondence with $X_{iij} \sqcup X_{iji} \sqcup X_{ijk}$.

As a last note, this interpretation already preludes the more general, less constrained weight sharing pattern advocated by the ReIGN(2) framework, which prescribes, for example, parameters specific to root- and non-root-updates. See Figure 3. This will become more clear in the following (see Equation 18).

B.1.3 Updating orbit representations

A 3-IGN architecture has the following form:

$$(A, X) \mapsto \big(m \circ h \circ \mathcal{I}\big)(A, X)\,, \qquad \mathcal{I} = L^{(T)} \circ \sigma \ldots \circ \sigma \circ L^{(1)} \tag{16}$$

where m is an MLP, h is an invariant linear 'pooling' layer and L's are equivariant linear k-IGN-layers, with $\mathtt{k} \leq 3$. From here onwards we will assume σ's are ReLU non-linearities.

Albooyeh et al. [2] show that, effectively, a linear 3-IGN-layer L updates each orbit representation such that output $X_{\omega'}$ is obtained as the sum of linear equivariant transformations of input orbit representations X_ω[14]:

$$\mathcal{Y}^{(t+1)} = L(\mathcal{Y}^t) \cong \bigsqcup_{\omega' \in \Omega} X_{\omega'}^{(t+1)} \tag{17}$$

$$X_{\omega'}^{(t+1)} = \sum_{\omega \in \Omega} \boldsymbol{W}^{\omega \to \omega'}(X_\omega^{(t)}) \tag{18}$$

where, as the authors show, each $\boldsymbol{W}^{\omega \to \omega'}$ corresponds to a linear combination of all pooling-broadcasting operations defined between input-output orbit representation $X_\omega, X_{\omega'}$:

$$\boldsymbol{W}^{\omega \to \omega'}(X_\omega) = \sum_{\substack{\mathbb{P} \subseteq [m] \\ \mathbb{B} \subseteq \langle 1, \ldots, m' \rangle \\ |\mathbb{B}| = m - |\mathbb{P}|}} W_{\mathbb{B},\mathbb{P}}^{\omega \to \omega'} \mathtt{Broad}_{\mathbb{B},m'}\big(\mathtt{Pool}_{\mathbb{P}}(X_\omega)\big) \tag{19}$$

with m the size of input orbit representation X_ω and m' the size of the output one. Broad and Pool are defined in [2] as follows.

Pooling Let $X_{i_1,\ldots i_m}$ be a generic face-vector of size m indexed by $i_1, \ldots i_m$. Let $\mathbb{P} = \{p_1, \ldots, p_\ell\} \subseteq [m]$. $\mathtt{Pool}_{\mathbb{P}}$ sums over the indexes in $\mathbb{P}$:

$$\mathtt{Pool}_{\mathbb{P}}\big(X_{i_1,\ldots i_m}\big) = \sum_{\substack{i_{p_1} \neq \ldots \neq i_{p_\ell} \\ i_{p_1} \in [n], \ldots, i_{p_\ell} \in [n]}} X_{i_1,\ldots i_m} \tag{20}$$

where the inequality constraints in the summation derive from the fact that $X_{i_1,\ldots i_m}$ represents an orbit of the permutation group. To shorten the notation, we will write pooling operations as:

$$\mathtt{Pool}_{\mathbb{P}}\big(X_{i_1,\ldots i_m}\big) = \boldsymbol{\pi}_{out}\, X_{i_1,\ldots i_m}$$

where $out = \{i_p \,|\, p \in [m] \setminus \mathbb{P}\}$ i.e. the set of indexes which are *not* pooled over, from which it follows that the cardinality of out states the size of the resulting object. For example, $\boldsymbol{\pi}_{i_1}\, X_{i_1,i_2}$ returns a size-1 object from a size-2 face-vector by summing over index variable i_2.

The pooling operation applies in the same way when we repeat index variables in the subscript of the input orbit representation: as more concrete examples, when interpreting $\mathcal{Y}$ as a bag of subgraphs, $\boldsymbol{\pi}_i\, X_{ijj}$ sums the representations of all non-root nodes (subgraph readout) as:

$$\Big(\mathtt{Pool}_j\big(X_{ijj}\big)\Big)_1 = \big(\boldsymbol{\pi}_i\, X_{ijj}\big)_1 = \Big(\sum_{j \in [n], j \neq i} (\mathcal{Y})_{i,j,j}\Big)_1 = \sum_{j \in [n], j \neq 1} (\mathcal{Y})_{1,j,j}$$

Similarly, $\boldsymbol{\pi}_j\, X_{ijj}$ sums non-root node representations across subgraphs (cross-subgraph aggregation). Set out can be empty, in which case pooling amounts to global summation: e.g., $\boldsymbol{\pi}\, X_{iii}$ sums the representations of all root nodes across the bag. Pooling boils down to the identity operation when out replicates the free indexes in X – as no pooling is effectively performed. We will refrain from explicitly writing this operation.

[14] Even if omitted, each face-vector update equation includes a bias term.

Broadcasting Let $X_{i_1,\dots i_m}$ be a generic face-vector of size m indexed by $i_1,\dots i_m$ and $\mathbb{B} = (b_1,\dots,b_m)$ a tuple of m indexes, with $b_j \in [m'], j = 1,\dots m, m' \geq m$. Operation $\texttt{Broad}_{\mathbb{B},m'}$ "broadcasts" X over a target size-m' face-vector in the sense that it identifies X by the target index sequence $\mathbb{B}$ and broadcasts across the remaining $m' - m$ indexes:

$$\Big(\texttt{Broad}_{\mathbb{B},m'}\big(X_{i_1,\dots,i_m}\big)\Big)_{i_1,\dots,i_{m'}} = X_{i_{b_1},\dots,i_{b_m}} \tag{21}$$

For example, if input X_{i_1,i_2} is a size-2 face-vector and output Y_{i_1,i_2,i_3} is a size-3 face-vector, $\texttt{Broad}_{(1,2),3}\big(X_{i_1,i_2}\big)$ maps X onto the first two indexes of Y, and broadcasts along the third. As another example, for output size-2 face-vector Z_{i_1,i_2}, $\texttt{Broad}_{(2,1),2}\big(X_{i_1,i_2}\big)$ effectively implements the 'transpose' operation. Similarly as above, we shorten the notation. Let us define ι such that, $\forall \ell \in [m']$:

$$\iota(\ell) = \begin{cases} j \text{ s.t. } b_j = \ell & \text{if } \ell \in \mathbb{B}, \\ * & \text{otherwise.} \end{cases}$$

where $*$ indicates an index over which broadcasting is performed. We write $\mathbb{C} = (i_{\iota(1)},\dots,i_{\iota(m')})$ and rewrite the broadcast operation as:

$$\texttt{Broad}_{\mathbb{B},m'}\big(X_{i_1,\dots,i_m}\big) = \boldsymbol{\beta}_{\mathbb{C}}\, X_{i_1,\dots,i_m}$$

Accordingly, the examples above are rewritten as $\boldsymbol{\beta}_{i_1,i_2,*}\, X_{i_1,i_2}, \boldsymbol{\beta}_{i_2,i_1}\, X_{i_1,i_2}$:

$$\big(Y_{i_1,i_2,i_3}\big)_{1,2,3} = \big(\texttt{Broad}_{(1,2),3}\big(X_{i_1,i_2}\big)\big)_{1,2,3} = \big(\boldsymbol{\beta}_{i_1,i_2,*}\, X_{i_1,i_2}\big)_{1,2,3} = \big(X_{i_1,i_2}\big)_{1,2}$$
$$\big(Z_{i_1,i_2}\big)_{1,2} = \big(\texttt{Broad}_{(2,1),2}\big(X_{i_1,i_2}\big)\big)_{1,2} = \big(\boldsymbol{\beta}_{i_2,i_1}\, X_{i_1,i_2}\big)_{1,2} = \big(X_{i_1,i_2}\big)_{2,1}$$

In the subscript of $\boldsymbol{\beta}$, we can conveniently retain the equality pattern of the orbit representation where we are broadcasting onto. For a concrete example, $X_{ijj} = \boldsymbol{\beta}_{i,*j,*j}\, X_{iii}$ broadcasts the root node representations over non-root ones, in a way that each non-root node j in subgraph i gets the representation of root node i. It has to be noted that, in these cases, the length of tuple $\mathcal{C}$ may not correspond to the size of the output face-vector, i.e. in those cases where indexes repeat, as above. Finally, let us note that, when both input and target face-vectors have size m and $\mathbb{B} = [m]$, the broadcasting operation boils down to the identity, e.g. $\boldsymbol{\beta}_{ijk}\, X_{ijk}$. We will omit it in writing in these cases.

The above results suggest that a way to describe a `3-IGN` stacking $\mathcal{I} = L^{(T)} \circ \sigma \dots \circ \sigma \circ L^{(1)}$ is to specify how each orbit representation $X_{\omega'}$ is updated from time step (t) to $(t+1)$, according to Equation 18, expanded as per Equation 19. In other words, stacking $\mathcal{I}$ is described by specifying, for each layer $L^{(t)}$, every linear operator $W^{\omega\to\omega'}_{\mathbb{B},\mathbb{P},t}$ in Equation 19. This is the main strategy we adopt in the proofs described in the following.

As a last note, in an effort to ease the notation, we will:

1. Describe updates for $X_{\omega'}$'s (in the form of Equation 18) only when non-trivial;
2. (For each of the above) specify only the non-null linear operators $W^{\omega\to\omega'}_{\mathbb{B},\mathbb{P},t}$ and corresponding terms.

For example, if layer $L^{(t)}$ only applies linear transformation $W^{iii\to iii}_{(1),\varnothing,t} = W$ to orbit representation $X^{(t)}_{iii}$, we will simply write:

$$X^{(t+1)}_{iii} = W \cdot X^{(t)}_{iii}$$

implying that, according to 2., all other terms in Equation 19 are nullified by operator $\mathbf{0}$ and, according to 1., all other orbit updates read as $X^{(t+1)}_{\omega} = I_d \cdot X^{(t)}_{\omega}$.

B.1.4 Pointwise operations

We define as 'pointwise' those operations which only apply to the feature dimension(s) and implement a form of channel mixing. By operating independently on the feature dimension(s), these are trivially equivariant. As these operations can be performed on any orbit representation, we will not specify

them in the following descriptions, and will simply assume to be working with generic tensors X, Y, Z.

Linear transformations are the most natural pointwise operations the `3-IGN` framework supports. Some of these are of particular interest as they will be heavily used in our proofs. We describe them below and define convenient notation for them.

Copy/Routing Pointwise linear operators can copy some specific feature channels in the input tensor and route them into some other output channels. Let X refer to a tensor representing orbit elements with d_{in} channels, and Y to an output tensor with d_{out} channels. We will write:

$$Y = \boldsymbol{\kappa}_{e:f}^{a:b} \, X$$

to refer to the operation which writes channels a to b (included) in X into channels e to f (included) in Y, with $a \leq b \leq d_{in}$, $e \leq f \leq d_{out}$, $b - a = f - e$. Here, $\boldsymbol{\kappa}_{e:f}^{a:b}$ is used to conveniently denote operator W: a matrix $d_{out} \times d_{in}$ where the square submatrix $W_{e:f,a:b} = I_{b-a+1}$ and other entries are 0. When omitting left indices we start from the first channel, i.e., $\boldsymbol{\kappa}_{e:f}^{:b} = \boldsymbol{\kappa}_{e:f}^{1:b}$. When omitting right indices we end at the last channel, i.e., $\boldsymbol{\kappa}_{e:}^{a:b} = \boldsymbol{\kappa}_{e:f}^{a:b}$ for f output channels. We will use notation $\boldsymbol{\kappa}_{c:d/(e)}^{a:b}$ to specify the target has e channels, whenever not clear from the context.

Selective copy/routing With a slight notation overload, we also write $\boldsymbol{\kappa}_{out}^{in}$ — with in, out being index tuples of the same cardinality ℓ — to refer to specific channels in, respectively, input and output tensors. For instance, $\boldsymbol{\kappa}_{d,e,f}^{a,b,c}$ copies (or routes) input channels a, b, c into output channels d, e, f, with such indices being not necessarily contiguous. Again, this operation is linear and is implemented by a matrix W having 1 in all entries in the form $(out_k, in_k), k \in [\ell]$, 0 elsewhere.

Concatenation Two (compatible) operands can be concatenated by means of the copy/routing operation above along with summation. For example, if the two are d dimensional, it is sufficient to route them into the two distinct halves of a $2d$-dimensional output tensor and then sum the two:

$$Z = \boldsymbol{\kappa}_{:d}^{:} \, X + \boldsymbol{\kappa}_{d+1:2d}^{:} \, Y$$

Concurrent linear transformations We note that one single linear operator can apply multiple linear transformations on (a specific subset of) channels of the input tensor. Let W_1, W_2 be two operators of size $d_{out} \times d_{in}$. Obtained as the vertical stacking of W_1, W_2, operator W can be applied to tensor X with d_{in} channels. It produces an output tensor Y with $2 \cdot d_{out}$ channels, where the first d_{out} channels store the result of applying W_1, channels $d_{out} + 1$ to $2 \cdot d_{out}$ store that from the application of W_2. We write:

$$Y = [W_1 \;\; W_2] \, X$$

Pre-multiplying routing operators allows these transformations to be applied to a selection of a subset of input channels. As an example, let X be an input with $2 \cdot d$ channels, and W_1, W_2 be two $d \times d$ linear operators. Expression:

$$Y = [W_1 \cdot \boldsymbol{\kappa}_{:d}^{:d} \;\; W_2 \cdot \boldsymbol{\kappa}_{:d}^{d+1:2d} \,] \, X$$

effectively applies W_1 to the first d channels of X, W_2 to channels $d+1$ to $2d$. In fact, $[W_1 \cdot \boldsymbol{\kappa}_{:d}^{:d} \;\; W_2 \cdot \boldsymbol{\kappa}_{:d}^{d+1:2d} \,]$ consists, as a whole, of a block diagonal matrix made up of operators W_1 (leftmost upper block) and W_2 (rightmost lower block). Clearly, these operations can be extended to more than two concurrent linear operators.

We note that this notation also captures the following 'replication' operation:

$$Y = [I_d \;\; I_d] \, X$$

which outputs two (stacked) copies of d-dimensional input tensor X.

Concurrent transformations and channel-wise summation Let X be an tensor with $2 \cdot d$ channels, and W_1, W_2 two $d \times d$ linear operators. The following expression applies W_1 to the first d channels of X, W_2 to channels $d + 1$ to $2d$ *and* sums the result channel by channel:

$$Y = [W_1 \,||\, W_2] \, X$$

In fact, $[W_1 \,||\, W_2]$ can be interpreted as single linear operator $d \times 2 \cdot d$ obtained by horizontally stacking W_1, W_2. As a particular case, we can simply sum the two halves of X by $[I_d \,||\, I_d] \, X$.

A note on non-linearities A 3-IGN-layer stacking is in the form $\mathcal{I} = L^{(T)} \circ \sigma \ldots \circ \sigma \circ L^{(1)}$, where L's are linear equivariant layers and σ's are ReLU non-linearities. In principle, these non-linearities in between layers may alter the result of linear computation they perform. For example, in order to perform an exact copy of input representation X, it may not be sufficient to simply choose an identity weight matrix I_d: the following ReLU non-linearity would clip negative entries to 0, thus invalidating the correctness of the operation. However, we note that the identity function can be implemented by a ReLU-network, as $y = x = \sigma(x) - \sigma(-x)$. This means that the copy operation can be realised by a 3-IGN-layer stacking as:

$$Y = [I_d \,||\, -I_d] \cdot \Big(\sigma\big([I_d \;\; -I_d]\, X\big)\Big)$$

This effectively provides us with a way to 'choose', in a 3-IGN layer stacking, when to apply σ's and when not to. Indeed, we can always work with $2d$ channels where all entries are non-negative: the positive entries in the first d channels store the originally positive ones, those in the second d channels store the originally negative ones, negated. This expansion can be realised by one layer as $Y = \sigma\big([I_d \;\; -I_d]\, X\big)$ and is such that ReLU activations act neutrally. Any linear transformation W is now applied as $Y = \sigma\big(UX\big)$, with $U = [I_d \;\; -I_d] \cdot W \cdot [I_d \,||\, -I_d]$. Whenever computation requires the application of ReLUs after linear transformation W, it is sufficient to perform the following: $Y = [I_d \;\; -I_d] \cdot \Big(\sigma\big(VX\big)\Big)$, with $V = W \cdot [I_d \,||\, -I_d]$. Operator $[I_d \;\; -I_d]$ will effectively be absorbed by the linear transformation in the following layer. This doubled representation also allows to apply non-linearities to some particular channels only. This can be realised by $Y = \sigma\big(U'X\big)$, with U' constructed as U above, but with the difference being that entries in its $(d+e)$-th row are set to 0, if e is an output channel where the ReLU non-linearity takes effect.

These considerations show that, in fact, interleaving linear (equivariant) layers with ReLU non-linearities does not hinder the possibility of performing (partially) linear computation, which can always be recovered at the cost of having additional channels and/or layers. In view of the above observations, and in an effort to ease the notation, in the proofs reported in the following sections we will thus assume to be allowed to stack linear layers with no ReLU activations in between.

Multi-Layer Perceptron 3-IGNs can naturally implement the application of a Multi-Layer Perceptron (MLP) to the feature dimension(s) of a particular orbit representation, as it stacks linear layers, interspersed with non-linearities. Each of these dense linear layers is trivially equivariant, and so is the overall stacking. We generally write:

$$Y = \boldsymbol{\varphi}^{(\boldsymbol{f})}\, X$$

to indicate the application of an MLP implementing (or approximating) function f. Additionally, we use the notation $\boldsymbol{\varphi}^{(\boldsymbol{f})in}_{out}$ to indicate that $\boldsymbol{\varphi}^{(\boldsymbol{f})}$ acts on the in channels of its input and writes over channels out of the output. This behaviour can be obtained by multiplying the MLP inputs by operator $\boldsymbol{\kappa}^{in}$ and its output by operator $\boldsymbol{\kappa}_{out}$.

MLP-copy We can also combine copy and MLP operations together. In other words, we can apply an MLP on some particular channels while copying some others; we write this operation as

$$Y = [\boldsymbol{\kappa}^{in}_{out} \;\; \boldsymbol{\varphi}^{in'}_{out'}]\, X$$

This operation can be implemented by 'embedding' the weights of the MLP in appropriately sized matrices where remaining entries perform copy/routing operations and are not affected by non-linearities (see discussion above). More in specific, to see how this is implemented, let the MLP $\boldsymbol{\varphi}^{in'}_{out'}$ above have weight matrices $\big(W_1, W_2, \ldots, W_L\big)$ with $W_1 \in \mathbb{R}^{d_1 \times |in'|}$, $W_l \in \mathbb{R}^{d_l \times d_{l-1}}, \forall l = 2 \ldots L-1$, $W_L \in \mathbb{R}^{|out'| \times d_{L-1}}$. Then, Y is obtained by stacking:

$$Y = \big(U_L \circ \sigma \ldots \circ \sigma \circ U_1\big) X$$

where $U_l, l \in [L]$ are linear operators obtained as follows.

$$\begin{aligned} U_1 &= [I_{(1)} \;\; -I^*_{(1)}] \cdot [\boldsymbol{\kappa}^{in}_{:} \;\; W_1 \cdot \boldsymbol{\kappa}^{in'}_{:}] \\ I_{(1)} &= I_{|in|+d_1} \\ I^*_{(1)} &= [[I_{|in|} \,||\, \mathbf{0}_{|in| \times d_1}] \;\; \mathbf{0}_{d_1 \times (|in|+d_1)}] \end{aligned}$$

For any $l = 2 \dots L-1$:

$$
\begin{aligned}
U_l &= [I_{(l)} \;\; -I^*_{(l)}] \cdot V_l \cdot [I_{|in|+d_{l-1}} \,||\, -I_{|in|+d_{l-1}}] \\
V_l &= [[I_{|in|} \,||\, \mathbf{0}_{|in|\times d_{l-1}}] \;\; [\mathbf{0}_{d_l \times |in|} \,||\, W_l]\,] \\
I_{(l)} &= I_{|in|+d_l} \\
I^*_{(l)} &= [[I_{|in|} \,||\, \mathbf{0}_{|in|\times d_l}] \;\; \mathbf{0}_{d_l \times (|in|+d_l)}]
\end{aligned}
$$

Finally:

$$
\begin{aligned}
U_L &= \boldsymbol{\kappa}^{:}_{(out||out')} \cdot [I_{(L)} \;\; -I^*_{(L)}] \cdot V_L \cdot [I_{|in|+d_{L-1}} \,||\, -I_{|in|+d_{L-1}}] \\
V_L &= [[I_{|in|} \,||\, \mathbf{0}_{|in|\times d_{L-1}}] \;\; [\mathbf{0}_{|out'|\times|in|} \,||\, W_L]\,] \\
I_{(L)} &= I_{|in|+|out'|} \\
I^*_{(L)} &= [[I_{|in|} \,||\, \mathbf{0}_{|in|\times|out'|}] \;\; \mathbf{0}_{|out'|\times(|in|+|out'|)}]
\end{aligned}
$$

with $(out||out')$ the concatenation of the two output index tuples out and out'.

Logical AND For inputs in $\{0, 1\}$, it is possible to *exactly* implement the logical AND function $y = f(a, b) = a \wedge b$ as $y = \sigma\big(+2 \cdot a + 2 \cdot b - 3\big)$, with σ being the ReLU non-linearity. As `3-IGN`s can implement pointwise MLPs, this operation can be performed as well when operands are on two distinct channels of the same orbit representation. In particular, for a d-dimensional input X we write:

$$
Y = \boldsymbol{\varphi}_c^{(\wedge)a,b}\, X
$$

to indicate the operation that applies a logical AND between channels a and b of input X and writes the result into channel c in output Y, with $a, b, c \in [d]$. For this operation in particular, we also imply that the rest of X is written in the remaining output channels, that is, we imply we are, in fact, performing $[\boldsymbol{\kappa}^{[d]\setminus\{c\}}_{[d]\setminus\{c\}} \;\; \boldsymbol{\varphi}_c^{(\wedge)a,b}]$.

Clipping An MLP equipped with one hidden layer and ReLU activation can exactly implement the 1-clipping function $f_\downarrow = \min(x, 1)$. In practice, $f_\downarrow$ clips inputs at the value of 1. For a scalar input, this is realised as:

$$
y = -\sigma\big(-x + 1\big) + 1
$$

An MLP $\boldsymbol{\varphi}^{(\downarrow)}$ implementing this function on each channel of a multi-dimensional input X is constructed as:

$$
Y = -I_d\, \sigma\big(-I_d\, X + \mathbf{1}_d\big) + \mathbf{1}_d
$$

where $\mathbf{1}_d$ is the d-dimensional one-vector. The existence of such an MLP entails that `3-IGN`s can exactly implement the clipping function as well, as a pointwise operation.

B.2 Implementing node-based selection policies

We now show how `IGN`s can compute node-based selection policies, proving Lemma 4. We will make use of concepts introduced above; the partitioning into orbits and the computational primitives in particular.

Proof of Lemma 4. We assume to be given an n-node graph G in input, represented by tensor $A \in \mathbb{R}^{n\times n\times d}$. A is subject to S_n symmetry, which partitions it into two distinct orbits: on-diagonal terms A_{ii} and off-diagonal terms $A_{ij}, i \neq j$. A_{ii} store d-dimensional node features; A_{ij} the binary graph connectivity in its first channels, with others being 0-padded.

The first operation, common to the implementation of all the policies, consists of lifting the two-way tensor A to the three-way tensor $\mathcal{Y} \in \mathbb{R}^{n^3\times d}$ interpreted as a bag of subgraphs and partitioned into orbit tensors as described above in Section B.1.1. This step is realised by the following broadcasting

operations[15]:

$$X^{(0)}_{iii} = \boldsymbol{\beta}_{i,i,i}\, A_{ii}$$
$$X^{(0)}_{jii} = \boldsymbol{\beta}_{*,i,i}\, A_{ii}$$
$$X^{(0)}_{iij} = \boldsymbol{\beta}_{i,i,j}\, A_{ij}$$
$$X^{(0)}_{iji} = \boldsymbol{\beta}_{i,j,i}\, A_{ij}$$
$$X^{(0)}_{kij} = \boldsymbol{\beta}_{*,i,j}\, A_{ij}$$

We now focus on each of the considered policies in particular.

[***node-deletion***] Given that X_{iij}, X_{iji} contain all and only those connections involving root nodes, it is sufficient to zero them out to recover a node-deleted bag. We thus perform the following operations:

$$X_{iij} = \mathbf{0} \cdot X^{(0)}_{iij}$$
$$X_{iji} = \mathbf{0} \cdot X^{(0)}_{iji}$$

[***node-marking***] adds a special 'mark' to root nodes only. We implement it by adding one additional dimension to node features and by setting that to 1 only for root nodes via the bias term:

$$X_{iii} = \boldsymbol{\kappa}^{1:d}_{1:d/(d+1)}\, X^{(0)}_{iii} + \mathbb{1}_{d+1}$$
$$X_{ijj} = \boldsymbol{\kappa}^{1:d}_{1:d/(d+1)}\, X^{(0)}_{ijj} + \mathbf{0}_{d+1}$$
$$X_{iij} = \boldsymbol{\kappa}^{1:d}_{1:d/(d+1)}\, X^{(0)}_{iij} + \mathbf{0}_{d+1}$$
$$X_{iji} = \boldsymbol{\kappa}^{1:d}_{1:d/(d+1)}\, X^{(0)}_{iji} + \mathbf{0}_{d+1}$$
$$X_{ijk} = \boldsymbol{\kappa}^{1:d}_{1:d/(d+1)}\, X^{(0)}_{ijk} + \mathbf{0}_{d+1}$$

where $\mathbb{1}_{d+1}$ is a (one-hot) $(d+1)$-dimensional vector being 1 in dimension $d+1$, 0 elsewhere; $\mathbf{0}_{d+1}$ is the $(d+1)$-dimensional zero vector.

[***ego-networks(h)***] So far, we have mostly made use of the orbit-partitioning that is induced by the S_n symmetry group, which has allowed us to implement the *node-deletion* and *node-marking* policies with one single `3-IGN` layer. We now show that, in order to implement the *ego-networks* policy, multiple layers are required, as a `3-IGN` effectively needs to perform Breadth-First-Search for each node in the graph to construct h-hop neighbourhoods. We illustrate the required steps below, which mainly articulate in (i) the construction of h-hop neighbourhoods around nodes; (ii) extraction of egonets from such neighbourhoods. The yet-to-describe `3-IGN` will realise part (i) by storing a 'reachability' patterns in an additional channel in X_{ijj}: element $\left(X^{d+1}_{ijj}\right)_{i=v,j=w}$ will be set to 1 if node w is reachable from node v in h hops, 0 otherwise. In part (ii), these patterns will be utilised, for each subgraph, to nullify the connectivity involving unreachable nodes, thus effectively extracting h-hop egonets. We start by describing the layers implementing part (i).

(*Immediate neighbourhood*) For immediate neighbours, the reachability pattern is already (implicitly) stored in X_{iij}, as it contains the direct connectivity involving root nodes. We therefore copy this information into an additional channel in X_{ijj}. This value will be updated iteratively as we explore higher-order neighborhoods. In the following, we conveniently set $e = d+1$ to ease the notation.

$$X^{(1)}_{ijj} = \boldsymbol{\kappa}^{:d}_{:d/(e)}\, X^{(0)}_{ijj} + \boldsymbol{\kappa}^{:1}_{e:}\, \boldsymbol{\beta}_{i,j,j}\, X^{(0)}_{iij}$$

(*Higher-order neighbourhoods*) We repeat the following steps $(h-1)$ times, and describe the generic l-th step. We first broadcast the current reachability pattern into X_{ijk}, writing it into the second channel (the first contains the original graph connectivity). Essentially, this operation 'propagates' the subgraph-wise reachability pattern copying it row-by-row.

$$X^{(l,1)}_{ijk} = X^{(l-1)}_{ijk} + \boldsymbol{\kappa}^{e:}_{2:2}\, \boldsymbol{\beta}_{i,*,j}\, X^{(l-1)}_{ijj}$$

[15] This layer effectively implements the *null* policy, see Appendix G.

Having placed the pattern as described above, we perform a logical AND between the first two channels of X_{ijk} and write back the result into the second channel.

$$X^{(l,2)}_{ijk} = \boldsymbol{\varphi}^{(\wedge)1:2}_{2:2/_{(e)}}\, X^{(l,1)}_{ijk}$$

For a specific node w in a given subgraph v, this operation spots the neighbours of w that are currently marked in v, effectively propagating the reachability information one hop farther. At this point, pooling over rows counts the number of such neighbours: if at least one is reachable, then node w becomes reachable as well, and its corresponding entry must be set to 1 in the updated reachability pattern. We therefore complete the l-th hop step by updating the pattern accordingly and by clipping it to 1.

$$\begin{aligned} X^{(l,3)}_{ijj} &= X^{(l,2)}_{ijj} + \boldsymbol{\kappa}^{2:2}_{e:}\, \boldsymbol{\beta}_{i,j,j}\, \boldsymbol{\pi}_{i,j}\, X^{(l,2)}_{ijk} \\ X^{(l)}_{ijj} &= [\boldsymbol{\kappa}^{:d}_{:d/_{(e)}} \quad \boldsymbol{\varphi}^{(\downarrow)e:e}_{e:e}\,]\, X^{(l,3)}_{ijj} \end{aligned}$$

(*Egonet extraction*) We complete the implementation of the policy by leveraging the computed reachability pattern to extract the required egonets. We do this by nullifying the connectivity entries in X_{ijk} for those nodes still unreached, i.e. we zero out row- and column-elements for nodes whose entry in the reachability pattern is 0. To perform this operation we appropriately broadcast the pattern and use it as an argument into a logical AND:

$$\begin{aligned} X^{(x,1)}_{ijk} &= X^{(h)}_{ijk} + \boldsymbol{\kappa}^{e:}_{2:2}\, \boldsymbol{\beta}_{i,j,*}\, X^{(h)}_{ijj} \\ X^{(x,2)}_{ijk} &= \boldsymbol{\varphi}^{(\wedge)1:2}_{2:2}\, X^{(x,1)}_{ijk} \\ X^{(x,3)}_{ijk} &= X^{(x,2)}_{ijk} + \boldsymbol{\kappa}^{e:}_{3:3}\, \boldsymbol{\beta}_{i,*,j}\, X^{(x,2)}_{ijj} \\ X^{(x,4)}_{ijk} &= \boldsymbol{\varphi}^{(\wedge)1:3}_{3:3}\, X^{(x,3)}_{ijk} \\ X^{(x)}_{ijk} &= \boldsymbol{\varphi}^{(\wedge)2:3}_{:1}\, X^{(x,4)}_{ijk} \end{aligned}$$

Finally, we save the reachability pattern in channel 2 of X_{iij}; this information effectively conveys, for each subgraph, the membership of each node to that specific subgraph. At the same time, we bring all other orbit tensors to the original dimension d:

$$\begin{aligned} X_{iii} &= \boldsymbol{\kappa}^{:d}_{:d}\, X^{(x)}_{iii} \\ X_{ijj} &= \boldsymbol{\kappa}^{:d}_{:d}\, X^{(x)}_{ijj} \\ X_{iij} &= \boldsymbol{\kappa}^{:1}_{:1/_{(d)}}\, X^{(x)}_{iij} + \boldsymbol{\kappa}^{e:}_{2:2/_{(d)}}\, \boldsymbol{\beta}_{i,i,j}\, X^{(x)}_{ijj} \\ X_{iji} &= \boldsymbol{\kappa}^{:d}_{:d}\, X^{(x)}_{iji} \\ X_{ijk} &= \boldsymbol{\kappa}^{:d}_{:d}\, X^{(x)}_{ijk} \end{aligned}$$

[***Retaining original connectivity***] In all the derivations above we have overwritten the first channel of orbit representations $X_{iij}, X_{iji}, X_{ijk}$ with the computed subgraph connectivity. However, certain Subgraph GNNs may require to retain the original graph connectivity, see, e.g., Equations (9) and (12). In that case it is sufficient to first replicate the first channel of the aforementioned orbit representations into another one before altering it to obtain the subgraph connectivity. □

B.3 Implementing Subgraph GNN layers

Before proceeding to prove Lemma 5, we report the equation of a GNN layer in the form due to Morris et al. [36], which we assume is the base-encoder of the Subgraph GNN layers considered in the following.

$$x^{(t+1)}_i = \sigma\big(W_{1,t} \cdot x^{(t)}_i + W_{2,t} \cdot \sum_{j \sim i} x^{(t)}_j\big) \tag{22}$$

Proof of Lemma 5. We will implement the update equations for a generic bag $B \in \{B^{(t)}_1, B^{(t)}_2\}$ represented by $\mathbb{R}^{n^3 \times d}$ tensor $\mathcal{Y}^{(t)} \cong X^{(t)}_{iii} \sqcup X^{(t)}_{ijj} \sqcup X^{(t)}_{iij} \sqcup X^{(t)}_{iji} \sqcup X^{(t)}_{ijk}$. When necessary, we will

use an additional subscript to indicate which of the two input bags the tensor is representing, as in $X^{(t)}_{(1),ijk}$. In the following we assume B_1 is the bag for graph G_1 of n_1 nodes, B_2 is the bag for graph G_2 of n_2 nodes.

[***DS-GNN***] When equipped with Morris et al. [36] base-encoder, DS-GNN updates the representation of node i in subgraph k as:

$$x_i^{k,(t+1)} = \sigma\big(W_{1,t} \cdot x_i^{k,(t)} + W_{2,t} \cdot \sum_{j \sim_k i} x_j^{k,(t)}\big) \tag{23}$$

([1] *Message broadcasting*) One first `3-IGN` layer propagates the current node representations in a way to prepare them for the following aggregation. Node representations X_{ijj} are written over X_{ijk}, X_{iij}; the ones in X_{iii} over X_{iji}: This will allow matching them with the subgraph connectivity stored in the first channel of such tensors.

$$\begin{aligned}
X^{(t,1)}_{iij} &= \boldsymbol{\kappa}^{:d}_{:d/(2d)}\, X^{(t)}_{iij} + \boldsymbol{\kappa}^{:}_{d+1:2d}\, \boldsymbol{\beta}_{i,i,j}\, X^{(t)}_{ijj} \\
X^{(t,1)}_{iji} &= \boldsymbol{\kappa}^{:d}_{:d/(2d)}\, X^{(t)}_{iji} + \boldsymbol{\kappa}^{:}_{d+1:2d}\, \boldsymbol{\beta}_{i,*,i}\, X^{(t)}_{iii} \\
X^{(t,1)}_{ijk} &= \boldsymbol{\kappa}^{:d}_{:d/(2d)}\, X^{(t)}_{ijk} + \boldsymbol{\kappa}^{:}_{d+1:2d}\, \boldsymbol{\beta}_{i,*,j}\, X^{(t)}_{ijj}
\end{aligned}$$

([2] *Message sparsification & aggregation*) `3-IGN`s only possess *global* pooling as computational primitive, while message-passing requires a form of local aggregation in accordance to the connectivity at hand. For each node, we realise this by first nullifying messages from non-adjacent nodes followed by global summation. We make use of a result by Yun et al. [57] to show that the aforementioned nullification, over the two bags in input, can be exactly implemented by a (small) ReLU network memorising a properly assembled dataset. Let us first report the result of interest [57, Theorem 3.1]:

Theorem 13 (Theorem 3.1 from Yun et al. [57])**.** *Consider any datasaset $\{(x_i, y_i)\}_{i=1}^N$ such that all x_i's are distinct and all $y_i \in [-1,+1]^{d_y}$. If a 3-layer ReLU-like MLP $f_{\boldsymbol{\theta}}$ satisfies $4\lfloor d_1/4 \rfloor \lfloor d_2/(4d_y) \rfloor \geq N$, then there exists a parameter $\boldsymbol{\theta}$ such that $y_i = f_{\boldsymbol{\theta}}(x_i)$ for all $i \in [N]$.*

The theorem guarantees the existence of a properly sized ReLU network able to memorise an input dataset satisfying the reported conditions. We note that one of these conditions can, in a sense, be relaxed:

Proposition 14 (Memorisation)**.** *Consider any dataset $D = \{(x_i, y_i)\}_{i=1}^N$ such that all x_i's $\in \mathbb{R}^{d_x}$ are distinct and all $y_i \in \mathbb{R}^{d_y}$. There exists a 3-layer ReLU-like MLP $\boldsymbol{\varphi}^{(\boldsymbol{D})}$ such that $y_i = \boldsymbol{\varphi}^{(\boldsymbol{D})}(x_i)$ for all $i \in [N]$.*

Proof. Let $M = \max\{\max_{i\in[N]} |y_i|, \mathbf{1}_{d_y}\}$, where $\max$ is intended to be applied element-wise. Let $\tilde{D} = \{(x_i, \tilde{y}_i) \,|\, \tilde{y}_i = y_i \oslash M\}_{i=1}^N$, where $\oslash$ is element-wise division. Dataset $\tilde{D}$ satisfies the assumptions in Theorem 13, as targets $\tilde{y}_i$ are now all necessarily in $[-1,+1]^{d_y}$. Hence, there exists a 3-layer ReLU MLP $f_{\boldsymbol{\theta}}$ memorising $\tilde{D}$. Let (W_l, b_l) refer to its weight matrix and bias vector at the l-th layer, $l = 1, 2, 3$. Let $\bar{W} = \mathrm{diag}(M)$, i.e. a diagonal matrix in $\mathbb{R}^{d_y \times d_y}$ such that $\bar{W}_{ii} = M_i, i \in [d_y]$. To conclude the proof it is sufficient to construct a 3-layer ReLU MLP $\boldsymbol{\varphi}^{(\boldsymbol{D})}$ with parameter stacking $\{(W_l^D, b_l^D)\}_{l=1,2,3}$ such that: $(W_1^D, b_1^D) = (W_1, b_1), (W_2^D, b_2^D) = (W_2, b_2), (W_3^D, b_3^D) = (\bar{W} \cdot W_3, \bar{W} \cdot b_3)$. □

We now continue our proof. Formally, we seek to find two MLPs $\boldsymbol{\varphi}^{(\odot_{iij})}, \boldsymbol{\varphi}^{(\odot_{ijk})}$ implementing, respectively, functions $f^{\odot}_{iij}, f^{\odot}_{ijk}$ satisfying the following. $f^{\odot}_{iij}$ is such that $\forall a, b \in [n], a \neq b$:

$$f^{\odot}_{iij}\big(X^{(t,1)}_{aab}\big) = \begin{cases} \mathbf{0}_d & \text{if } X^{(t,1),1}_{aab} = 0, \\ X^{(t,1),d+1:}_{aab} & \text{otherwise.} \end{cases}$$

Likewise, $f^{\odot}_{ijk}$ is such that: $\forall a, b, c \in [n], a \neq b \neq c$:

$$f^{\odot}_{ijk}\big(X^{(t,1)}_{abc}\big) = \begin{cases} \mathbf{0}_d & \text{if } X^{(t,1),1}_{abc} = 0, \\ X^{(t,1),d+1:}_{abc} & \text{otherwise.} \end{cases}$$

We construct two datasets:

$$D_{iij} = \Big\{ \big(x, f^{\odot}_{iij}(x)\big) \,\big|\, x = X^{(t,1)}_{(1),aab} \;\; \forall a, b \in [n_1], a \neq b \Big\} \cup \\ \cup \Big\{ \big(x, f^{\odot}_{iij}(x)\big) \,\big|\, x = X^{(t,1)}_{(2),aab} \;\; \forall a, b \in [n_2], a \neq b \Big\}$$

$$D_{ijk} = \Big\{ \big(x, f^{\odot}_{ijk}(x)\big) \,\big|\, x = X^{(t,1)}_{(1),abc} \;\; \forall a, b, c \in [n_1], a \neq b \neq c \Big\} \cup \\ \cup \Big\{ \big(x, f^{\odot}_{ijk}(x)\big) \,\big|\, x = X^{(t,1)}_{(2),abc} \;\; \forall a, b, c \in [n_2], a \neq b \neq c \Big\}$$

Here, as all targets are the output of a well-defined function, these datasets satisfy, by construction, the hypothesis of Preposition 14, which we apply on both. This guarantees the existence of $\boldsymbol{\varphi}^{(\odot_{iij})}$, $\boldsymbol{\varphi}^{(\odot_{ijk})}$; their application allows global pooling to effectively recover sparse message aggregation. We also notice that, when updating representations of non-root nodes, roots may be amongst their neighbours, so that it may be needed to additionally sum their representations in X_{iii} to X_{ijj}, conditioned on the subgraph connectivity information stored in X_{iji}. Accordingly, let us define function $f^{\odot}_{iji}$:

$$f^{\odot}_{iji}\big(X^{(t,1)}_{aba}\big) = \begin{cases} \mathbf{0}_d & \text{if } X^{(t,1),1}_{aba} = 0, \\ X^{(t,1),d+1:}_{aba} & \text{otherwise.} \end{cases}$$

We construct dataset:

$$D_{iji} = \Big\{ \big(x, f^{\odot}_{iji}(x)\big) \,\big|\, x = X^{(t,1)}_{(1),aba} \;\; \forall a, b \in [n_1], a \neq b \Big\} \cup \\ \cup \Big\{ \big(x, f^{\odot}_{iji}(x)\big) \,\big|\, x = X^{(t,1)}_{(2),aba} \;\; \forall a, b \in [n_2], a \neq b \Big\}$$

Invoking Proposition 14 on D_{iji} guarantees the existence of $\boldsymbol{\varphi}^{(\odot_{iji})}$ memorising D_{iji}. We let the described `3-IGN` implement such networks:

$$X^{(t,2)}_{iij} = [\boldsymbol{\kappa}^{:d}_{:d} \;\; \boldsymbol{\varphi}^{(\odot_{iij}):}_{d+1:}] \; X^{(t,1)}_{iij} \\ X^{(t,2)}_{iji} = [\boldsymbol{\kappa}^{:d}_{:d} \;\; \boldsymbol{\varphi}^{(\odot_{iji}):}_{d+1:}] \; X^{(t,1)}_{iji} \\ X^{(t,2)}_{ijk} = [\boldsymbol{\kappa}^{:d}_{:d} \;\; \boldsymbol{\varphi}^{(\odot_{ijk}):}_{d+1:}] \; X^{(t,1)}_{ijk}$$

This last layer completes message aggregation:

$$X^{(t,3)}_{iii} = \boldsymbol{\kappa}^{:d}_{:d} \; X^{(t,2)}_{iii} + \boldsymbol{\kappa}^{d+1:}_{d+1:} \; \boldsymbol{\beta}_{iii} \; \boldsymbol{\pi}_i \; X^{(t,2)}_{iij} \tag{24}$$

$$X^{(t,3)}_{ijj} = \boldsymbol{\kappa}^{:d}_{:d} \; X^{(t,2)}_{ijj} + \boldsymbol{\kappa}^{d+1:}_{d+1:} \; \boldsymbol{\beta}_{ijj} \; X^{(t,2)}_{iji} + \boldsymbol{\kappa}^{d+1:}_{d+1:} \; \boldsymbol{\beta}_{ijj} \; \boldsymbol{\pi}_{ij} \; X^{(t,2)}_{ijk} \tag{25}$$

([3] *Update*) We finally describe the statements implementing linear transformations operated by parameters $W_{1,t}, W_{2,t}$, other than bringing the other orbit representations to dimension d:

$$X^{(t+1)}_{iii} = \sigma\big(\, [W_{1,t} \,||\, W_{2,t}] \; X^{(t,3)}_{iii} \, \big) \tag{26}$$

$$X^{(t+1)}_{ijj} = \sigma\big(\, [W_{1,t} \,||\, W_{2,t}] \; X^{(t,3)}_{ijj} \, \big) \tag{27}$$

$$X^{(t+1)}_{iij} = \boldsymbol{\kappa}^{:1}_{:1/(d)} \; X^{(t,3)}_{iij} \\ X^{(t+1)}_{iji} = \boldsymbol{\kappa}^{:1}_{:1/(d)} \; X^{(t,3)}_{iji} \\ X^{(t+1)}_{ijk} = \boldsymbol{\kappa}^{:1}_{:1/(d)} \; X^{(t,3)}_{ijk}$$

[***DSS-GNN***] When equipped with Morris et al. [36] base-encoder, DSS-GNN updates representation of node i in subgraph k as:

$$x^{k,(t+1)}_i = \sigma\big(W^1_{1,t} \cdot x^{k,(t)}_i + W^1_{2,t} \cdot \sum_{j \sim_k i} x^{k,(t)}_j + W^2_{1,t} \cdot \sum_h x^{h,(t)}_i + W^2_{2,t} \cdot \sum_{j \sim i} \sum_h x^{h,(t)}_j \big) \tag{28}$$

([0] *Cross-bag aggregation*) We start by performing those operations above of the form $\sum_h$:

$$X^{(t,0)}_{iii} = [I_d \;\; I_d]\; X^{(t)}_{iii} + \boldsymbol{\kappa}^{:}_{d+1:2d}\, \boldsymbol{\beta}_{j,j,j}\, \boldsymbol{\pi}_j\, X^{(t)}_{ijj}$$
$$X^{(t,0)}_{ijj} = \boldsymbol{\kappa}^{:}_{:d}\, X^{(t)}_{ijj} + \boldsymbol{\kappa}^{:}_{d+1:2d}\, \boldsymbol{\beta}_{*,j,j}\, \boldsymbol{\pi}_j\, X^{(t)}_{ijj} + \boldsymbol{\kappa}^{:}_{d+1:2d}\, \boldsymbol{\beta}_{*,i,i}\, X^{(t)}_{iii}$$

([1] *Message broadcasting*) Similarly as in DS-GNN, we propagate node representations — and their cross-bag aggregated counterparts — on those orbits storing (sub)graph connectivity.

$$X^{(t,1)}_{iij} = \boldsymbol{\kappa}^{:d}_{:d/(3d)}\, X^{(t,0)}_{iij} + \boldsymbol{\kappa}^{:}_{d+1:3d}\, \boldsymbol{\beta}_{i,i,j}\, X^{(t,0)}_{ijj}$$
$$X^{(t,1)}_{iji} = \boldsymbol{\kappa}^{:d}_{:d/(3d)}\, X^{(t,0)}_{iji} + \boldsymbol{\kappa}^{:}_{d+1:3d}\, \boldsymbol{\beta}_{i,*,i}\, X^{(t,0)}_{iii}$$
$$X^{(t,1)}_{ijk} = \boldsymbol{\kappa}^{:d}_{:d/(3d)}\, X^{(t,0)}_{ijk} + \boldsymbol{\kappa}^{:}_{d+1:3d}\, \boldsymbol{\beta}_{i,*,j}\, X^{(t,0)}_{ijj}$$

([2] *Message sparsification & aggregation*) We now follow the same rationale as for DS-GNN, and construct datasets that allow the invocation of Proposition 14. This will guarantee the existence of an MLP that can be applied to retain, for each node, only those messages coming from direct neighbours, according to the subgraph connectivity (stored in channel 1) or the original one (which we assume to be stored in channel 2). Precisely, we would like to memorise the following functions:

$$f^{\odot,\sim_i}_{iij}\big(X^{(t,1)}_{aab}\big) = \begin{cases} \mathbf{0}_d & \text{if } X^{(t,1),1}_{aab} = 0, \\ X^{(t,1),d+1:2d}_{aab} & \text{otherwise.} \end{cases} \quad f^{\odot,\sim_i}_{iji}\big(X^{(t,1)}_{aba}\big) = \begin{cases} \mathbf{0}_d & \text{if } X^{(t,1),1}_{aba} = 0, \\ X^{(t,1),d+1:2d}_{aba} & \text{otherwise.} \end{cases}$$

$$f^{\odot,\sim_i}_{ijk}\big(X^{(t,1)}_{abc}\big) = \begin{cases} \mathbf{0}_d & \text{if } X^{(t,1),1}_{abc} = 0, \\ X^{(t,1),d+1:2d}_{abc} & \text{otherwise.} \end{cases}$$

$$f^{\odot,\sim}_{iij}\big(X^{(t,1)}_{aab}\big) = \begin{cases} \mathbf{0}_d & \text{if } X^{(t,1),2}_{aab} = 0, \\ X^{(t,1),2d+1:}_{aab} & \text{otherwise.} \end{cases} \quad f^{\odot,\sim}_{iji}\big(X^{(t,1)}_{aba}\big) = \begin{cases} \mathbf{0}_d & \text{if } X^{(t,1),2}_{aba} = 0, \\ X^{(t,1),2d+1:}_{aba} & \text{otherwise.} \end{cases}$$

$$f^{\odot,\sim}_{ijk}\big(X^{(t,1)}_{abc}\big) = \begin{cases} \mathbf{0}_d & \text{if } X^{(t,1),2}_{abc} = 0, \\ X^{(t,1),2d+1:}_{abc} & \text{otherwise.} \end{cases}$$

and construct the corresponding datasets:

$$D^{\sim_i}_{iij} = \Big\{ \big(x, f^{\odot,\sim_i}_{iij}(x)\big) \,\big|\, x = X^{(t,1)}_{(1),aab} \;\; \forall a,b \in [n_1], a \neq b \Big\} \cup \Big\{ \big(x, f^{\odot,\sim_i}_{iij}(x)\big) \,\big|\, x = X^{(t,1)}_{(2),aab} \;\; \forall a,b \in [n_2], a \neq b \Big\}$$

$$D^{\sim_i}_{iji} = \Big\{ \big(x, f^{\odot,\sim_i}_{iji}(x)\big) \,\big|\, x = X^{(t,1)}_{(1),aba} \;\; \forall a,b \in [n_1], a \neq b \Big\} \cup \Big\{ \big(x, f^{\odot,\sim_i}_{iij}(x)\big) \,\big|\, x = X^{(t,1)}_{(2),aba} \;\; \forall a,b \in [n_2], a \neq b \Big\}$$

$$D^{\sim_i}_{ijk} = \Big\{ \big(x, f^{\odot,\sim_i}_{ijk}(x)\big) \,\big|\, x = X^{(t,1)}_{(1),abc} \;\; \forall a,b,c \in [n_1], a \neq b \neq c \Big\} \cup \Big\{ \big(x, f^{\odot,\sim_i}_{ijk}(x)\big) \,\big|\, x = X^{(t,1)}_{(2),abc} \;\; \forall a,b,c \in [n_2], a \neq b \neq c \Big\}$$

$$D^{\sim}_{iij} = \Big\{ \big(x, f^{\odot,\sim}_{iij}(x)\big) \,\big|\, x = X^{(t,1)}_{(1),aab} \;\; \forall a,b \in [n_1], a \neq b \Big\} \cup \Big\{ \big(x, f^{\odot,\sim}_{iij}(x)\big) \,\big|\, x = X^{(t,1)}_{(2),aab} \;\; \forall a,b \in [n_2], a \neq b \Big\}$$

$$D^{\sim}_{iji} = \Big\{ \big(x, f^{\odot,\sim}_{iji}(x)\big) \,\big|\, x = X^{(t,1)}_{(1),aba} \;\; \forall a,b \in [n_1], a \neq b \Big\} \cup \Big\{ \big(x, f^{\odot,\sim}_{iij}(x)\big) \,\big|\, x = X^{(t,1)}_{(2),aba} \;\; \forall a,b \in [n_2], a \neq b \Big\}$$

$$D^{\sim}_{ijk} = \Big\{ \big(x, f^{\odot,\sim}_{ijk}(x)\big) \,\big|\, x = X^{(t,1)}_{(1),abc} \;\; \forall a,b,c \in [n_1], a \neq b \neq c \Big\} \cup \Big\{ \big(x, f^{\odot,\sim}_{ijk}(x)\big) \,\big|\, x = X^{(t,1)}_{(2),abc} \;\; \forall a,b,c \in [n_2], a \neq b \neq c \Big\}$$

These, by Proposition 14, are memorised by, respectively, MLPs $\boldsymbol{\varphi}^{(\odot\widetilde{\boldsymbol{iij}}^{\boldsymbol{i}})}$, $\boldsymbol{\varphi}^{(\odot\widetilde{\boldsymbol{iji}}^{\boldsymbol{i}})}$, $\boldsymbol{\varphi}^{(\odot\widetilde{\boldsymbol{ijk}}^{\boldsymbol{i}})}$, $\boldsymbol{\varphi}^{(\odot\widetilde{\boldsymbol{iij}})}$, $\boldsymbol{\varphi}^{(\odot\widetilde{\boldsymbol{iji}})}$, $\boldsymbol{\varphi}^{(\odot\widetilde{\boldsymbol{ijk}})}$. We let our 3-IGN model apply these:

$$
\begin{aligned}
X^{(t,2)}_{iij} &= \big[\boldsymbol{\kappa}^{:d}_{:d}\ \boldsymbol{\varphi}^{(\odot\widetilde{\boldsymbol{iij}}^{\boldsymbol{i}}):}_{d+1:2d}\ \boldsymbol{\varphi}^{(\odot\widetilde{\boldsymbol{iij}}):}_{2d+1:}\big] X^{(t,1)}_{iij} \\
X^{(t,2)}_{iji} &= \big[\boldsymbol{\kappa}^{:d}_{:d}\ \boldsymbol{\varphi}^{(\odot\widetilde{\boldsymbol{iji}}^{\boldsymbol{i}}):}_{d+1:2d}\ \boldsymbol{\varphi}^{(\odot\widetilde{\boldsymbol{iji}}):}_{2d+1:}\big] X^{(t,1)}_{iji} \\
X^{(t,2)}_{ijk} &= \big[\boldsymbol{\kappa}^{:d}_{:d}\ \boldsymbol{\varphi}^{(\odot\widetilde{\boldsymbol{ijk}}^{\boldsymbol{i}}):}_{d+1:2d}\ \boldsymbol{\varphi}^{(\odot\widetilde{\boldsymbol{ijk}}):}_{2d+1:}\big] X^{(t,1)}_{ijk}
\end{aligned}
$$

It is only left to aggregate messages via global pooling:

$$
\begin{aligned}
X^{(t,3)}_{iii} &= \boldsymbol{\kappa}^{:2d}_{:2d/(4d)}\ X^{(t,2)}_{iii} + \boldsymbol{\kappa}^{d+1:}_{2d+1:4d}\ \boldsymbol{\beta}_{iii}\ \boldsymbol{\pi}_i\ X^{(t,2)}_{iij} \\
X^{(t,3)}_{ijj} &= \boldsymbol{\kappa}^{:2d}_{:2d/(4d)}\ X^{(t,2)}_{ijj} + \boldsymbol{\kappa}^{d+1:}_{2d+1:4d}\ \boldsymbol{\beta}_{ijj}\ X^{(t,2)}_{iji} + \boldsymbol{\kappa}^{d+1:}_{2d+1:4d}\ \boldsymbol{\beta}_{ijj}\ \boldsymbol{\pi}_{ij}\ X^{(t,2)}_{ijk}
\end{aligned}
$$

([4] *Update*) We describe the statements implementing the final linear transformations:

$$
\begin{aligned}
X^{(t+1)}_{iii} &= \sigma\Big([W^1_{1,t} \,||\, W^2_{1,t} \,||\, W^1_{2,t} \,||\, W^2_{2,t}]\ X^{(t,3)}_{iii}\Big) \\
X^{(t+1)}_{ijj} &= \sigma\Big([W^1_{1,t} \,||\, W^2_{1,t} \,||\, W^1_{2,t} \,||\, W^2_{2,t}]\ X^{(t,3)}_{ijj}\Big) \\
X^{(t+1)}_{iij} &= \boldsymbol{\kappa}^{:2}_{:2/(d)}\ X^{(t,3)}_{iij} \\
X^{(t+1)}_{iji} &= \boldsymbol{\kappa}^{:2}_{:2/(d)}\ X^{(t,3)}_{iji} \\
X^{(t+1)}_{ijk} &= \boldsymbol{\kappa}^{:2}_{:2/(d)}\ X^{(t,3)}_{ijk}
\end{aligned}
$$

[***GNN-AK-ctx***] When equipped with Morris et al. [36] base-encoder, GNN-AK-ctx updates representation of node i in subgraph k as:

$$
\begin{aligned}
x^{k,(t,0)}_i &= x^{k,(t)}_i \\
x^{k,(t,l+1)}_i &= \sigma\big(W_{1,t,l} \cdot x^{k,(t,l)}_i + W_{2,t,l} \cdot \sum_{j \sim_k i} x^{k,(t,l)}_j\big),\ \ l = 0, \ldots, L-1 \qquad [S] \qquad (29) \\
x^{k,(t+1)}_i &= x^{i,(t,L)}_i + \sum_j x^{j,(t,L)}_i + \sum_j x^{i,(t,L)}_j \qquad [A] \qquad (30)
\end{aligned}
$$

([S]) In order to implement block [S], it is sufficient to repeat steps [1–3] in the DS-GNN derivation L times, i.e. the desired number of message-passing steps. We obtain representations $X^{(t,L)}$.

([A]) Block [A] is implemented as:

$$
\begin{aligned}
X^{(t+1)}_{iii} &= 3 \cdot X^{(t,L)}_{iii} + \boldsymbol{\beta}_{i,i,i}\ \boldsymbol{\pi}_i\ X^{(t,L)}_{ijj} + \boldsymbol{\beta}_{j,j,j}\ \boldsymbol{\pi}_j\ X^{(t,L)}_{ijj} \\
X^{(t+1)}_{ijj} &= 3 \cdot \boldsymbol{\beta}_{*,i,i}\ \cdot X^{(t,L)}_{iii} + \boldsymbol{\beta}_{*,i,i}\ \boldsymbol{\pi}_i\ X^{(t,L)}_{ijj} + \boldsymbol{\beta}_{*,j,j}\ \boldsymbol{\pi}_j\ X^{(t,L)}_{ijj}
\end{aligned}
$$

In the original paper [61], the second and third terms in block [A] only operate on the nodes which are members of the ego-networks at hand:

$$
x^{k,(t+1)}_i = x^{i,(t,L)}_i + \sum_{j \in V^i} x^{j,(t,L)}_i + \sum_{j \in V^i} x^{i,(t,L)}_j \qquad [A]
$$

We show that 3-IGNs can implement this block formulation as well, by resorting to the same sparsification technique employed in the derivation of DS-GNN. Let us recall that, as already mentioned above, the *ego-networks* policy can store reachability patterns in orbit representation X_{iij}: they convey, for each node j, its membership to subgraph i. This information can be used to sparsify node representations being aggregated by the global pooling operations taking place in the equations above. We start by placing node representations X_{ijj} onto X_{iij}, X_{iji}. Let us also replicate reachability patterns into the second channel of X_{iji}.

$$
\begin{aligned}
X^{(t,p)}_{iij} &= \boldsymbol{\kappa}^{:d}_{:d}\ X^{(t,L)}_{iij} + \boldsymbol{\kappa}^{:d}_{d+1:2d}\ \boldsymbol{\beta}_{i,i,j}\ X^{(t,L)}_{ijj} \\
X^{(t,p)}_{iji} &= \boldsymbol{\kappa}^{:d}_{:d}\ X^{(t,L)}_{iji} + \boldsymbol{\kappa}^{2:2}_{2:2}\ \boldsymbol{\beta}_{i,j,i}\ X^{(t,L)}_{iij} + \boldsymbol{\kappa}^{:d}_{d+1:2d}\ \boldsymbol{\beta}_{j,i,j}\ X^{(t,L)}_{ijj}
\end{aligned}
$$

We would like to memorise the following sparsification functions:

$$f_{iij}^{\odot,V^i}\big(X_{aab}^{(t,p)}\big) = \begin{cases} \mathbf{0}_d & \text{if } X_{aab}^{(t,p),2} = 0, \\ X_{aab}^{(t,p),d+1:} & \text{otherwise.} \end{cases} \quad f_{iji}^{\odot,V^i}\big(X_{aba}^{(t,p)}\big) = \begin{cases} \mathbf{0}_d & \text{if } X_{aba}^{(t,p),2} = 0, \\ X_{aba}^{(t,p),d+1:} & \text{otherwise.} \end{cases}$$

so we construct the following datasets:

$$\begin{aligned} D_{iij}^{V^i} &= \Big\{ \big(x, f_{iij}^{\odot,V^i}(x)\big) \,\big|\, x = X_{(1),aab}^{(t,p)} \;\; \forall a,b \in [n_1], a \neq b \Big\} \cup \\ &\qquad \cup \Big\{ \big(x, f_{iij}^{\odot,V^i}(x)\big) \,\big|\, x = X_{(2),aab}^{(t,p)} \;\; \forall a,b \in [n_2], a \neq b \Big\} \\ D_{iji}^{V^i} &= \Big\{ \big(x, f_{iji}^{\odot,V^i}(x)\big) \,\big|\, x = X_{(1),aba}^{(t,p)} \;\; \forall a,b \in [n_1], a \neq b \Big\} \cup \\ &\qquad \cup \Big\{ \big(x, f_{iji}^{\odot,V^i}(x)\big) \,\big|\, x = X_{(2),aba}^{(t,p)} \;\; \forall a,b \in [n_2], a \neq b \Big\} \end{aligned}$$

Again, we invoke Proposition 14, which guarantees the existence of MLPs $\boldsymbol{\varphi}^{(\odot_{iij}^{V^i})}$, $\boldsymbol{\varphi}^{(\odot_{iji}^{V^i})}$. Let the `3-IGN` model implement them:

$$\begin{aligned} X_{iij}^{(t,p+1)} &= [\boldsymbol{\kappa}_{:d}^{:d} \;\; \boldsymbol{\varphi}_{d+1:2d}^{(\odot_{iij}^{V^i}):}] \, X_{iij}^{(t,p)} \\ X_{iji}^{(t,p+1)} &= [\boldsymbol{\kappa}_{:d}^{:d} \;\; \boldsymbol{\varphi}_{d+1:2d}^{(\odot_{iji}^{V^i}):}] \, X_{iji}^{(t,p)} \end{aligned}$$

Then, we perform the last global pooling step to complete the implementation of block $[A]$:

$$X_{iii}^{(t+1)} = 3 \cdot \boldsymbol{\kappa}_{:d}^{:d} \, X_{iii}^{(t,p+1)} + \boldsymbol{\kappa}_{:d}^{d+1:2d} \, \boldsymbol{\beta}_{i,i,i} \, \boldsymbol{\pi}_i \, X_{iij}^{(t,p+1)} + \boldsymbol{\kappa}_{:d}^{d+1:2d} \, \boldsymbol{\beta}_{i,i,i} \, \boldsymbol{\pi}_i \, X_{iji}^{(t,p+1)} \tag{31}$$

$$X_{ijj}^{(t+1)} = 3 \cdot \boldsymbol{\kappa}_{:d}^{:d} \, \boldsymbol{\beta}_{*,i,i} \, X_{iii}^{(t,p+1)} + \boldsymbol{\kappa}_{:d}^{d+1:2d} \, \boldsymbol{\beta}_{*,i,i} \, \boldsymbol{\pi}_i \, X_{iij}^{(t,p+1)} + \boldsymbol{\kappa}_{:d}^{d+1:2d} \, \boldsymbol{\beta}_{*,i,i} \, \boldsymbol{\pi}_i \, X_{iji}^{(t,p+1)} \tag{32}$$

$$\begin{aligned} X_{iij}^{(t+1)} &= \boldsymbol{\kappa}_{1:2/(d)}^{1:2} \, X_{iij}^{(t,p+1)} \\ X_{iji}^{(t+1)} &= \boldsymbol{\kappa}_{1:1/(d)}^{1:1} \, X_{iji}^{(t,p+1)} \\ X_{ijk}^{(t+1)} &= \boldsymbol{\kappa}_{1:1/(d)}^{1:1} \, X_{ijk}^{(t,p+1)} \end{aligned}$$

[***GNN-AK***] In the case of $[A]$ operating only on those nodes in the ego-networks at hand, it is sufficient to rewrite Equations 31, 32 as:

$$\begin{aligned} X_{iii}^{(t+1)} &= 2 \cdot \boldsymbol{\kappa}_{:d}^{:d} \, X_{iii}^{(t,p+1)} + \boldsymbol{\kappa}_{:d}^{d+1:2d} \, \boldsymbol{\beta}_{i,i,i} \, \boldsymbol{\pi}_i \, X_{iij}^{(t,p+1)} \\ X_{ijj}^{(t+1)} &= 2 \cdot \boldsymbol{\kappa}_{:d}^{:d} \, \boldsymbol{\beta}_{*,i,i} \, X_{iii}^{(t,p+1)} + \boldsymbol{\kappa}_{:d}^{d+1:2d} \, \boldsymbol{\beta}_{*,i,i} \, \boldsymbol{\pi}_i \, X_{iij}^{(t,p+1)} \end{aligned}$$

These equations would also implement the more general block $[A]$ in Equation (30).

[***ID-GNN***] With Morris et al. [36] base-encoder, ID-GNN updates node representations as:

$$x_i^{k,(t+1)} = \sigma\big(W_{1,t} x_i^{k,(t)} + W_{2,t} \sum_{j \sim^k i, j \neq k} x_j^{k,(t)} + \mathbb{1}_{[k \sim^k i]} \cdot W_{3,t} x_k^{k,(t)}\big) \tag{33}$$

Message passing is performed according to the same 3-IGN programme as in DS-GNN, with the only modifications required to Equations 24,25,26,27. Equations 24 and 25 are rewritten as:

$$\begin{aligned} X_{iii}^{(t,3)} &= \boldsymbol{\kappa}_{:d}^{:d} \, X_{iii}^{(t,2)} + \boldsymbol{\kappa}_{d+1:}^{:d} \, W_{2,t} \boldsymbol{\kappa}_{:d}^{d+1:} \, \boldsymbol{\beta}_{iii} \, \boldsymbol{\pi}_i \, X_{iij}^{(t,2)} \\ X_{ijj}^{(t,3)} &= \boldsymbol{\kappa}_{:d}^{:d} \, X_{ijj}^{(t,2)} + \boldsymbol{\kappa}_{d+1:}^{:d} \, W_{3,t} \boldsymbol{\kappa}_{:d}^{d+1:} \, \boldsymbol{\beta}_{ijj} \, X_{iji}^{(t,2)} + \boldsymbol{\kappa}_{d+1:}^{:d} \, W_{2,t} \boldsymbol{\kappa}_{:d}^{d+1:} \, \boldsymbol{\beta}_{ijj} \, \boldsymbol{\pi}_{ij} \, X_{ijk}^{(t,2)} \end{aligned}$$

whereas Equations 26, 27 as:

$$\begin{aligned} X_{iii}^{(t+1)} &= \sigma\big(\, [W_{1,t} \,||\, I_d] \, X_{iii}^{(t,3)} \, \big) \\ X_{ijj}^{(t+1)} &= \sigma\big(\, [W_{1,t} \,||\, I_d] \, X_{ijj}^{(t,3)} \, \big) \end{aligned}$$

[***NGNN***] Using a Morris et al. [36] base-encoder, the update equation for the *inner* siamese GNN in a Nested GNN [59] exactly match that of Equation 23. It is therefore sufficient for the `3-IGN` to execute the same programme employed in the DS-GNN derivation. □

B.4 Upperbounding Subgraph GNNs

Proof of Thereom 6. Subgraph GNN $\mathcal{N}_\Theta$ distinguishes G_1, G_2 if they are assigned distinct representations, that is: $y_{G_1} = \mathcal{N}_\Theta\big(A_1, X_1\big) \neq \mathcal{N}_\Theta\big(A_2, X_2\big) = y_{G_2}$. Naturally, a `3-IGN` instance $\mathcal{M}_\Omega$ implementing $\mathcal{N}_\Theta$ on the same pair of graphs would distinguish them as well. We prove the theorem by showing that such an instance exists.

We seek to find a `3-IGN` model $\mathcal{M}_\Omega$ in the form of Equation 16 such that: $\mathcal{M}_\Omega\big(A_1, X_1\big) = \mathcal{N}_\Theta\big(A_1, X_1\big) = y_{G_1}$ and $\mathcal{M}_\Omega\big(A_2, X_2\big) = \mathcal{N}_\Theta\big(A_2, X_2\big) = y_{G_2}$. According to Equation 1, $\mathcal{N}_\Theta\big(\cdot\big) = \big(\mu \circ \rho \circ \mathcal{S} \circ \pi\big)_\Theta(\cdot)$. We will show how to construct $\mathcal{M}_\Omega$ as an appropriate stacking of `3-IGN` layers exactly implementing each of the components $\pi, \mathcal{S}, \rho, \mu$ when applied to graphs G_1, G_2. We assume, w.l.o.g., that stacking $\mathcal{S}$ has the form $\mathcal{S} = L^{(T)} \circ L^{(T-1)} \circ \ldots \circ L^{(1)}$, where L's are $\mathcal{N}$-layers.

By the definition of class Υ, π in $\mathcal{N}_\Theta$ is such that $\pi \in \Pi$, thus, by Lemma 4, there exists a stacking of `3-IGN` layers $\mathcal{M}_\pi$ implementing π. At the same time, for each $\mathcal{N}$-layer $L^{(t)}$, Lemma 5 has its hypotheses satisfied, hence there exists a `3-IGN`-stacking $\mathcal{M}^{(t)}$ implementing $L^{(t)}$ on both G_1, G_2. We can compose such stacks so that, overall, we have: $\big(\mathcal{M}^{(T)} \circ \ldots \circ \mathcal{M}^{(1)} \circ \mathcal{M}_\pi\big) \cong_{\{G_1,G_2\}} \big(\mathcal{S} \circ \pi\big)$, $\cong_{\{G_1,G_2\}}$ denoting *implementation* over set $\{G_1, G_2\} \subset \mathcal{G}$.

We are left with implementing blocks μ, ρ. We show this for every Subgraph GNN in Υ.

[***DS-GNN** & **DSS-GNN***] perform graph readout on each subgraph and then apply a Deep Sets network to these obtained representations:

$$x^{k,(T)} = \sum_i x_i^{k,(T)}$$
$$y_G = \psi\big(\sum_k \phi(x^{k,(T)})\big)$$

The following instruction implements subgraph readout as a `3-` to `1-` equivariant layer:

$$X_i^{\rho,(1)} = \boldsymbol{\pi}_i \; X_{ijj}^{(T)} + X_{iii}^{(T)}$$

Transformation ϕ is implemented by a stacking of `1-IGN` layers:

$$X_i^{\rho,(2)} = \boldsymbol{\varphi}^{(\boldsymbol{\phi})} \; X_i^{\rho,(1)} \tag{34}$$

Finally, we let module h in the `3-IGN` model implement summation $\sum_k$, and choose MLP m in the `3-IGN` such that $m \equiv \psi$:

$$x_G = h\big(X_i^{\rho,(2)}\big) = \sum_i X_i^{\rho,(2)} \tag{35}$$
$$y_G = m\big(x_G\big) = \psi\big(x_G\big)$$

It is possible for the DeepSets network to implement a late invariant-aggregation strategy, so that $\mu \circ \rho$ is realised as:

$$x^{k,(T)} = \sum_i x_i^{k,(T)}$$
$$x^{k,(T+1)} = \sigma\big(W_T^1 x^{k,(T)} + \sum_h W_T^2 x^{h,(T)}\big)$$
$$\ldots$$
$$x^{k,(T+L)} = \sigma\big(W_{T+L-1}^1 x^{k,(T+L-1)} + \sum_h W_{T+L-1}^2 x^{h,(T+L-1)}\big)$$
$$y_G = \psi\big(\sum_k x^{k,(T+L)}\big)$$

In this case, it is sufficient to rewrite Equation 34 as:

$$X_i^{\rho,(1+l)} = \sigma\big(W_l^1 X_i^{\rho,(l)} + W_l^2 \boldsymbol{\beta}_* \; \boldsymbol{\pi} \; X_i^{\rho,(l)}\big)$$

with l ranging from 1 to L, so that then Equation (35) becomes:

$$x_G = h\big(X_i^{\rho,(1+L)}\big) = \sum_i X_i^{\rho,(1+L)}$$

[***GNN-AK***, ***GNN-AK-ctx*** & **ID-GNN**] do not perform subgraph pooling, rather pool the representations of root nodes directly:

$$y_G = \mu\big(\sum_h x_h^{h,(T)}\big)$$

Block h implements pooling on roots:

$$x_G = h(\mathcal{Y}^{(T)}) = \sum_i X_{iii}^{(T)}$$

and it is then sufficient to choose block m such that $m \equiv \mu$.

[***NGNN***], in its most general form, performs L layers of message passing on subgraph pooled representations over the original graph connectivity:

$$\begin{aligned}
x_v^{(T)} &= \sum_{w \in V^v} x_w^{v,(T)} \\
x_v^{(T+1)} &= \sigma\big(W_T^1 x_v^{(T)} + W_T^2 \sum_{w \sim v} x_w^{(T)}\big) \\
&\dots \\
x_v^{(T+L)} &= \sigma\big(W_{T+L-1}^1 x_v^{(T+L-1)} + W_{T+L-1}^2 \sum_{w \sim v} x_w^{(T+L-1)}\big) \\
y_G &= \mu\big(\sum_w x_w^{(T+L)}\big)
\end{aligned}$$

We assume the original graph connectivity has been retained in the third channel of orbit representations $X_{iij}, X_{iji}, X_{ijk}$, while the second channel in X_{iij} hosts reachability patterns (see Section B.2, [**ego-networks(**h**)**] and [***Retaining original connectivity***]). First, we pool representations of nodes in each subgraph, excluding those nodes not belonging to the ego-nets. We need to extend the summation only to those nodes belonging to the ego-networks. This information is stored in the reachability pattern in X_{iij}, and we make use of this information to mask node representations before aggregating them. First, we place node representations in X_{ijj} over X_{iij}:

$$X_{iij}^{\rho,(1)} = \boldsymbol{\kappa}_{:d/(2d)}^{:d} \, X_{iij} + \boldsymbol{\kappa}_{d+1:2d}^{:} \, \boldsymbol{\beta}_{iij} \, X_{ijj}^{(T)}$$

We note that it is needed to memorise the following sparsification function:

$$f_{iij}^{\odot,V^i}\big(X_{aab}^{\rho,(1)}\big) = \begin{cases} \mathbf{0}_d & \text{if } X_{aab}^{\rho,(1),2} = 0, \\ X_{aab}^{\rho,(1),d+1:} & \text{otherwise.} \end{cases}$$

and construct the following dataset:

$$\begin{aligned}
D_{iij}^{V^i} = &\Big\{ \big(x, f_{iij}^{\odot,V^i}(x)\big) \,\big|\, x = X_{(1),aab}^{\rho,(1)} \;\; \forall a, b \in [n_1], a \neq b \Big\} \cup \\
&\cup \Big\{ \big(x, f_{iij}^{\odot,V^i}(x)\big) \,\big|\, x = X_{(2),aab}^{\rho,(1)} \;\; \forall a, b \in [n_2], a \neq b \Big\}
\end{aligned}$$

Proposition 14 can be invoked, guaranteeing the existence of MLP $\boldsymbol{\varphi}^{(\odot_{iij}^{V^i})}$ memorising such dataset. We let the `3-IGN` implement it:

$$X_{iij}^{\rho,(2)} = [\boldsymbol{\kappa}_{:d}^{:d} \;\; \boldsymbol{\varphi}_{d+1:2d}^{(\odot_{iij}^{V^i}):} \,] \, X_{iij}^{\rho,(1)}$$

and complete the subgraph readout via a global pooling operation:

$$X^{\rho,(3)}_{iii} = \boldsymbol{\kappa}^{:d}_{:d}\, X^{\rho,(3)}_{iii} + \boldsymbol{\kappa}^{d+1:}_{:d}\, \boldsymbol{\beta}_{iii}\, \boldsymbol{\pi}_i\, X^{\rho,(2)}_{iij}$$

At this point it is left to perform message passing on these pooled representations for L steps on the original connectivity. We note that it is sufficient to broadcast these onto X_{ijj} and run the same message passing steps in parallel on each subgraph, using the same original graph connectivity:

$$X^{\rho,(4)}_{ijj} = \boldsymbol{\beta}_{*,i,i}\, X^{\rho,(3)}_{iii}$$

Such message-passing steps are implemented with the same programme provided in the Proof of Lemma 5 for DS-GNN, with the only difference being that the sparsification functions are defined based on the third channel of $X_{iij}, X_{iji}, X_{ijk}$:

$$f^{\odot}_{iij}\big(X^{\rho,(4+l)}_{aab}\big) = \begin{cases} \mathbf{0}_d & \text{if } X^{\rho,(4+l),3}_{aab} = 0, \\ X^{\rho,(4+l),d+1:}_{aab} & \text{otherwise.} \end{cases}$$

$$f^{\odot}_{ijk}\big(X^{\rho,(4+l)}_{abc}\big) = \begin{cases} \mathbf{0}_d & \text{if } X^{\rho,(4+l),3}_{abc} = 0, \\ X^{\rho,(4+l),d+1:}_{abc} & \text{otherwise.} \end{cases}$$

$$f^{\odot}_{iji}\big(X^{\rho,(4+l)}_{aba}\big) = \begin{cases} \mathbf{0}_d & \text{if } X^{\rho,(4+l),3}_{aba} = 0, \\ X^{\rho,(4+l),d+1:}_{aba} & \text{otherwise.} \end{cases}$$

Datasets to be memorised are defined accordingly. This construction is repeated L times. Afterwards, blocks h and m in the `3-IGN` model pool the root representations and apply MLP μ on the obtained embedding. These are implemented as shown above for GNN-AK, GNN-AK-ctx, ID-GNN. The proof concludes. □

Proof of Corollary 7. We prove the corollary by contradiction. Suppose there exist non-isomorphic but `3-WL`-equivalent graphs G_1, G_2 distinguished by instance $\mathcal{N}_\Theta$ of $\mathcal{N} \in \Upsilon$. That is, $\mathcal{N}_\Theta\big(G_1\big) \neq \mathcal{N}_\Theta\big(G_2\big)$. In view of Theorem 6, there must exists a `3-IGN` instance $\mathcal{M}_\Omega$ such that $\mathcal{M}_\Omega\big(G_1\big) \neq \mathcal{M}_\Omega\big(G_2\big)$. We note that the expressive power of `k-IGN`s has been fully characterised by Azizian and Lelarge [5], Geerts [21]. In particular, let us report Geerts [21, Theorem 2]:

Theorem 15 (Expressive power of `k-IGN`s, Theorem 2 in Geerts [21])**.** *For any two graphs G_1 and G_2, if `k-WL` does not distinguish G_1, G_2 then any `k-IGN` does not distinguish them either, i.e., it assigns G_1, G_2 the same (tensorial) representations.*

This theorem equivalently asserts that if there exists a `k-IGN` distinguishing G_1, G_2, then these two graphs must be distinguished by the `k-WL` algorithm. Thus, given the existence of `3-IGN` model $\mathcal{M}_\Omega$, the theorem ensures us that `3-WL` distinguishes graphs G_1, G_2, against our hypothesis. □

Let us conclude this section by reporting the following

Remark 16. *Any Subgraph Network $\mathcal{N} \in \Upsilon$ equipped with policy $\pi_{\mathrm{EGO}(h)}$ (or $\pi_{\mathrm{EGO+}(h)}$) is at most as expressive as `3-WL`, for* any *$h > 0$.*

In other words, given the results proved above, deeper ego-networks may increase the expressive power of a model, but not in a way to exceed that of `3-WL`.

C Illustrated comparison of Subgraph GNNs

In this section we explain in detail Figure 6 (corresponding to Figure 3 in the main paper) by linking the coloured updates of each Subgraph GNN to its corresponding formulation in Appendix A. We consider grids of n subgraphs with n nodes. The figure shows the aggregation and update rules in Subgraph GNNs for both diagonal (i, i) and off-diagonal (k, i) entries, which correspond respectively to updates of root and non-root nodes. Each color represents a different parameter. We use squares to indicate global pooling and triangles for local pooling.

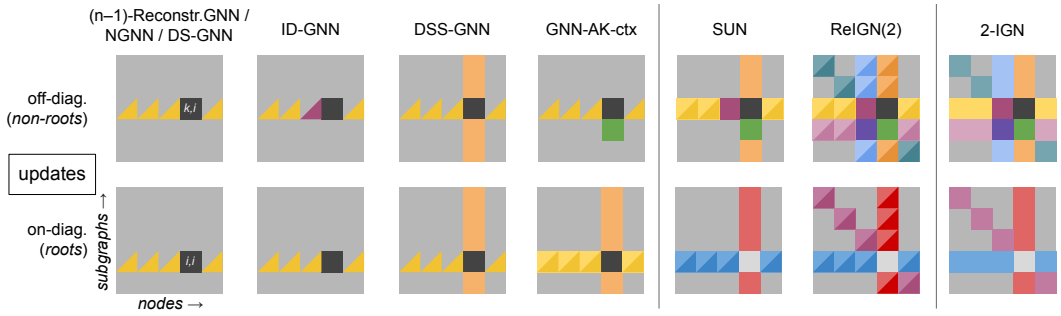

Figure 6: A comparison of aggregation and update rules in Subgraph GNNs, illustrated on an $n \times n$ matrix holding n subgraphs with n node features. Top row shows off-diagonal updates, bottom row shows diagonal (root node) updates. Each colour represents a different parameter. Full squares represent global sum pooling; triangles represent local pooling. Two triangles represent both local and global pooling.

Reconstruction GNN / NGNN / DS-GNN. These methods do not distinguish between root and non-root nodes, effectively sharing the parameters between the two (same yellow colour). The representation of a node in a subgraph is obtained via message passing and aggregation within the subgraph, thus, locally.

ID-GNN. ID-GNN performs message passing on each subgraph but distinguishes messages coming from the root (purple instead of yellow), resulting in an additional parameter for non-root updates.

DSS-GNN. DSS allows information sharing between subgraphs. Indeed, it does not only perform message passing within each subgraph (yellow), but also on the aggregated adjacency matrix. The message passing on the aggregated adjacency matrix uses the original connectivity and it is therefore still local (triangle, yellow). However, it uses node representations obtained by aggregating node representations globally across subgraphs (orange).

GNN-AK-ctx. GNN-AK-ctx distinguishes between root and non-root updates. Non-root node are updated by first copying the diagonal representation of the corresponding node (green) and then performing message passing locally (yellow). Root nodes are updated first by performing a local message passing (yellow), and then by also considering the subgraph readout (yellow squares) and the aggregated representation of the node across subgraphs (orange).

SUN. `SUN` distinguishes root and non-root updates. Each non-root node is updated with: (1) the representation of the node at the previous iteration (black), (2) the representation of the root of the subgraph in which the current node is located (purple), (3) the representation of the node in the subgraph where it is root (green), (4) the readout on the subgraph (yellow squares), (5) message passing on the subgraph (yellow triangles), (6) message passing on the aggregated connectivity (yellow triangles and orange squares). For root nodes many of these terms collapse and the node is updated by only considering (1) (bright green), (4) (blue squares), (5) (blue triangles), (6) (blue triangles and red squares).

2-IGN and ReIGN(2). The node representations are updated according to Equation (4). In the `2-IGN` case, the operations are all global (squares), whilst for `ReIGN(2)` each aggregation can also be performed locally (triangles), as prescribed by the connectivity of the subgraph or by the original connectivity.

D Proofs for Section 6 – Subgraph GNNs and ReIGN(2)

D.1 ReIGN(2) expansion of aggregation terms

We report in Table 3 the expansion rules which allow to derive the `ReIGN(2)` equations from the `2-IGN` ones (Equation 4), which we copy here below for convenience.

$$x_i^{i,(t+1)} = \upsilon_{\theta_1}\left(x_i^{i,(t)}, \square_j x_j^{j,(t)}, \square_{j\neq i} x_j^{i,(t)}, \square_{h\neq i} x_i^{h,(t)}, \square_{h\neq j} x_j^{h,(t)}\right)$$

$$x_i^{k,(t+1)} = \upsilon_{\theta_2}\left(x_i^{k,(t)}, x_k^{i,(t)}, \square_{h\neq j} x_j^{h,(t)}, \square_{h\neq i} x_i^{h,(t)}, \square_{j\neq k} x_j^{k,(t)}, \square_{j\neq i} x_j^{i,(t)}, \square_{h\neq k} x_k^{h,(t)}, x_k^{k,(t)}, x_i^{i,(t)}, \square_j x_j^{j,(t)}\right)$$

In Table 3 we assign each term an identifier (id.) which will allow us to easily refer to specific terms in the proofs we report below. We additionally provide an interpretation for each of the three expanded terms in the last column. Global and local 'vertical' aggregations are dubbed 'needle's in analogy with what the authors in Bevilacqua et al. [7, Definition 5] define as 'needle' colours in their DSS- Weisfeiler-Leman variant.

Table 3: `ReIGN(2)` expansion rules. For each of the `2-IGN` global aggregation terms in Equation 4, `ReIGN(2)` additionally considers two more *local* aggregation terms, which sparsify the aggregation to only include factors adjacent according to the subgraph or original graph connectivities.

target	id.	`2-IGN` term	`ReIGN(2)` expansion	interpretation
x_i^i	#1.on	$\square_j\, x_j^j$	$\big[\sum_{j/j\sim_i i/j\sim i} x_j^j\big]$	root-readout / root-msg for i (on i)
	#2.on	$\square_{j\neq i}\, x_j^i$	$\big[\sum_{j\neq i/j\sim_i i/j\sim i} x_j^i\big]$	i-readout / i-msg for i (on i)
	#3.on	$\square_{h\neq i}\, x_i^h$	$\big[\sum_{h\neq i/h\sim_i i/h\sim i} x_i^h\big]$	i-'needle' / local i-'needle' for i (on i)
	#4.on	$\square_{h\neq j}\, x_j^h$	$\big[\sum_{h/h\sim_i i/h\sim i}\sum_{j/j\sim_h h/j\sim h} x_j^h\big]$	non-root-readout / joint local needle for i (on i) and msg for h (on h)
x_i^k	#1.off	$\square_{h\neq j}\, x_j^h$	$\big[\sum_{h/h\sim_k i/h\sim i}\sum_{j/j\sim_h i/j\sim i} x_j^h\big]$	non-root-readout / joint local needle and msg for i (on k and h)
	#2.off	$\square_{h\neq i}\, x_i^h$	$\big[\sum_{h\neq i/h\sim_k i/h\sim i} x_i^h\big]$	i-'needle' / local i-'needle' for i (on k)
	#3.off	$\square_{j\neq k}\, x_j^k$	$\big[\sum_{j\neq k/j\sim_k i/j\sim i} x_j^k\big]$	k-readout / k-msg for i (on k)
	#4.off	$\square_{h\neq i}\, x_h^i$	$\big[\sum_{h\neq i/h\sim_k i/h\sim i} x_h^i\big]$	i-readout / i-msg for i (on k)
	#5.off	$\square_{h\neq k}\, x_k^h$	$\big[\sum_{h\neq k/h\sim_k i/h\sim i} x_k^h\big]$	k-'needle' / local k-'needle' for i (on k)
	#6.off	$\square_j\, x_j^j$	$\big[\sum_{j/j\sim_k i/j\sim i} x_j^j\big]$	root-readout / root-msg for i (on k)

Interestingly, expansions in Table 3 could be extended to also include global summations extending only over subgraph nodes as already proposed in Zhang and Li [59], Zhao et al. [61]. For example, term [#3.off] could also include summation $\sum_{j\in V^k} x_j^k$, where V^k is the vertex set of subgraph k. As a last note, we remark how all subgraph-local aggregations updating target x_i^k (second expansions) consider the connectivity of subgraph k. We believe it could be possible to extend `ReIGN(2)` to also make use of a different subgraph connectivity, e.g. to define a variant of term [#2.off] which includes expansion $\sum_{h\sim_i i} x_i^h$. We defer these enquiries to future works.

D.2 Proofs for Section 6.1

Proof of Theorem 8. Any Subgraph GNN in class Υ has the following form:

$$\mathcal{N} = \big(\mu \circ \rho \circ \mathcal{S} \circ \pi\big)$$

with μ any MLP, ρ a permutation invariant pooling function, $\pi \in \Pi$ and $\mathcal{S}$ a stacking $\mathcal{S} = L_T \circ \dots L_1$. Any `ReIGN(2)` model has exactly the same form, with the only (important) difference that layers L_t's in the stacking are `ReIGN(2)` layers. Therefore, the theorem is proved by showing that, for any $\mathcal{N} \in \Upsilon$, the $\mathcal{N}$-layer equations can be implemented by an appropriate `ReIGN(2)` layer stacking. This effort consists in describing (a series of) linear functions υ_1, υ_2 as in Equation 4 implementing the layer equation for model $\mathcal{N} \in \Upsilon$. In practice, this will involve specifying which linear transformation W is applied to each of the terms in Equation 4 after expanding each summation according to the rules in Table 3. For convenience, we will directly omit terms assigned a 'nullifying' linear transformation $\mathbf{0}$.

[***DS-GNN***] has its layer equations in the form of Equation 23. These are recovered with one `ReIGN(2)` layer by linearly transforming the second expansion for aggregated terms [#2.on] and [#3.off], and by sharing parameters between off- and on-diagonal updates:

$$x_i^{i,(t+1)} = \sigma\Big(W_{1,t} x_i^{i,(t)} + W_{2,t} \sum_{j\sim_i i} x_j^{i,(t)}\Big)$$
$$x_i^{k,(t+1)} = \sigma\Big(W_{1,t} x_i^{k,(t)} + W_{2,t} \sum_{j\sim_k i} x_j^{k,(t)}\Big)$$

[***DSS-GNN***] has its update rule in the form of Equation 28. It is needed to stack two linear `ReIGN(2)` layers to recover these. The first layer computes message passing on each subgraph as in DS-GNN

and cross-bag aggregation of features. We expand the hidden dimension to $2d$ so that the first half stores the result from the former, the second that of the latter. We 'utilise' terms [#2.on] and [#3.off] in their second expansion for the message-passing operation and terms [#3.on] and [#2.off] in their global version for cross-bag aggregation:

$$x_i^{i,(t,1)} = [W_{1,t}^1 \;\; I_d]\, x_i^{i,(t)} + \boldsymbol{\kappa}_{:d}^{:} W_{2,t}^1 \sum_{j \sim_i i} x_j^{i,(t)} + \boldsymbol{\kappa}_{d+1:2d}^{:} \sum_{h \neq i} x_i^{h,(t)}$$
$$x_i^{k,(t,1)} = \boldsymbol{\kappa}_{:d}^{:} W_{1,t}^1 x_i^{k,(t)} + \boldsymbol{\kappa}_{:d}^{:} W_{2,t}^1 \sum_{j \sim_k i} x_j^{k,(t)} + \boldsymbol{\kappa}_{d+1:2d}^{:} \sum_{h \neq i} x_i^{h,(t)} + \boldsymbol{\kappa}_{d+1:2d}^{:} x_i^{i,(t)}$$

The second layer reduces the dimensionality back to d and completes the implementation by performing message-passing of the cross-bag-aggregated representations over the original graph. This is realised by employing terms [#2.on] and [#3.off] in their third expansion.

$$x_i^{i,(t+1)} = \sigma\Big([I_d \,||\, W_{1,t}^2]\, x_i^{i,(t,1)} + W_{2,t}^2 \boldsymbol{\kappa}_{:d}^{d+1:2d} \sum_{j \sim i} x_j^{i,(t,1)}\Big)$$
$$x_i^{k,(t+1)} = \sigma\Big([I_d \,||\, W_{1,t}^2]\, x_i^{k,(t,1)} + W_{2,t}^2 \boldsymbol{\kappa}_{:d}^{d+1:2d} \sum_{j \sim i} x_j^{k,(t,1)}\Big)$$

[***GNN-AK-ctx & GNN-AK***] Equations 29 and 30 describe the update equations for these models. First, block [S] performs independent message-passing on each subgraph for L steps. The l-th update, $l = 1, \ldots, (L-1)$ is implemented as for DS-GNN, that is by employing terms [#2.on] and [#3.off] as follows:

$$x_i^{i,(t,l+1)} = \sigma\Big(W_{1,t,l} x_i^{i,(t,l)} + W_{2,t,l} \sum_{j \sim_i i} x_j^{i,(t,l)}\Big)$$
$$x_i^{k,(t,l+1)} = \sigma\Big(W_{1,t,l} x_i^{k,(t,l)} + W_{2,t,l} \sum_{j \sim_k i} x_j^{k,(t,l)}\Big)$$

Block [A] in GNN-AK-ctx is implemented by one `ReIGN(2)` layer via aggregated terms [#2.on], [#3.on], [#2.off], [#4.off] all in their global version:

$$x_i^{i,(t+1)} = 3 \cdot I_d\, x_i^{i,(t,L)} + \sum_{h \neq i} x_i^{h,(t,L)} + \sum_{j \neq i} x_j^{i,(t,L)}$$
$$x_i^{k,(t+1)} = 3 \cdot I_d\, x_i^{i,(t,L)} + \sum_{h \neq i} x_i^{h,(t,L)} + \sum_{j \neq i} x_j^{i,(t,L)}$$

In the case of GNN-AK, Block [A] is implemented more simply as

$$x_i^{i,(t+1)} = 2 \cdot I_d\, x_i^{i,(t,L)} + \sum_{j \neq i} x_j^{i,(t,L)}$$
$$x_i^{k,(t+1)} = 2 \cdot I_d\, x_i^{i,(t,L)} + \sum_{j \neq i} x_j^{i,(t,L)}$$

where terms [#3.on], [#2.off] are nullified.

[***ID-GNN***] Implements the update rule in Equation 33, which we report here for convenience:

$$x_i^{k,(t+1)} = \sigma\big(W_{1,t} x_i^{k,(t)} + W_{2,t} \sum_{j \sim_k i, j \neq k} x_j^{k,(t)} + \mathbb{1}_{[k \sim_k i]} \cdot W_{3,t} x_k^{k,(t)}\big)$$

We observe that we can rewrite this equation as follows:

$$x_i^{k,(t+1)} = \sigma\big(W_{1,t} x_i^{k,(t)} + \sum_{j \sim_k i} W_{(\mathbb{1}_{[j=k]}+2),t} x_j^{k,(t)}\big) \tag{36}$$

where $(\mathbb{1}_{[j=k]} + 2) = 3$ if $j = k$, 2 otherwise. That is: (i) we do not explicitly exclude the root node from the set of i's neighbours; (ii) messages are computed via $W_{3,t}$ if from root nodes, via $W_{2,t}$ otherwise. This update equation can be implemented by two `ReIGN(2)` layers. Similarly as in

the DSS-GNN derivation, the first layer expands the hidden dimension to $2d$. The first d channels will store node representations transformed according to $W_{1,t}$, whilst the remaining $d+1$ to $2d$ channels will store node representations transformed according to $W_{3,t}, W_{2,t}$ for, respectively, on- and off-diagonal terms, namely root and non-root nodes:

$$x_i^{i,(t,1)} = [W_{1,t} \;\; W_{3,t}]\, x_i^{i,(t)}$$
$$x_i^{k,(t,1)} = [W_{1,t} \;\; W_{2,t}]\, x_i^{k,(t)}$$

The second `ReIGN(2)` layer effectively completes implementing message-passing and brings back the dimension to d. It combines and aggregates the resulting transformations via terms [#2.on] and [#3.off] in their second expansion as follows:

$$x_i^{i,(t+1)} = \sigma\Big(\boldsymbol{\kappa}_{:d}^{:d}\, x_i^{i,(t,1)} + \boldsymbol{\kappa}_{:d}^{d+1:2d} \sum_{j\sim_i i} x_j^{i,(t,1)}\Big)$$
$$x_i^{k,(t+1)} = \sigma\Big(\boldsymbol{\kappa}_{:d}^{:d}\, x_i^{k,(t,1)} + \boldsymbol{\kappa}_{:d}^{d+1:2d} \sum_{j\sim_k i} x_j^{k,(t,1)}\Big)$$

[***NGNN***] Computes independent subgraph-wise message passing as in DS-GNN: the same `ReIGN(2)` layer implements this one. □

Proof of Proposition 9. `ReIGN(2)` model $\mathcal{R}_{\rho,\Theta,\pi}$ distinguishes G_1, G_2 if they are assigned distinct representations, that is: $y_{G_1} = \mathcal{R}_{\rho,\Theta,\pi}(A_1, X_1) \neq \mathcal{R}_{\rho,\Theta,\pi}(A_2, X_2) = y_{G_2}$. A `3-IGN` instance $\mathcal{M}_\Omega$ implementing $\mathcal{R}_{\rho,\Theta,\pi}$ on the same pair of graphs would distinguish the same graphs as well. We will show the existence of such a model instance.

We seek to find a `3-IGN` model $\mathcal{M}_\Omega$ in the form of Equation 16 such that: $\mathcal{M}_\Omega(A_1, X_1) = \mathcal{R}_{\rho,\Theta,\pi}(A_1, X_1) = y_{G_1}$ and $\mathcal{M}_\Omega(A_2, X_2) = \mathcal{R}_{\rho,\Theta,\pi}(A_2, X_2) = y_{G_2}$, where $\mathcal{R}_{\rho,\Theta,\pi}(\,\cdot\,) = (\mu \circ \rho \circ \mathcal{S} \circ \pi)_\Theta(\cdot)$. From the hypotheses of the theorem, block ρ is `3-IGN`-computable, so there must exist a `3-IGN` layer stacking $\mathcal{M}_\rho$ such that $\mathcal{M}_\rho \cong \rho$. At the same time, $\pi \in \Pi$ so Lemma 4 ensures the existence of a `3-IGN` stacking $\mathcal{M}_\pi$ such that $\mathcal{M}_\pi \cong \pi$. It is left to show the existence of a `3-IGN` stacking $\mathcal{M}_\mathcal{S}$ implementing the `ReIGN(2)` stacking $\mathcal{S}$ on the same pair of graphs. Without loss of generality, it is sufficient to show the existence of a `3-IGN` stacking $\mathcal{M}_L$ implementing one single `ReIGN(2)` intermediate layer L defined as per Equations 4 and the aggregated term expansions in Table 3. We will then show how to construct $\mathcal{M}_L$ for a generic step t in the following. In order to more explicitly reflect the index notation used in Table 3 (i refers to nodes, k to subgraphs) we will refer to the `3-IGN` orbit representations with different subscripts: $\mathcal{Y} \cong X_{iii} \sqcup X_{iij} \sqcup X_{kik} \sqcup X_{kii} \sqcup X_{kij}$, that is we rename X_{iji} as X_{kik}, X_{ijj} as X_{kii}, X_{ijk} as X_{kij}.

We note that the summation of all non-aggregated and globally aggregated terms is recovered by just one `3-IGN` layer, including their linear transformations. In the yet-to-construct stacking, the first layer performs this computation and stores the result into d-auxiliary channels. The layer also replicates the current representations $x^{k,(t),i}, x^{i,(t),i}$ in the first d channels. The implementation of local aggregations, i.e. second and third expansions in Table 3, will require a larger number of layers: this aforementioned input replication allows them to operate on the original representations even after having implemented non-aggregated globally aggregated terms, as required. The result of their computation will then be used to update the intermediate term in channels $d+1$ to $2d$, as we shall see next. Let us start by describing the first `3-IGN` layer, constructed as follows:

$$X_{iii}^{(t,1)} = [I_d \;\; \theta_{1,t}^{(i,i)}]\, X_{iii}^{(t)} + \sum_{o_1 \in O_1} \boldsymbol{\kappa}_{d+1:2d}^{:}\, o_1$$
$$X_{kii}^{(t,1)} = [I_d \;\; \theta_{2,t}^{(k,i)}]\, X_{kii}^{(t)} + \sum_{o_2 \in O_2} \boldsymbol{\kappa}_{d+1:2d}^{:}\, o_2$$

with set O_1 being:

$$O_1 = \Big\{\theta_{1,t}^{(j,j)} \boldsymbol{\beta}_{*i,*i,*i}\, \boldsymbol{\pi}\, X_{iii}^{(t)}, \theta_{1,t}^{(i,j)} \boldsymbol{\beta}_{i,i,i}\, \boldsymbol{\pi}_i\, X_{ijj}^{(t)}, \theta_{1,t}^{(h,i)} \boldsymbol{\beta}_{j,j,j}\, \boldsymbol{\pi}_j\, X_{ijj}^{(t)}, \theta_{1,t}^{(h,j)} \boldsymbol{\beta}_{*i,*i,*i}\, \boldsymbol{\pi}\, X_{ijj}^{(t)}\Big\}$$

and set O_2 being:

$$O_2=\Big\{\theta_{2,t}^{(i,k)}\boldsymbol{\beta}_{i,k,k}\,X_{kii}^{(t)},\theta_{2,t}^{(h,j)}\boldsymbol{\beta}_{*k,*i,*i}\,\boldsymbol{\pi}\,X_{kii}^{(t)},\theta_{2,t}^{(h,i)}\boldsymbol{\beta}_{*,i,i}\,\boldsymbol{\pi}_i\,X_{kii}^{(t)},\theta_{2,t}^{(k,j)}\boldsymbol{\beta}_{k,*i,*i}\,\boldsymbol{\pi}_k\,X_{kii}^{(t)}$$
$$\theta_{2,t}^{(i,j)}\boldsymbol{\beta}_{*,k,k}\,\boldsymbol{\pi}_k\,X_{kii}^{(t)},\theta_{2,t}^{(h,k)}\boldsymbol{\beta}_{i,*k,*k}\,\boldsymbol{\pi}_i\,X_{kii}^{(t)},\theta_{2,t}^{(k,k)}\boldsymbol{\beta}_{i,*k,*k}\,X_{iii}^{(t)},\theta_{2,t}^{(i,i)}\boldsymbol{\beta}_{*,i,i}\,X_{iii}^{(t)},$$
$$\theta_{2,t}^{(j,j)}\boldsymbol{\beta}_{*k,*i,*i}\,\boldsymbol{\pi}\,X_{iii}^{(t)}\Big\}$$

We now focus on the following layers. The l-th local aggregation in Table 3 (second and third expansions) can be obtained by a `3-IGN` layer stacking implementing the steps of: (1) *Message broadcasting*, (2) *Message sparsification*, (3) *Message aggregation*, (4) *Update*, similarly to what already shown for the Proof of Lemma 5. More in detail, the underlying construction will be such such that: first, messages are placed on the third axis of the cubed tensor on which the `3-IGN` operates (broadcasting, 1); they are then sparsified consistently with the (sub)graph connectivity (sparsification, 2); aggregated via pooling operations on the same axis (aggregation, 3); finally, linearly transformed with their specific linear operator and used to update the intermediate representation(s) in channels $d+1$ to $2d$ (update, 4). We note that for each local aggregation term, these steps essentially differ in the way messages are propagated (1) and in the specific linear transformations applied (4), while the same computation is shared for the sparsification (2) and aggregation (3) steps. Thus, we deem it convenient to first describe these steps and then show how specific choices for (1), (4) recover each desired term.

Here, we assume that $\mathcal{M}_\pi$ writes in $X_{kij}, i\neq j$, the connectivity between nodes i,j in subgraph k (first channel) as well as that prescribed by the original graph connectivity (second channel) — once more, see discussion [***Retaining original connectivity***] in the Proof of Lemma 4. In order to implement this step on the input graph pair, it is sufficient to have `3-IGN` layers applying an MLP which sparsifies messages according to the aforementioned connectivities and then to aggregate the sparsified messages by global summation, effectively realising *both* the second and third expansion for terms in Table 3. Step (2) is realised as:

$$X_{iij}^{(t,l,\text{sp.})}=\big[\boldsymbol{\kappa}_{:d}^{:d}\;\boldsymbol{\varphi}_{d+1:2d}^{(\odot_{\boldsymbol{iij}}^{\boldsymbol{\sim i}}):}\;\boldsymbol{\varphi}_{2d+1:}^{(\odot_{\boldsymbol{iij}}^{\boldsymbol{\sim}}):}\big]X_{iij}^{(t,l,\text{broad.})}\tag{37}$$
$$X_{kik}^{(t,l,\text{sp.})}=\big[\boldsymbol{\kappa}_{:d}^{:d}\;\boldsymbol{\varphi}_{d+1:2d}^{(\odot_{\boldsymbol{kik}}^{\boldsymbol{\sim k}}):}\;\boldsymbol{\varphi}_{2d+1:}^{(\odot_{\boldsymbol{kik}}^{\boldsymbol{\sim}}):}\big]X_{kik}^{(t,l,\text{broad.})}\tag{38}$$
$$X_{kij}^{(t,l,\text{sp.})}=\big[\boldsymbol{\kappa}_{:d}^{:d}\;\boldsymbol{\varphi}_{d+1:2d}^{(\odot_{\boldsymbol{kij}}^{\boldsymbol{\sim k}}):}\;\boldsymbol{\varphi}_{2d+1:}^{(\odot_{\boldsymbol{kij}}^{\boldsymbol{\sim}}):}\big]X_{kij}^{(t,l,\text{broad.})}\tag{39}$$

where $X_{iij}^{(t,l,\text{broad.})},X_{kik}^{(t,l,\text{broad.})},X_{kij}^{(t,l,\text{broad.})}$ are computed by the yet-to-describe step (1) and MLPs $\boldsymbol{\varphi}^{(\odot_{\boldsymbol{iij}}^{\boldsymbol{\sim i}})},\boldsymbol{\varphi}^{(\odot_{\boldsymbol{iij}}^{\boldsymbol{\sim}})},\boldsymbol{\varphi}^{(\odot_{\boldsymbol{kik}}^{\boldsymbol{\sim k}})},\boldsymbol{\varphi}^{(\odot_{\boldsymbol{kik}}^{\boldsymbol{\sim}})},\boldsymbol{\varphi}^{(\odot_{\boldsymbol{kij}}^{\boldsymbol{\sim k}})},\boldsymbol{\varphi}^{(\odot_{\boldsymbol{kij}}^{\boldsymbol{\sim}})}$ compute the required sparsifications. We do not describe how to construct such MLPs, but their existence is guaranteed by Proposition 14, which we can invoke by constructing the same datasets as shown in the Proof of Lemma 5 for the DSS-GNN derivation. Step (3) aggregates these sparsified messages; concurrently the same layer linearly transforms the result and adds it to the current, intermediate node representations, performing step (4):

$$X_{iii}^{(t,l+1)}=\boldsymbol{\kappa}_{:2d}^{:2d}\,X_{iii}^{(t,l,\text{sp.})}+\boldsymbol{\kappa}_{d+1:2d}^{:}\,[\mathbf{0}\,||\,\theta_{1,l,t}^{\sim i}\,||\,\theta_{1,l,t}^{\sim}]\,\boldsymbol{\beta}_{iii}\,\boldsymbol{\pi}_i\,X_{iij}^{(t,l,\text{sp.})}$$
$$X_{kii}^{(t,l+1)}=\boldsymbol{\kappa}_{:2d}^{:2d}\,X_{kii}^{(t,l,\text{sp.})}+\boldsymbol{\kappa}_{d+1:2d}^{:}\,[\mathbf{0}\,||\,\theta_{2,l,t}^{\sim k}\,||\,\theta_{2,l,t}^{\sim}]\,\boldsymbol{\beta}_{kii}\,X_{kik}^{(t,l,\text{sp.})}+$$
$$+\boldsymbol{\kappa}_{d+1:2d}^{:}\,[\mathbf{0}\,||\,\theta_{2,l,t}^{\sim k}\,||\,\theta_{2,l,t}^{\sim}]\,\boldsymbol{\beta}_{kii}\,\boldsymbol{\pi}_{ki}\,X_{kij}^{(t,l,\text{sp.})}$$

Here, parameters $\theta_{1,l,t}^{\sim i},\theta_{1,l,t}^{\sim},\theta_{2,l,t}^{\sim k},\theta_{2,l,t}^{\sim}$ will depend on the specific term being implemented.

As for step (1), one `3-IGN` layer suffices to properly broadcast the current input representations $X_{iii}^{(t,l)},X_{kii}^{(t,l)}$ over, respectively, $X_{iji}^{(t,l,\text{broad.})}$ and $X_{kik}^{(t,l,\text{broad.})},X_{kij}^{(t,l,\text{broad.})}$. We will now show the required broadcasting operations in a way that, then, the following layers described above will

effectively implement the second and third expansions of the terms in Table 3:

$$
\begin{aligned}
[\#1.\text{on}] \quad & X^{(t,l,\text{broad.})}_{iij} = \boldsymbol{\kappa}^{:d}_{:d}\, X^{(t,l)}_{iij} + \boldsymbol{\kappa}^{:2d}_{d+1:3d}\, [\boldsymbol{\kappa}^{:d}_{:d} \;\; \boldsymbol{\kappa}^{:d}_{:d}]\, \boldsymbol{\beta}_{*,*,i}\, X^{(t,l)}_{iii} \\
[\#2.\text{on}] \quad & X^{(t,l,\text{broad.})}_{iij} = \boldsymbol{\kappa}^{:d}_{:d}\, X^{(t,l)}_{iij} + \boldsymbol{\kappa}^{:2d}_{d+1:3d}\, [\boldsymbol{\kappa}^{:d}_{:d} \;\; \boldsymbol{\kappa}^{:d}_{:d}]\, \boldsymbol{\beta}_{k,k,i}\, X^{(t,l)}_{kii} \\
[\#3.\text{on}] \quad & X^{(t,l,\text{broad.})}_{iij} = \boldsymbol{\kappa}^{:d}_{:d}\, X^{(t,l)}_{iij} + \boldsymbol{\kappa}^{:2d}_{d+1:3d}\, [\boldsymbol{\kappa}^{:d}_{:d} \;\; \boldsymbol{\kappa}^{:d}_{:d}]\, \boldsymbol{\beta}_{i,i,k}\, X^{(t,l)}_{kii} \\
[\#2.\text{off}] \quad & X^{(t,l,\text{broad.})}_{kik} = \boldsymbol{\kappa}^{:d}_{:d}\, X^{(t,l)}_{kik} + \boldsymbol{\kappa}^{:2d}_{d+1:3d}\, [\boldsymbol{\kappa}^{:d}_{:d} \;\; \boldsymbol{\kappa}^{:d}_{:d}]\, \boldsymbol{\beta}_{*,i,*}\, X^{(t,l)}_{iii} \\
& X^{(t,l,\text{broad.})}_{kij} = \boldsymbol{\kappa}^{:d}_{:d}\, X^{(t,l)}_{kij} + \boldsymbol{\kappa}^{:2d}_{d+1:3d}\, [\boldsymbol{\kappa}^{:d}_{:d} \;\; \boldsymbol{\kappa}^{:d}_{:d}]\, \boldsymbol{\beta}_{*,i,k}\, X^{(t,l)}_{kii} \\
[\#3.\text{off}] \quad & X^{(t,l,\text{broad.})}_{kik} = \boldsymbol{\kappa}^{:d}_{:d}\, X^{(t,l)}_{kik} + \boldsymbol{\kappa}^{:2d}_{d+1:3d}\, [\boldsymbol{\kappa}^{:d}_{:d} \;\; \boldsymbol{\kappa}^{:d}_{:d}]\, \boldsymbol{\beta}_{i,*,i}\, X^{(t,l)}_{iii} \\
& X^{(t,l,\text{broad.})}_{kij} = \boldsymbol{\kappa}^{:d}_{:d}\, X^{(t,l)}_{kij} + \boldsymbol{\kappa}^{:2d}_{d+1:3d}\, [\boldsymbol{\kappa}^{:d}_{:d} \;\; \boldsymbol{\kappa}^{:d}_{:d}]\, \boldsymbol{\beta}_{k,*,i}\, X^{(t,l)}_{kii} \\
[\#4.\text{off}] \quad & X^{(t,l,\text{broad.})}_{kik} = \boldsymbol{\kappa}^{:d}_{:d}\, X^{(t,l)}_{kik} + \boldsymbol{\kappa}^{:2d}_{d+1:3d}\, [\boldsymbol{\kappa}^{:d}_{:d} \;\; \boldsymbol{\kappa}^{:d}_{:d}]\, \boldsymbol{\beta}_{*,i,*}\, X^{(t,l)}_{iii} \\
& X^{(t,l,\text{broad.})}_{kij} = \boldsymbol{\kappa}^{:d}_{:d}\, X^{(t,l)}_{kij} + \boldsymbol{\kappa}^{:2d}_{d+1:3d}\, [\boldsymbol{\kappa}^{:d}_{:d} \;\; \boldsymbol{\kappa}^{:d}_{:d}]\, \boldsymbol{\beta}_{*,k,i}\, X^{(t,l)}_{kii} \\
[\#5.\text{off}] \quad & X^{(t,l,\text{broad.})}_{kik} = \boldsymbol{\kappa}^{:d}_{:d}\, X^{(t,l)}_{kik} + \boldsymbol{\kappa}^{:2d}_{d+1:3d}\, [\boldsymbol{\kappa}^{:d}_{:d} \;\; \boldsymbol{\kappa}^{:d}_{:d}]\, \boldsymbol{\beta}_{i,*,i}\, X^{(t,l)}_{iii} \\
& X^{(t,l,\text{broad.})}_{kij} = \boldsymbol{\kappa}^{:d}_{:d}\, X^{(t,l)}_{kij} + \boldsymbol{\kappa}^{:2d}_{d+1:3d}\, [\boldsymbol{\kappa}^{:d}_{:d} \;\; \boldsymbol{\kappa}^{:d}_{:d}]\, \boldsymbol{\beta}_{i,*,k}\, X^{(t,l)}_{kii} \\
[\#6.\text{off}] \quad & X^{(t,l,\text{broad.})}_{kik} = \boldsymbol{\kappa}^{:d}_{:d}\, X^{(t,l)}_{kik} + \boldsymbol{\kappa}^{:2d}_{d+1:3d}\, [\boldsymbol{\kappa}^{:d}_{:d} \;\; \boldsymbol{\kappa}^{:d}_{:d}]\, \boldsymbol{\beta}_{i,*,i}\, X^{(t,l)}_{iii} \\
& X^{(t,l,\text{broad.})}_{kij} = \boldsymbol{\kappa}^{:d}_{:d}\, X^{(t,l)}_{kij} + \boldsymbol{\kappa}^{:2d}_{d+1:3d}\, [\boldsymbol{\kappa}^{:d}_{:d} \;\; \boldsymbol{\kappa}^{:d}_{:d}]\, \boldsymbol{\beta}_{*,*,i}\, X^{(t,l)}_{iii}
\end{aligned}
$$

Terms [#4.on], [#1.off] involve two sparse summations and thus require a slightly different construction. In particular, they are concurrently implemented by computing steps (1,2,3) twice, in sequence, followed by computation of step (4). The first brodcasting step (1) is realised as follows:

$$
\begin{aligned}
X^{(t,l,1^{st}\text{broad.})}_{iij} &= \boldsymbol{\kappa}^{:d}_{:d}\, X^{(t,l)}_{iij} + \boldsymbol{\kappa}^{:2d}_{d+1:3d}\, [\boldsymbol{\kappa}^{:d}_{:d} \;\; \boldsymbol{\kappa}^{:d}_{:d}]\, \boldsymbol{\beta}_{k,k,i}\, X^{(t,l)}_{kii} \\
X^{(t,l,1^{st}\text{broad.})}_{kik} &= \boldsymbol{\kappa}^{:d}_{:d}\, X^{(t,l)}_{kik} + \boldsymbol{\kappa}^{:2d}_{d+1:3d}\, [\boldsymbol{\kappa}^{:d}_{:d} \;\; \boldsymbol{\kappa}^{:d}_{:d}]\, \boldsymbol{\beta}_{i,*,i}\, X^{(t,l)}_{iii} \\
X^{(t,l,1^{st}\text{broad.})}_{kij} &= \boldsymbol{\kappa}^{:d}_{:d}\, X^{(t,l)}_{kij} + \boldsymbol{\kappa}^{:2d}_{d+1:3d}\, [\boldsymbol{\kappa}^{:d}_{:d} \;\; \boldsymbol{\kappa}^{:d}_{:d}]\, \boldsymbol{\beta}_{k,*,i}\, X^{(t,l)}_{kii}
\end{aligned}
$$

that is, in the same way as in the implementation of terms [#2.on], [#3.off]. Then, the first sparsification step (2) is computed as per Equations (37) to (39), generating $X^{(t,l,1^{st}\text{sp.})}_{iij}, X^{(t,l,1^{st}\text{sp.})}_{kik}, X^{(t,l,1^{st}\text{sp.})}_{kij}$. The first aggregation step (3) is performed jointly with the second broadcasting step (1) as:

$$
\begin{aligned}
X^{(t,l,2^{nd}\text{broad.})}_{iij} &= \boldsymbol{\kappa}^{:d}_{:d}\, X^{(t,l,1^{st}\text{sp.})}_{iij} + \boldsymbol{\kappa}^{d+1:3d}_{d+1:3d}\, \boldsymbol{\beta}_{*,*,i}\, \boldsymbol{\pi}_i\, X^{(t,l,1^{st}\text{sp.})}_{iij} \\
X^{(t,l,2^{nd}\text{broad.})}_{kik} &= \boldsymbol{\kappa}^{:d}_{:d}\, X^{(t,l,1^{st}\text{sp.})}_{kik} + \boldsymbol{\kappa}^{d+1:3d}_{d+1:3d}\, \boldsymbol{\beta}_{k,i,k}\, \boldsymbol{\pi}_{k,i}\, X^{(t,l,1^{st}\text{sp.})}_{kij} + \\
&\quad + \boldsymbol{\kappa}^{:2d}_{d+1:3d}\, [\boldsymbol{\kappa}^{:d}_{:d} \;\; \boldsymbol{\kappa}^{:d}_{:d}]\, \boldsymbol{\beta}_{i,*,i}\, X^{(t,l,1^{st}\text{sp.})}_{iii} \\
X^{(t,l,2^{nd}\text{broad.})}_{kij} &= \boldsymbol{\kappa}^{:d}_{:d}\, X^{(t,l,1^{st}\text{sp.})}_{kij} + \boldsymbol{\kappa}^{d+1:3d}_{d+1:3d}\, \boldsymbol{\beta}_{*,i,k}\, X^{(t,l,1^{st}\text{sp.})}_{kik} + \boldsymbol{\kappa}^{d+1:3d}_{d+1:3d}\, \boldsymbol{\beta}_{*,i,k}\, \boldsymbol{\pi}_{k,i}\, X^{(t,l,1^{st}\text{sp.})}_{kij}
\end{aligned}
$$

where, crucially, the results from pooling are broadcast back into orbit tensors $X_{iij}, X_{kik}, X_{kij}$, given that one more local summation is required. Next, one more sparsification takes place in the form of Equations (37) to (39), generating $X^{(t,l,2^{nd}\text{sp.})}_{iij}, X^{(t,l,2^{nd}\text{sp.})}_{kik}, X^{(t,l,2^{nd}\text{sp.})}_{kij}$. Finally, second aggregation step (3) is performed jointly with the final update step (4), which writes back into orbit tensors X_{iii}, X_{kii}:

$$
\begin{aligned}
X^{(t,l+1)}_{iii} &= \boldsymbol{\kappa}^{:2d}_{:2d}\, X^{(t,l,2^{nd}\text{sp.})}_{iii} + \boldsymbol{\kappa}^{:}_{d+1:2d}\, [\mathbf{0} \,||\, \theta^{\sim_i}_{1,l,t} \,||\, \theta^{\sim}_{1,l,t}]\, \boldsymbol{\beta}_{i,i,i}\, \boldsymbol{\pi}_i\, X^{(t,l,2^{nd}\text{sp.})}_{iij} \\
X^{(t,l+1)}_{kii} &= \boldsymbol{\kappa}^{:2d}_{:2d}\, X^{(t,l,2^{nd}\text{sp.})}_{kii} + \boldsymbol{\kappa}^{:}_{d+1:2d}\, [\mathbf{0} \,||\, \theta^{\sim_k}_{2,l,t} \,||\, \theta^{\sim}_{2,l,t}]\, \boldsymbol{\beta}_{kii}\, X^{(t,l,2^{nd}\text{sp.})}_{kik} + \\
&\quad + \boldsymbol{\kappa}^{:}_{d+1:2d}\, [\mathbf{0} \,||\, \theta^{\sim_k}_{2,l,t} \,||\, \theta^{\sim}_{2,l,t}]\, \boldsymbol{\beta}_{kii}\, \boldsymbol{\pi}_{k,i}\, X^{(t,l,2^{nd}\text{sp.})}_{kij}
\end{aligned}
$$

When all terms are implemented and combined together, it is only left to bring back the dimensionality to d, overwriting the previous node representations with the newly computed one:

$$X_{iii}^{(t+1)} = \sigma\Big(\boldsymbol{\kappa}_{:d}^{d+1:}\ X_{iii}^{(t,L)}\Big)$$
$$X_{kii}^{(t+1)} = \sigma\Big(\boldsymbol{\kappa}_{:d}^{d+1:}\ X_{kii}^{(t,L)}\Big)$$

□

Proof of Corollary 10. We proceed by contradiction as in the Proof of Corollary 7. Suppose there exist non-isomorphic but 3-WL-equivalent graphs G_1, G_2 distinguished by instance $\mathcal{R}_{\rho,\Theta,\bar{\pi}}$. That is, $\mathcal{R}_{\rho,\Theta,\bar{\pi}}\big(G_1\big) \neq \mathcal{R}_{\rho,\Theta,\bar{\pi}}\big(G_2\big)$. In view of Theorem 9, there must exists a 3-IGN instance $\mathcal{M}_\Omega$ such that $\mathcal{M}_\Omega\big(G_1\big) \neq \mathcal{M}_\Omega\big(G_2\big)$. By Theorem 15, if there exists a 3-IGN distinguishing G_1, G_2, then these two graphs must be distinguished by the 3-WL algorithm, against our hypothesis. □

D.3 Proofs for Section 6.2

SUN in linear form

$$x_i^{i,(t+1)} = \sigma\Big(U_{r,t}^2 \cdot x_i^{i,(t)} + U_{r,t}^3 \cdot \sum_j x_j^{i,(t)} + \\ + U_{r,t}^4 \cdot \sum_{j\sim_i i} x_j^{i,(t)} + U_{r,t}^5 \cdot \sum_h x_i^{h,(t)} + U_{r,t}^6 \cdot \sum_{j\sim i}\sum_h x_j^{h,(t)}\Big) \tag{40}$$

$$x_i^{k,(t+1)} = \sigma\Big(U_t^0 \cdot x_i^{i,(t)} + U_t^1 \cdot x_k^{k,(t)} + U_t^2 \cdot x_i^{k,(t)} + U_t^3 \cdot \sum_j x_j^{k,(t)} + \\ + U_t^4 \cdot \sum_{j\sim_k i} x_j^{k,(t)} + U_t^5 \cdot \sum_h x_i^{h,(t)} + U_t^6 \cdot \sum_{j\sim i}\sum_h x_j^{h,(t)}\Big) \tag{41}$$

Proof of Proposition 11. We construct a stacking of 2 ReIGN(2) layers implementing one SUN layer as per Equations 40 and 41. The first layer expands the dimension of the hidden representations to $2d$. The first d channels store the sum of linear transformations operated by $U_{r,t}^2, U_{r,t}^3, U_{r,t}^4$ in Equation 40 and those operated by $U_t^0, U_t^1, U_t^2, U_t^3, U_t^4$ in Equation 41. Channels $d+1$ to $2d$ will store terms $\sum_h x_i^{h,(t)}$:

$$x_i^{i,(t,1)} = [(U_{r,t}^2 + I_d)\ \ I_d]\ x_i^{i,(t)} + \boldsymbol{\kappa}_{:d/(2d)}^{:}\ U_{r,t}^3 \cdot \sum_{j\neq i} x_j^{i,(t)} + \\ + \boldsymbol{\kappa}_{:d/(2d)}^{:}\ U_{r,t}^4 \cdot \sum_{j\sim_i i} x_j^{i,(t)} + \boldsymbol{\kappa}_{d+1:2d}^{:} \sum_{h\neq i} x_i^{h,(t)}$$

$$x_i^{k,(t,1)} = [U_t^0\ \ I_d]\ x_i^{i,(t)} + \boldsymbol{\kappa}_{:d/(2d)}^{:}\ (U_t^1 + I_d) \cdot x_k^{k,(t)} + \boldsymbol{\kappa}_{:d/(2d)}^{:}\ U_t^2 \cdot x_i^{k,(t)} + \\ + \boldsymbol{\kappa}_{:d/(2d)}^{:}\ U_t^3 \cdot \sum_{j\neq k} x_j^{k,(t)} + \boldsymbol{\kappa}_{:d/(2d)}^{:}\ U_t^4 \cdot \sum_{j\sim_k i} x_j^{k,(t)} + \boldsymbol{\kappa}_{d+1:2d}^{:} \sum_{h\neq i} x_i^{h,(t)}$$

where we have used the following aggregated terms. First equation: [#2.on] in its global version and second expansion, [#3.on] in its global version. Second equation: [#2.off] in its global version, [#3.off] in its global version and second expansion. Non-appearing ReIGN(2) terms are nullified. The second ReIGN(2) layer completes the computation by implementing linear transformations $U_{t,r}^5, U_{t,r}^6, U_t^5, U_t^6$, and by contracting the dimensionality back to d:

$$x_i^{i,(t+1)} = \sigma\Big(\big[I_d \,||\, U_{r,t}^5\big]\ x_i^{i,(t,1)} + U_{r,t}^6 \cdot \boldsymbol{\kappa}_{:d}^{d+1:2d} \sum_{j\sim i} x_j^{i,(t,1)}\Big)$$

$$x_i^{k,(t+1)} = \sigma\Big(\big[I_d \,||\, U_t^5\big]\ x_i^{k,(t,1)} + U_t^6 \cdot \boldsymbol{\kappa}_{:d}^{d+1:2d} \sum_{j\sim i} x_j^{k,(t,1)}\Big)$$

where we have used aggregated terms [#2.on] and [#3.off] in their third expansion. □

Proof of Proposition 12. We describe how a stacking of SUN layers in the form of Equations 40 and 41 implements layers of models in Υ with Morris et al. [36] base-encoders. As usual, we proceed model by model.

[***DS-GNN***] updates root and non-root nodes in the same manner. Thus, we seek to find a choice of linear operators in Equations 40 and 41 in a way that the two coincide and exactly correspond to Equation 23. To this aim, it is sufficient to set:

- $U^2_{r,t} = U^2_t = W_{1,t}$
- $U^4_{r,t} = U^4_t = W_{2,t}$

and all other weight matrices U to $\mathbf{0}$.

[***DSS-GNN***] implements Equation 28. We proceed similarly as above, setting:

- $U^2_{r,t} = U^2_t = W^1_{1,t}$
- $U^4_{r,t} = U^4_t = W^1_{2,t}$
- $U^5_{r,t} = U^5_t = W^2_{1,t}$
- $U^6_{r,t} = U^6_t = W^2_{2,t}$

and all other weight matrices U to $\mathbf{0}$.

[***GNN-AK-ctx & GNN-AK***] We seek to recover Equations 29 ([S]) and 30 ([A]). Each message passing layer in [S] is implemented by one SUN layer similarly as above, that is by setting:

- $U^2_{r,t,l} = U^2_{t,l} = W_{1,t,l}$
- $U^4_{r,t,l} = U^4_{t,l} = W_{2,t,l}$

and all other weight matrices U to $\mathbf{0}$. Then, block [A] is implemented by one SUN layer by setting:

- $U^2_{r,t} = U^3_{r,t} = U^5_{r,t} = I$
- $U^0_t = U^3_t = U^5_t = I$

and all other weight matrices U to $\mathbf{0}$. In the case of GNN-AK, we instead require $U^5_{r,t} = U^5_t = \mathbf{0}$. No activation σ is applied after this layer.

[***ID-GNN***] Two SUN layers can implement one ID-GNN layer as in Equation 36, similarly as shown for `ReIGN(2)` in the Proof of Theorem 8. The first layer doubles the representation dimension and applies projections $W_{1,t}, W_{2,t}, W_{3,t}$, by setting:

- $U^2_{r,t,1} = [W_{1,t} \;\; W_{3,t}]$
- $U^2_{t,1} = [W_{1,t} \;\; W_{2,t}]$

and all other weight matrices U to $\mathbf{0}$. Here, as usual, $\left[\cdot\,\cdot\right]$ indicates vertical concatenation. No activation σ is applied after this layer.

The second layer has its weight matrices set to:

- $U^2_{r,t,2} = U^2_{t,2} = \boldsymbol{\kappa}^{:d}_{:d}$
- $U^4_{r,t,2} = U^4_{t,2} = \boldsymbol{\kappa}^{d+1:2d}_{:d}$

and all other weight matrices U to $\mathbf{0}$.

[***NGNN***] layers perform independent message passing on each subgraph. `SUN` implements these as shown for DS-GNN. □

E Future research directions

The following are promising directions for future work:

1. *Extension to higher-order node policies.* The prior works of Cotta et al. [14], Papp et al. [43] suggested using more complex policies that depend on tuples of nodes rather than a single node. Since there are exactly n^k distinct k-tuples, and each subgraph is defined by a second-order adjacency tensor, we conjecture that Subgraph GNNs applied to such policies are bounded by `(k+2)-WL`. See Appendix F for additional details.
2. *Beyond `3-WL`.* Our results suggest two directions for breaking the `3-WL` representational limit: (i) Using policies not computable by `3-IGN`s (ii) Using higher-order node-based policies as mentioned above.
3. *Layers vs. policies.* We make an interesting observation regarding the relationship between layer structure and subgraph selection policies: Having a non-shared set of parameters for root and non-root nodes, `SUN` may be capable of learning the policies $\pi_{\text{NM}}, \pi_{\text{ND}}$ by itself. This raises the question of whether we should let the model learn a policy or specify one in advance.
4. *Lower bound on `SUN` and `ReIGN(2)`.* In this work we have proved a `3-WL` *upper bound* on the expressive power of `SUN`, `ReIGN(2)` and other node-based Subgraph GNNs by showing their computation on a given graph pair can be simulated by a `3-IGN`. It is natural to ask whether a (tighter) *lower bound* exists as well. In this sense, it is reasonable to believe that node-based Subgraph GNNs are not capable of implementing `3-IGN`s, as they inherently operate on a second-order object. However, this does not necessarily imply these models are less expressive than `3-IGN`s, when considering graph separation. For example, they may still be able to distinguish between the same pairs of graphs distinguished by 3-IGNs, hence attaining `3-WL` expressive power. It is because of this reason that we believe studying the expressivity gap between `ReIGN(2)` (or any of the subsumed Subgraph GNNs) and `3-WL` represents an interesting open question that could be addressed in future work.
5. *Expressive power of subgraph selection policies.* Another interesting direction for future work would be to better characterise the impact of subgraph selection policies on the expressive power of Subgraph GNNs. Bevilacqua et al. [7] already showed that the DS-GNN model can distinguish some Strongly Regular graphs in the same family when equipped with edge-deletion policy, but not with node-deletion or depth-n ego-networks [7, Proposition 3]. However, edge-deletion is *not* a node-based policy since subgraphs are not in a bijection with nodes in the original graph. It still remains unclear whether a stratification in expressive power exists amongst node-based policies in particular, and under which conditions – if any – this last holds.

We note that, related to 3. and concurrently to the present work, Qian et al. [46] experiment with directly learning policies by back-propagating through discrete structures via perturbation-based differentiation [41].

F Extension to higher-order node policies

Constructing a higher-order subgraph selection policy (Appendix E, direction 1.), amounts to defining *selection function* f on a graph and a k*-tuple* of its nodes: For a graph $G \in \mathcal{G}$, the subgraphs of such a policy are obtained as $G_{(v_1,\ldots,v_k)} = f\big(G, (v_1, \ldots, v_k)\big)$. The policy contains a subgraph for each possible tuple $(v_1, \ldots, v_k)$. We refer to such policies as k*-order node policies*. The k-node deletion policy suggested by Cotta et al. [14] is a natural example as the bag of subgraphs contains all subgraphs that are obtained by removing k distinct nodes from the original graph. Since there are exactly n^k distinct tuples, and each subgraph is defined by a second-order adjacency tensor in $\mathbb{R}^{n^2}$, these bags of subgraphs can be arranged into tensors in $\mathbb{R}^{n^{k+2}}$. Noting that the symmetry of

Table 4: TUDatasets. The top three are highlighted by **First**, **Second**, **Third**.

Dataset	MUTAG	PTC	PROTEINS	NCI1	NCI109	IMDB-B	IMDB-M
DCNN [4]	N/A	N/A	61.3±1.6	56.6±1.0	N/A	49.1±1.4	33.5±1.4
DGCNN [60]	85.8±1.8	58.6±2.5	75.5±0.9	74.4±0.5	N/A	70.0±0.9	47.8±0.9
IGN [33]	83.9±13.0	58.5±6.9	76.6±5.5	74.3±2.7	72.8±1.5	72.0±5.5	48.7±3.4
PPGNs [32]	90.6±8.7	66.2±6.6	**77.2**±4.7	83.2±1.1	**82.2**±1.4	73.0±5.8	50.5±3.6
NATURAL GN [15]	89.4±1.6	66.8±1.7	71.7±1.0	82.4±1.3	N/A	73.5±2.0	51.3±1.5
GSN [11]	**92.2**±7.5	**68.2**±7.2	76.6±5.0	83.5±2.0	N/A	**77.8**±3.3	**54.3**±3.3
SIN [10]	N/A	N/A	76.4±3.3	82.7±2.1	N/A	75.6±3.2	52.4±2.9
CIN [9]	**92.7**±6.1	**68.2**±5.6	**77.0**±4.3	83.6±1.4	**84.0**±1.6	75.6±3.7	52.7±3.1
GIN [55]	89.4±5.6	64.6±7.0	76.2±2.8	82.7±1.7	**82.2**±1.6	75.1±5.1	52.3±2.8
ID-GNN (GIN) [56]	90.4±5.4	67.2±4.3	75.4±2.7	82.6±1.6	82.1±1.5	76.0±2.7	52.7±4.2
DROPEDGE [48]	91.0±5.7	64.5±2.6	73.5±4.5	82.0±2.6	**82.2**±1.4	76.5± 3.3	52.8± 2.8
DS-GNN (GIN) (ND) [7]	89.4±4.8	66.3±7.0	**77.1**±4.6	**83.8**±2.4	82.4±1.3	75.4±2.9	52.7±2.0
DS-GNN (GIN) (EGO) [7]	89.9±6.5	68.6±5.8	76.7±5.8	81.4±0.7	79.5±1.0	76.1±2.8	52.6±2.8
DS-GNN (GIN) (EGO+) [7]	91.0±4.8	68.7±7.0	76.7±4.4	82.0±1.4	80.3±0.9	**77.1**±2.6	53.2±2.8
DSS-GNN (GIN) (ND) [7]	91.0±3.5	66.3±5.9	76.1±3.4	83.6±1.5	**83.1**±0.8	76.1±2.9	**53.3**±1.9
DSS-GNN (GIN) (EGO) [7]	91.0±4.7	68.2±5.8	76.7±4.1	83.6±1.8	82.5±1.6	76.5±2.8	**53.3**±3.1
DSS-GNN (GIN) (EGO+) [7]	91.1±7.0	**69.2**±6.5	75.9±4.3	83.7±1.8	82.8±1.2	**77.1**±3.0	53.2±2.4
GIN-AK+ [61]	**91.3**±7.0	**67.8**±8.8	**77.1**±5.7	**85.0**±2.0	N/A	75.0±4.2	N/A
SUN (GIN) (NULL)	91.6±4.8	67.5±6.8	76.8±4.4	84.1±2.0	83.0±0.9	76.2±1.9	52.6±3.2
SUN (GIN) (NM)	91.0±4.7	67.0±4.8	75.7±3.4	84.2±1.5	**83.1**±1.5	76.1±2.9	**53.1**±2.5
SUN (GIN) (EGO)	**92.7**±5.8	67.2±5.9	76.8±5.0	83.7±1.3	83.0±1.0	**76.6**±3.4	52.7±2.3
SUN (GIN) (EGO+)	92.1±5.8	67.6±5.5	76.1±5.1	**84.2**±1.5	**83.1**±1.0	76.3±1.9	52.9±2.8

these tensors can be naturally defined by the diagonal action of S_n on $\{1, \dots, n\}^{k+2}$ we raise the following generalisation of Corollary 7:

Conjecture 1. *Subgraph GNNs equipped with k-order* node-deletion*, k-order* node-marking *or k-order* ego-networks *policies are bounded by $(k+2)$-WL.*

We believe that proving this conjecture can be accomplished by following the same steps as our proof, i.e., by showing that `(k+2)-IGN` can implement the bag and the update steps of Subgraph GNNs. We also note that `ReIGN(k)`, a higher order analogue of `ReIGN(2)`, can be obtained by following the steps in Section 6. We leave both directions for future work.

We end this section by noting that the statement in our conjecture is considered in a work concurrent to ours by Qian et al. [46].

G Experimental details and additional results

Table 5: Test mean metric on the Graph Properties dataset. All Subgraph GNNs employ a GIN base-encoder.

Method	Graph Properties ($\log_{10}$(MSE))		
	IsConnected	Diameter	Radius
GCN [27]	-1.7057	-2.4705	-3.9316
GIN [55]	-1.9239	-3.3079	-4.7584
PNA [13]	-1.9395	-3.4382	-4.9470
PPGN [32]	-1.9804	-3.6147	-5.0878
GNN-AK [61]	-1.9934	-3.7573	-5.0100
GNN-AK-CTX [61]	-2.0541	-3.7585	-5.1044
GNN-AK+ [61]	-2.7513	-3.9687	-5.1846
SUN (EGO)	-2.0001	-3.6671	-5.5720
SUN (EGO+)	-2.0651	-3.6743	-5.6356

G.1 Additional experiments

TUDatasets. We experimented the performances of `SUN` on the widely used datasets from the TUD repository [37], and include a comparison of different subgraph selection policies. Marking a first,

Table 6: Test mean and std for the corresponding metric on the synthetic tasks. A comparison with other methods can be found in Tables 1 and 5.

Method	Counting Substructures (MAE)			
	Triangle	Tailed Tri.	Star	4-Cycle
SUN (EGO)	0.0092±0.0002	0.0105±0.0010	0.0064±0.0006	0.0140±0.0014
SUN (EGO+)	0.0079±0.0003	0.0080±0.0005	0.0064±0.0003	0.0105±0.0006

Method	Graph Properties ($\log_{10}$(MSE))		
	IsConnected	Diameter	Radius
SUN (EGO)	-2.0001±0.0211	-3.6671±0.0078	-5.5720±0.0423
SUN (EGO+)	-2.0651±0.0533	-3.6743±0.0178	-5.6356±0.0200

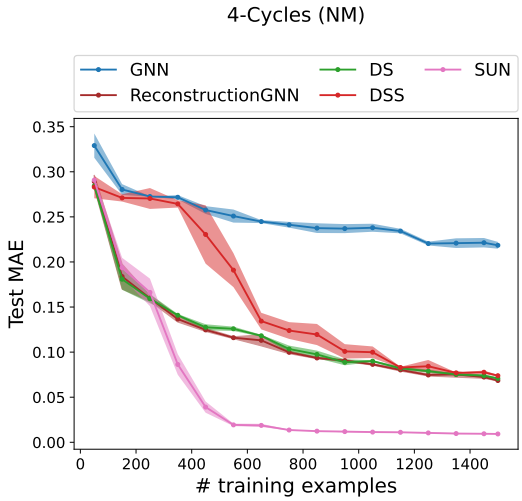

Figure 7: Generalisation capabilities of Subgraph GNNs in the counting prediction task with the node-marking (NM) selection policy.

preliminary, step in the future research direction (3) in Appendix E, we also experiment with a 'NULL' policy, i.e. by constructing bags by simply replicating the original graph n times, without any marking or connectivity alteration. Results are reported in Table 4. Notably, the EGO policies obtain the best results in 6 out of 7 datasets, while the NULL policy does not seem an advantageous strategy on this benchmarking suite. On average, SUN compares well with best performing approaches across domains, while featuring smaller result variations w.r.t. to GNN-AK+ [61].

Synthetic – Graph property prediction. Table 5 reports mean test $\log_{10}(\text{MSE})$ on the Graph Properties dataset. SUN achieves state-of-the art results on the "Radius" task, where each target is defined as the largest (in absolute value) eigenvalue of the graph's adjacency matrix. Table 6 gathers the standard deviation on the results for these benchmarks as well as "Counting Substructures" ones over 3 seeds as in Zhao et al. [61].

Generalisation from limited data – Node Marking. Figure 7 tests the generalisation abilities of Subgraph GNNs on the 4-Cycles task using the node-marking selection policy (NM). Similarly to Figures 4a and 4b, SUN outperforms all other Subgraph GNNs by a large margin and, except for a short initial phase where all Subgraph architectures perform similarly, SUN generalises better.

Analysis of generalisation. The GNN's poor performance on this set of experiments may be due to different reasons, e.g. underfitting vs. overfitting behaviours. In this sense, here we deepen our understanding on the 4-Cycles counting task by additionally inspecting characteristics of the train samples and performance thereon. Table 7 reports evaluation results on training and validation sets at the epoch of best validation performance, as well as the best overall training performance. We include the GNN and SUN models, along with a trivial predictor which always outputs the mean training target.

Table 7: Performances for the 4-Cycles counting task. The Trivial Predictor always outputs the mean training target.

	Best Train	Train	Val	Test
Trivial Predictor	0.9097	0.9097	0.9193	0.9275
GIN [55]	0.0283±0.0032	0.1432±0.0526	0.2148±0.0051	0.2185±0.0061
SUN (EGO+)	0.0072±0.0002	0.0072±0.0001	0.0097±0.0005	0.0105±0.0002

Table 8: Test results on ZINC dataset (GIN base-encoder). Each row reports a particular ablation applied on top of the ones in the upper rows.

Method	ZINC (MAE ↓)	
	EGO	EGO+
SUN	0.083±0.003	0.084±0.002
w/o $x_i^{i,(t)}, x_k^{k,(t)}$	0.089±0.004	0.089±0.002
$\theta_1 = \theta_2$	0.093±0.003	0.093±0.004
w/o $\sum_j x_j^{k,(t)}$	0.093±0.004	0.090±0.004
w/o $\sum_h x_i^{h,(t)}, \sum_{j\sim i} \sum_h x_j^{h,(t)}$	0.111±0.005	0.101±0.007

First, we observe that the GNN exhibits a relatively large gap between the two reported training MAEs if compared to SUN. This rules out scenarios of complete underfitting, especially considering the trivial predictor performs much worse than the GNN. This led us to evaluate the expressiveness class required to disambiguate all training and test samples: out of all possible graph pairs, we only found one not distinguished by a 1-WL test running 6 colour refinement rounds — same as the number of message passing layers in our GNN. As a consequence, the GNN baseline can effectively assign unique representations to almost all graphs, this justifying its superior performance w.r.t. the trivial predictor. Yet, SUN achieves much better results on all sets, while displaying a smaller train-test gap. This is an indication that, although the hypothesis class of the GNN is sufficiently large to avoid underfitting, it renders the overall learning procedure difficult, leading to suboptimal solutions and partial memorisation phenomena. These results are in line with the observations in Cotta et al. [14, Appendix G.1], where the authors have performed a similar analysis on real-world benchmarks.

Ablation study. To assess the impact of the terms in the SUN layer, we perform an ablation study by making sequential changes to Equations (5) and (6) until recovering an architecture similar to NGNN, DS-GNN. We considered the ZINC-12k molecular dataset, using GIN as base graph encoder. Table 8 reports the performances for the EGO and EGO+ policies. As it can be seen, each ablation generally produces some performance degradation, with the removal of $\sum_j x_j^{k,(t)}$ having no significant impact (EGO policy) or even being beneficial when the other changes are made (EGO+ policy). Interestingly, in the EGO+ policy case, although root nodes are explicitly marked, the architecture seems to still benefit from not sharing parameters between root and non-root updates. Indeed, imposing the weight sharing $\theta_1 = \theta_2$ deteriorates the overall performance, which gets similar to the one obtained for the EGO policy. These results indicates that, in the SUN layer, most of the terms concur to the strong empirical performance of the architecture, including the choice of not sharing parameters between root and non-root updates.

G.2 Experimental details

We implemented our model using Pytorch [44] and Pytorch Geometric [18] (available respectively under the BSD and MIT license). We ran our experiments on NVIDIA DGX V100, GeForce 2080, and TITAN V GPUs. We performed hyperparameter tuning using the Weight and Biases framework [8]. The time spent on each run depends on the dataset under consideration, with the largest being ogbg-molhiv which takes around 8 hours for 200 epochs and asam optimizer. The time for a single ZINC run is 1 hour and 10 minutes for 400 epochs. SUN uses the mean aggregator for the feature matrix and directly employs the adjacency matrix of the original graph as the aggregated adjacency (Equations (5) and (6)). We used the sum aggregator for all the other terms. Unless

otherwise specified, SUN uses the following update equations:

$$x_v^{v,(t+1)} = \sigma\Big(\mu_{t,r}^2\big(x_v^{v,(t)}\big) + \mu_{t,r}^3\big(\sum_w x_w^{v,(t)}\big) + \\ + \gamma_{t,r}^0\big(x_v^{v,(t)}, \sum_{w\sim_v v} x_w^{v,(t)}\big) + \gamma_{t,r}^1\big(\sum_h x_v^{h,(t)}, \sum_{w\sim v}\sum_h x_w^{h,(t)}\big)\Big) \tag{42}$$

$$x_v^{k,(t+1)} = \sigma\Big(\mu_t^0\big(x_v^{v,(t)}\big) + \mu_t^1\big(x_k^{k,(t)}\big) + \mu_t^2\big(x_v^{k,(t)}\big) + \mu_t^3\big(\sum_w x_w^{k,(t)}\big) + \\ + \gamma_t^0\big(x_v^{k,(t)}, \sum_{w\sim_k v} x_w^{k,(t)}\big) + \gamma_t^1\big(\sum_h x_v^{h,(t)}, \sum_{w\sim v}\sum_h x_w^{h,(t)}\big)\Big) \tag{43}$$

where μ's are two-layer MLPs and each γ consists of one GIN [55] convolutional layer whose internal MLP matches the dimensionality of μ's, e.g.,

$$\gamma_t^0\big(x_v^{k,(t)}, \sum_{w\sim_k v} x_w^{k,(t)}\big) = \hat{\mu}_t^0\Big((1+\epsilon)x_v^{k,(t)} + \sum_{w\sim_k v} x_w^{k,(t)}\Big)$$

where $\hat{\mu}_t^0$ is an MLP. Details on the hyperparameter grid and architectural choices specific for each dataset are reported in the following subsections.

G.2.1 Synthetic datasets

We used the dataset splits and evaluation procedure of Zhao et al. [61]. We considered a batch size of 128 and used Adam optimiser with a learning rate of 0.001 which is decayed by 0.5 every 50 epochs. Training is stopped after 250 epochs. We used GIN as base encoder, and tuned the number of layers in $\{5, 6\}$, and the embedding dimension in $\{64, 96, 110\}$. The depth of the ego-networks is set 2 and 3 in, respectively, the Counting and Graph Property tasks, in accordance with Zhao et al. [61]. Results of existing baselines reported in Tables 1 and 5 are taken from Zhao et al. [61].

G.2.2 ZINC-12k

We used the same dataset splits of Dwivedi et al. [17], and followed the evaluation procedure prescribed therein. We used Mean Absolute Error as training loss and evaluation metric. We considered batch size of 128, and Adam optimizer with initial learning rate of 0.001 which is decayed by 0.5 after the validation metric does not improve for a patience that we set of 40 epochs. Training is stopped after the learning rate reaches the value of 0.00001, at which time we compute the test metric. We re-trained all Subgraph GNNs to comply with the 500k parameter budget, and also to the above standard procedure in the case of GNN-AK and GNN-AK-ctx. For GNN-AK+, we reported the result $0.086\pm???$ specified by the authors in the rebuttal phase on Openreview, where the question marks indicate that the standard deviation was not provided. We also re-ran GNN-AK+ with the aforementioned standard procedure (learning rate decay and test at the time of early stopping) and obtained 0.091 ± 0.011. All Subgraph GNNs use 6 layers and ego-networks of depth 3. We use GIN as the base encoder and we set the embedding dimension to 128 for NGNN, DS- and DSS-GNN, to 100 for GNN-AK variants and to 64 for SUN. DS-GNN employs invariant deep sets layers [58] of the form $\rho(\frac{1}{n}\sum_{i=1}^n \phi(x_i))$ where x_i denotes the representation of subgraph i. We tuned ϕ and ρ to be either a 2-layers MLP or a single layer with dimensions in $\{64, 128\}$. All other parameters are left as in the original implementation of the corresponding method. We repeat the experiments with 10 different initialisation seeds, and report mean and standard deviation.

G.2.3 OGBG-molhiv dataset

We used the evaluation procedure proposed in Hu et al. [23], which prescribes running each experiment with 10 different seeds and reporting the results at the epoch achieving the best validation metric. Following Zhao et al. [61], we disabled the subgraph aggregation components $\mu_{t,r}^3\big(\sum_w x_w^{v,(t)}\big)$ and $\mu_t^3\big(\sum_w x_w^{k,(t)}\big)$ in Equations (42) and (43). We used the same architectural choices of Zhao et al. [61], namely depth-3 ego-networks, 2 GIN layers, residual connections and dropout of 0.3. We set the embedding dimension of the GNNs to be 64. Early experimentation with the common Adam optimiser revealed large fluctuations in the validation metric, which we found to considerably

oscillate across optimisation steps even for small learning rate values. Thus, given the non-uniform strategy adopted to generate train, validation and test splits, we considered employing the ASAM optimiser [29]. ASAM considers the sharpness of the training loss in each gradient descent step, effectively driving the optimisation towards flatter minima. We left its ρ parameter to its default value of 0.5. Additionally, to further prevent overfitting, we adopted linear layers in place of MLPs, as shown in Equations (44) and (45). These choices showed to greatly reduce the aforementioned fluctuations. Finally, we tuned the learning rate in $\{0.01, 0.005\}$ and the batch size in $\{32, 64\}$. The result in Table 2 corresponds to the configuration attaining best overall validation performance (ROC AUC 85.19 ± 0.82), with a batch size of 32 and a learning rate of 0.01. We note that other configurations performed comparably well. Amongst others, the configuration with a batch size of 64 and a learning rate of 0.005 attained a Test ROC AUC of 80.41 ± 0.76 with a Validation ROC AUC of 84.87 ± 0.55. We remark how these SUN configurations perform comparably well when contrasted with state-of-the-art GNN approaches which explicitly model (molecular) rings, crucially, *both* on test and validation sets, despite the non-uniform splitting procedure. As an example, CIN [9] reports a Test ROC AUC of 80.94 ± 0.57 with a Validation ROC AUC of 82.77 ± 0.99.

$$x_v^{v,(t+1)} = \sigma\Big(U_{t,r}^2 \cdot x_v^{v,(t)} + \gamma_{t,r}^0\big(x_v^{v,(t)}, \sum_{w \sim_v v} x_w^{v,(t)}\big) + \gamma_{t,r}^1\big(\sum_h x_v^{h,(t)}, \sum_{w \sim v} \sum_h x_w^{h,(t)}\big)\Big) \tag{44}$$

$$\begin{aligned} x_v^{k,(t+1)} = \sigma\Big(&U_t^0 \cdot x_v^{v,(t)} + U_t^1 \cdot x_k^{k,(t)} + U_t^2 \cdot x_v^{k,(t)} + \\ &+ \gamma_t^0\big(x_v^{k,(t)}, \sum_{w \sim_k v} x_w^{k,(t)}\big) + \gamma_t^1\big(\sum_h x_v^{h,(t)}, \sum_{w \sim v} \sum_h x_w^{h,(t)}\big)\Big) \end{aligned} \tag{45}$$

G.2.4 TUDatasets

We followed the evaluation procedure described in Xu et al. [55]. We conducted 10-fold cross validation and reported the performances at the epoch achieving the best averaged validation accuracy across the folds. We used the same hyperparameter grid of Bevilacqua et al. [7]. We used GIN as base encoder, setting the number of layers to 4 and tuning its embedding dimension in $\{16, 32\}$. We used Adam optimizer with batch size in $\{32, 128\}$, and initial learning rate in $\{0.01, 0.001\}$, which is decayed by 0.5 every 50 epochs. Training is stopped after 350 epochs. All ego-networks are of depth 2.

G.2.5 Generalisation from limited data

We select each architecture by tuning the hyperparameters with the entire training and validation sets, and choosing the configuration achieving the best validation performances. The hyperparameter grids for SUN are the ones in Appendices G.2.1 and G.2.2. In the 4-Cycles task, for NGNN, DS- and DSS-GNN we used the same grid but we tuned the embedding dimension in $\{64, 128, 256\}$ to allow them to have a similar number of parameters as SUN. For GNN-AK variants we used the best performing parameters as provided in Zhao et al. [61].

G.2.6 Ablation study

For every ablation we tuned the embedding dimension in $\{64, 96, 110, 128\}$ and chose the model obtaining the lowest validation MAE while still being complaint with the 500K parameter budget. The evaluation procedure and all the other hyperparameters are as specified in Appendix G.2.2.